TESIS DE LA UNIVERSIDAD DE ZARAGOZA

2018

10

Alba Pilar Martín Yebra

Assessment of ventricular repolarization instability and cardiac risk stratification in different pathological and abnormal conditions

Departamento

Instituto de Investigación en Ingeniería [I3A]

Director/es

Martínez Cortés, Juan Pablo
Caiani, Enrico

ISSN 2254-7606

Prensas de la Universidad Universidad Zaragoza

ISSN 2254-7606

Universidad Zaragoza
1542

Tesis Doctoral

ASSESSMENT OF VENTRICULAR REPOLARIZATION INSTABILITY AND CARDIAC RISK STRATIFICATION IN DIFFERENT PATHOLOGICAL AND ABNORMAL CONDITIONS

Autor

Alba Pilar Martín Yebra

Director/es

Martínez Cortés, Juan Pablo
Caiani, Enrico

UNIVERSIDAD DE ZARAGOZA

Instituto de Investigación en Ingeniería [I3A]

2017

POLITECNICO
MILANO 1863

Universidad
Zaragoza

Ph.D. Thesis

Assessment of ventricular repolarization instability and cardiac risk stratification in different pathological and abnormal conditions

Alba Pilar Martín Yebra

SUPERVISORS:

Prof. Enrico Gianluca Caiani

Prof. Juan Pablo Martínez Cortés

Ph.D. in Bioengineering

October, 2017
XXIX Cycle

Assessment of ventricular repolarization instability and cardiac risk stratification in different pathological and abnormal conditions

Alba Pilar Martín Yebra, 2017
Assessment of ventricular repolarization instability and cardiac risk stratification in different pathological and abnormal conditions.

Date of current version: October 5, 2017

This thesis was supported by a fellowship from the *Ministero dell'Istruzione, dell' Università e della Ricerca* (MIUR, Italy). The research presented in this thesis was also supported by the following projects: *TEC2013-42140-R* and *DPI2016-75458-R* funded by MINECO and FEDER and by the Italian Space Agency (*contract 2013-033-R.0*, recipient E. Caiani). In addition, it was supported by Gobierno de Aragón (Spain) and European Social Fund through Grupo Consolidado Biomedical Signal Interpretation and Computational Simulation (BSICoS), Ref: *T96*, and by CIBER-BBN through Instituto de Salud Carlos III. The computation of some parts of this thesis was performed at the High Performance Computing platform of the NANBIOSIS ICTS, CIBER-BBN and Aragón Institute of Engineering Research (I3A), Zaragoza, Spain.

Summary and conclusions

Cardiovascular diseases (CVDs) represents the leading cause of mortality worldwide. These pathological conditions are mainly characterized by a structurally abnormal heart, that is, a vulnerable substrate, prone to the abnormal generation and/or propagation of the electrical impulse, determining the onset of ventricular arrhythmias. In this context, the assessment of ventricular repolarization from the electrocardiogram (ECG) signal has been shown to provide with valuable information for risk stratification and several electrocardiographic indices have been proposed in the literature.

The main objective of this thesis is to propose methodological advances for the assessment of ventricular repolarization instability in pathological and abnormal conditions. These contributions are aimed at improving the prediction of ventricular arrhythmias and, consequently, better identifying sudden cardiac death (SCD) risk. In particular, we have addressed this objective by developing robust methodologies for the assessment of T-wave alternans (TWA) and ventricular repolarization instability, in invasive and non-invasive cardiac signals, that have been evaluated in both experimental and clinical conditions.

In the first part of the thesis, TWA was simultaneously characterized (prevalence, magnitude, time-course, and alternans waveform) in body-surface ECG and intracardiac electrograms (EGM) signals during coronary artery occlusion. Signals from both body surface ECG and intracardiac EGM recorded from 4 different anatomical heart locations (coronary sinus, epicardial space and left and right ventricles) were analyzed following a multilead strategy. Leads were linearly combined using the periodic component analysis (πCA), which maximizes the 2-beat periodicity (TWA periodicity) content present on the available leads. Then the Laplacian Likelihood Ratio method (LLRM) was applied for TWA detection and estimation. A sensitivity study for TWA detection from the 5 different locations of leads was

performed, revealing that it is the combination of the ECG leads that better performs. In addition, this multilead approach allowed us to find the optimal combination of intracardiac leads usable for in-vivo monitorization of TWA directly from an implantable device, with a sensitivity comparable to the ECG analysis. These results encourage further research to determine the feasibility of predicting imminent VT/VF episodes by TWA analysis implemented in implantable cardioverter defibrillator's (ICD) technology.

Then, we have studied the potential changes induced by a prolonged exposure to simulated microgravity on ventricular repolarization in structurally normal hearts. It is well known that this environmental condition affects the control of autonomic and cardiovascular systems, with a potential increase on cardiac electrical instability. The effects of short- (5 days), mid- (21 days) and long- (60 days) exposure to simulated microgravity on TWA using the head-down bed-rest (HDBR) model were assessed. TWA was evaluated before (PRE), during and after (POST) the immobilization period, by the long-term averaging technique in ambulatory ECG Holter recordings. Additionally, we proposed an adapted short-term averaging approach for shorter, non-stationary ECG signals obtained during two stress manoeuvres (head-up tilt-table and bicycle exercise tests). Both approaches are based on the multilead analysis used in the previous study. The absence of significant changes between PRE and POST-HDBR on TWA indices suggests that a long-term exposure to simulated microgravity is not enough to induce alterations in healthy myocardial substrate up to the point of reflecting electrical instability in terms of TWA on the ECG.

Finally, methodological advances were proposed for the assessment of ventricular repolarization instability from the ECG signal in the presence of sporadic (ventricular premature contractions, VPCs) and sustained (atrial fibrillation) rhythm disturbance.

On the one hand, a methodological improvement for the estimation of TWA amplitude in ambulatory ECG recordings was proposed, which deals with the possible phase reversal on the alternans sequence induced by the presence of VPCs. The performance of the algorithm was first evaluated using synthetic signals. Then, the effect of the proposed method in the prognostic value of TWA amplitude was assessed in real ambulatory ECG recordings from patients with chronic heart failure (CHF). Finally, circadian TWA changes were evaluated as well as the prognostic value of TWA at different times of the day. A clinical study demonstrated the enhancement in the predictive value of the index of average alternans (IAA) for

SCD stratification. In addition, results suggested that alternans activity is modulated by the circadian pattern, preserving its prognostic information when computed just during the morning, which is also the day interval with the highest reported SCD incidence. Thus, suggesting that time of the day should be considered for SCD risk prediction.

On the other hand, the high irregularity of the ventricular response in atrial fibrillation (AF) limits the use of the most common ECG-derived markers of repolarization heterogeneity, including TWA, under this clinical condition. A new method for assessing ventricular repolarization changes based on a selective averaging technique was developed and new non-invasive indices of repolarization variation were proposed. The positive impact in the prognostic value of the computed indices was demonstrated in a clinical study, by analyzing ECG Holter recordings from CHF patients with AF. To the best of our knowledge, this is the first study that attempts a non-invasive SCD stratification of patients under AF rhythm by assessing ventricular repolarization instability from the ECG signal.

To conclude, the research presented in this thesis sheds some light in the identification of pro-arrhythmic factors, which plays an important role in adopting efficient therapeutic strategies. In particular, the optimal configuration for real-time monitoring of repolarization alternans from intracardiac EGMs, together with the prognostic value of the proposed non-invasive indices of alternans activity and ventricular instability variations in case of AF rhythms demonstrated in two clinical studies, would increase the effectiveness of (ICD) therapy. Finally, the analysis of ECG signals recorded during HDBR experiments in structurally healthy hearts, also provides interesting information on cardiovascular alterations produced in immobilized or bedridden patients.

Keywords: Electrocardiogram; Intracardiac Electrogram; Ventricular Repolarization; Cardiac Electrical Instability; T-wave alternans; Sudden Cardiac Death; Risk Prediction; Advance Signal Processing; Implantable Cardioverter Defibrillator; Chronic Heart Failure; Atrial Fibrillation; Ischemia; Microgravity; Head-Down Bed-Rest.

Resumen y conclusiones

Las enfermedades cardiovasculares representan la principal causa de mortalidad en el mundo. Estas condiciones patológicas normalmente se caracterizan por presentar una estructura anormal del músculo cardiaco, esto es, un substrato vulnerable propenso a la generación y/o propagación anormal del impulso eléctrico, que resulta ser un factor determinante en el inicio de arritmias ventriculares. En este contexto, se ha demostrado que el estudio de la repolarización ventricular en la señal electrocardiográfica (ECG), reflejada en la onda T, puede proporcionar valiosa información para la estratificación de riesgo en pacientes, y varios índices electrocardiográficos han sido propuestos en la literatura.

El principal objetivo de esta tesis es proponer avances metodológicos para evaluar la inestabilidad de la repolarización ventricular en diferentes condiciones anormales y patológicas. Estas contribuciones están principalmente dirigidas a mejorar la predicción de arritmias ventriculares y, consecuentemente, identificar mejor el riesgo de padecer muerte súbita cardiaca (MSC). En particular, se han desarrollado métodos robustos para evaluar las alternancias de onda T (AOT) y la inestabilidad en la repolarización ventricular, en señales cardiacas invasivas y no invasivas. Estos métodos han sido evaluados en condiciones clínicas y experimentales.

En la primera parte de la tesis, se ha caracterizado el fenómeno de las AOT (prevalencia, magnitud, evolución temporal y forma de onda de la alternancia) simultáneamente en la señal ECG de superficie y en electrogramas (EGM) intracavitarios durante una oclusión coronaria. Tanto las señales de ECG de superficie como las señales intracavitarias, registradas en 4 localizaciones anatómicas diferentes (seno coronario, epicardio y los ventrículos izquierdo y derecho) se han analizado usando una estrategia multiderivacional. Las derivaciones disponibles se combinan linearmente usando el análisis de las componentes periódicas (πCA), que maximiza las

componentes de periodo 2 latidos presentes en las diferentes derivaciones. Tras ello, se aplica el método del cociente de verosimilitudes para ruido laplaciano (LLRM, de las siglas en inglés) para la detección y estimación de las AOT. Con un estudio de sensibilidad para la detección de la AOT desde las 5 regiones diferentes se ha demostrado que es el grupo de derivaciones del ECG de superficie el que mayor sensibilidad presenta. Además, esta estrategia multiderivacional ha permitido encontrar la combinación óptima de derivaciones intracavitarias de cara a la monitorización *in-vivo* de las AOT, directamente desde un dispositivo implantable, con una sensibilidad comparable a la obtenida con el ECG. Estos resultados animan a continuar el estudio de la posibilidad de predecir episodios inminenetes de taquicardia o fibrilación ventricular a través del análisis de AOT directamente implementado en la tecnología de un desfibrilador automático implantable (DAI).

Tras ello, hemos estudiado los potenciales cambios inducidos por un periodo prolongado de exposición a microgravedad simulada en sujetos sanos. Se sabe que esta condición ambiental afecta al control de los sistemas autonómico y cardiovascular, produciendo un potencial aumento de la inestabilidad eléctrica cardiaca. En concreto, se han estudiado los efectos sobre la AOT de la exposición a la microgravedad simulada usando el modelo *head-down bed-rest* (HDBR) en campañas de corta, media y larga duración (5, 21 y 60 días, respectivamente). Se han calculado las AOT antes (PRE), durante y después (POST) del periodo de inmobilización usando la técnica de promediado a largo plazo en registros ECG ambulatorios. Además, se ha propuesto una versión adaptada al análisis de registros no estacionarios de corta duración obtenidos durante dos maniobras de estrés (tilt-test y prueba de esfuerzo). Ambas estrategias están basadas en el análisis multiderivacional usado en el estudio anterior. La ausencia de cambios significativos entre PRE y POST-HDBR en los índices de AOT sugieren que 60 días de exposición a microgravedad simulada no es tiempo suficiente para inducir alteraciones en miocardios estructuralmente sanos, hasta el punto de reflejar inestabilidad eléctrica en términos de AOT.

Finalmente, se han propuesto avances metodológicos para determinar inestabilidades en la repolarización ventricular en el ECG en presencia de perturbaciones de ritmo esporádicas (contracciones ventriculares prematuras, CVP) o sostenidas (fibrilación auricular, FA).

Por un lado, se ha propuesto una mejora metodológica para la estimación de la amplitud de la AOT en registros ambulatorios, que tiene en cuenta la posible inversión de fase en la secuencia alternante inducida por la presencia

de CVPs. El algortítmo ha sido evaluado en primer lugar usando señales sintéticas. Tras ello, se ha evaluado también su efecto en el valor pronóstico de la amplitud de AOT en ECG ambulatorios de pacientes con insuficiencia cardiaca (IC). Finalmente, se han estudiado los cambios circadianos en las AOT, así como el valor pronóstico en diferentes intervalos del día. Mediante un estudio clínico se ha demostrado la mejora del valor predictivo del índice de alternancia promedio (IAA, de las siglas en inglés). Además, los resultados obtenidos del análisis circadiano sugieren que la actividad alternante está modulada por este patrón, manteniendo su valor pronóstico en las horas matinales, que se corresponden con el intervalo del día con mayor incidencia de MSC. Así pues, el periodo del día parece ser otro factor importante a la hora de determinar el riesgo de MSC.

Por otro lado, la irregularidad de la respuesta ventricular en pacientes con FA limita el uso de los índices electrocardiográficos más comunes, entre ellos las AOT, en registros con esta condición. Se ha desarrollado un nuevo método para cuantificar cambios en la repolarización ventricular basado el la técnica de promediado selectivo y se han propuesto varios índices de variación de la repolarización. El valor pronóstico de estos índices se ha demostrado en un estudio clínico, analizando registros ECG ambulatorios de pacientes con IC en FA. Hasta donde podemos saber, éste es el primer estudio que ha propuesto un método para cuantificar inestabilidades en la repolarización ventricular desde el ECG adecuado a pacientes en ritmo de FA.

En conclusión, el trabajo de investigación presentado en esta tesis arroja luz en la identificación de factores pro-arrítmicos, lo cual resulta crucial en la adopción terapias eficientes. En particular, la configuración óptima de derivaciones para monitorizar AOT en señales intracavitarias, junto con el valor pronóstico de los índices propuestos demostrado en dos estudios clínicos, pueden ayudar a mejorar la eficiencia de los DAIs. Finalmente, el análisis de señales ECG registradas durante experimentos de microgravedad simulada puede aportar información útil de alteraciones en el sistema cardiovascular a tener en cuenta en pacientes inmobilizados o encamados durante largos periodos.

Palabras clave: Electrocardiograma; electrograma intracavitario; repolarización ventricular; inestabilidad eléctrica cardiaca; alternancias de onda T; muerte súbita cardiaca; predicción de riesgo; procesado de señal avanzado; desfibrilador automático implantable; insuficiencia cardiaca; fibrilación auricular; isquemia; microgravedad; Head-Down Bed-Rest.

Riassunto e conclusioni

Le malattie cardiovascolari (MCD) sono la principale causa di morte al mondo. Queste condizioni patologiche sono normalmente caratterizzate da difetti cardiaci a livello strutturale, e rendono perciò il cuore una struttura vulnerabile, incline alla generazione e/o propagazione anomala di impulsi elettrici che determinano l'instaurarsi di aritmie ventricolari. In questo contesto, è stato mostrato come la misura della ripolarizzazione ventricolare a partire dall'elettrocardiogramma (ECG), possibile tramite l'onda T, fornisca informazioni importanti per una stratificazione del rischio, per la quale sono stati proposti diversi indici elettrocardiografici.

L'obiettivo principale di questa tesi è il proporre sviluppi metodologici per la valutazione della ripolarizzazione ventricolare in condizioni patologiche e non fisiologiche. I contributi qui presentati sono volti al miglioramento della predizione delle aritmie ventricolari e, di conseguenza, a migliorare la diagnosi di rischio di arresto cardiaco improvviso. In particolare, il nostro approccio ha previsto lo sviluppo di metodi robusti per la valutazione dell'alternanza dell'onda T (TWA) e dell'instabilità della ripolarizzazione ventricolare, usando segnali cardiaci invasivi e non, e validando i metodi in condizioni sperimentali e cliniche.

Nella prima parte della tesi, la TWA è stata caratterizzata (prevalenza, ampiezza, andamento e forma d'onda) usando ECG di superficie ed elettrogrammi (EGM) intracardiaci acquisiti in simultanea durante occlusione dell'arteria coronarica. I segnali provenienti dall'ECG di superficie e dall'EGM acquisito in 4 differenti posizioni (seno coronarico, interstizio epicardiale ed entrambi i ventricoli) sono stati analizzati seguendo una strategia *multilead*. Le derivazioni sono state combinate linearmente usando l'analisi di componenti periodiche (πCA), che massimizza il contenuto periodico del segnale compreso tra 2 battiti (periodicità della TWA) sulle derivazioni disponibili. Quindi, un metodo basato sul Rapporto di Verosimiglianza Lapla-

ciano (ad esempio LLRM) è stato applicato per la detenzione e la stima della TWA. Uno studio di sensitività per la detezione della TWA dalle 5 registrazioni disponibili ha mostrato che le prestazioni migliori si sono riscontrate combinando le derivazioni ECG. Inoltre, questo approccio multilead ha permesso di identificare la combinazione ottima di derivazioni intracardiache per il monitoraggio della TWA in-vivo tramite un dispositivo impiantabile, con una sensitività paragonabile a quella data dall'ECG. Questi risultati incoraggiano lo studio della fattibilità di predire episodi di VT/VF tramite l'analisi della TWA implementato all'interno di un ICD.

In seguito, ci si è dedicati alla valutazione delle potenziali variazioni indotte da un'esposizione prolungata a microgravità simulata sulla ripolarizzazione ventricolare in strutture cardiache strutturalmente sane. È noto che queste condizioni ambientali hanno ripercussioni sul controllo dei sistemi autonomico e cardiovascolare, con un potenziale aumento di instabilità elettrica cardiaca a livello della ripolarizzazione ventricolare. Gli effetti di un'esposizione breve (5 giorni), media (21 giorni) e prolungata (60 giorni) a microgravità simulata sulla TWA sono stati misurati usando il modello chiamato *head-down bed-rest* (HBDR). La TWA è stata valutata prima (PRE), durante e dopo (POST) il periodo di immobilità, usando la media sul lungo periodo su registrazioni di ECG ambulatoriali. In aggiunta, si è proposto un approccio di calcolo degli indici della TWA sul breve periodo modificato, per l'applicazione su registrazioni ECG non stazionarie e più brevi, acquisite durante due manovre sperimentali che inducono una condizione di stress (head-up tilt-test e test di sforzo). Entrambi gli approcci proposti sono basati sullanalisi multilead utilizzata nello studio precedente. L'assenza di variazioni significative tra PRE e POST-HBDR negli indici di TWA, seppur in presenza di trend in direzione di un aumento del rischio, suggerisce che l'esposizione prolungata a microgravità simulata non basta ad introdurre in un miocardio sano alterazioni tali da portare ad instabilità elettrica rilevabile dall'ECG tramite la misura della TWA.

Infine, sono stati proposti sviluppi metodologici per la valutazione dell'instabilità della ripolarizzazione ventricolare misurata sul segnale ECG in presenza di disturbi sporadici del ritmo (contrazioni ventricolari premature, CVP) e sostenuti (fibrillazione atriale, FA).

Da una parte, si è presentato un miglioramento nel metodo per la stima dell'ampiezza della TWA in registrazioni ECG ambulatoriali, che tiene in conto della possibile inversione di fase nella sequenza dell'alternanza dovuta alla presenza di CVP. Le prestazioni dell'algoritmo sono state valutate dap-

prima tramite simulazioni. In seguito, il contributo del metodo proposto al valore prognostico dell'ampiezza della TWA è stato valutato usando ECG reali di pazienti con scompenso cardiaco. Infine, le variazioni circadiane di TWA sono state valutate insieme al valore prognostico della TWA a differenti ore della giornata. Uno studio clinico ha dimostrato un miglior valore predittivo dell'indice di alternanza medio (IAA) per la stratificazione di rischio soffrire arresto cardiaco.

Allo stesso tempo, l'elevata irregolarità della risposta ventricolare durante FA limita l'uso dei marker più comuni di eterogeneità della ripolarizzazione derivanti dall'ECG, inclusa la TWA, in presenza di questa patologia. È stato quindi proposto un nuovo metodo, basato su una tecnica di media selettiva, per la valutazione delle variazioni di ripolarizzazione ventricolare, e sono stati introdotti nuovi indici di variazione della ripolarizzazione non invasivi. Uno studio clinico ha misurato il contributo positivo al valore prognostico fornito da tali indici, analizzando registrazioni ECG Holter da pazienti con scompenso cardiaco che presentavano FA. Per quanto ci risulta, questo è stato il primo tentativo di stratificazione non-invasiva di pazienti con arresto cardiaco durante FA, sfruttando la misura di instabilità di ripolarizzazione ventricolare dal segnale ECG.

In conclusione, il lavoro qui presentato contribuisce ad una migliore identificazione di fattori che predispongono ad aritmie, fondamentale per l'adozione di strategie terapeutiche efficaci. In particolare, la configurazione ottimale per il monitoraggio in tempo reale dell'alternanza di ripolarizzazione da segnali EGM intracardiaci, insieme al valore prognostico degli indici di alternanza ed instabilità ventricolare non-invasivi durante fibrillazione atriale, dimostrato in due studi clinici, può contribuire all'efficacia della terapia ICD. Infine, anche l'analisi di segnali ECG registrati durante esperimenti HDBR in soggetti sani fornisce informazioni sul sistema cardiovascolare di cui tener conto in caso di pazienti immobilizzati o costretti a letto per lunghi periodi.

Parole chiave: Elettrocardiogramma; Elettrogramma Intracardiaco; Ripolarizzazione Ventricolare; Instabilità Elettrica; Alternanza dell'onda T; Arresto Cardiaco improvviso; Predizione di Rischio; Elaborazione di Segnali; Defibrillatore Impiantabile; Scompenso Cardiaco; Fibrillazione Atriale; Ischemia; Microgravità; Head-Down Bed-Rest.

Acknowledgments

I would like to thank my supervisors, Juan Pablo Martínez and Enrico Caiani, for all their constant support, availability, patience and the contagious enthusiasm that I have received along all these years. It has been a pleasure to have them as supervisors.

I would also like to extend my thankfulness to Pablo Laguna, for his continuous help, infinite ideas and fruitful discussions that have contributed to the realization of this thesis.

Many thanks to all members of BSICoS group (Universidad de Zaragoza) and the B3-Lab (Politecnico di Milano), because all of you have contributed to this work in one way or another.

Of course, this work would have never finished without the unconditional support from my family and friends.

Thank you all.

Contents

List of Figures

List of Tables

List of Acronyms

AP	Action potential
APD	Action potential duration
APDR	Action potential duration restitution
AHF	Acute heart failure
ANR	Alternans-to-noise ratio
ACEI	Angiotensin-converting enzyme inhibitor
AF	Atrial fibrillation
AV	Atrioventricular
ANS	Autonomic nervous system
BNP	B-type natriuretic peptide
BDC	Baseline data collection
BAS	Baseline interval
BASE	Baseline recording
CMR	Cardiac magnetic resonance
CRT	Cardiac resynchronization therapy
CVDs	Cardiovascular diseases
CHF	Chronic heart failure
CHD	Coronary heart disease
CS	Coronary sinus
CM	Countermeasure
DLR	Deutsches Zentrum für Luft- und Raumfahrt e.V
ECG	Electrocardiogram
EGM	Electrogram

EPI Epicardial space

ESA European Space Agency

EX1 First 5-min step of cycling (25% workload)

EX2 Second 5-min step of cycling (50% workload)

GLRT Generalized likelihood ratio test

HDBR Head-down bed-rest

HF Heart failure

HR Heart rate

HRV Heart rate variability

ICD Implantable cardioverter defibrillator

IAA Index of average alternans

$IAAn$ Index of average normalized alternans

$IAA^{\mathbf{ST}}$ Index of short-term average alternans

$IAAn^{\mathbf{ST}}$ Index of short-term average normalized alternans

IHD Ischemic heart disease

LLRM Laplacian likelihood ratio method

LBBB Left bundle branch block

LCX Left circumflex artery

LV Left ventricle

LVEF Left ventricular ejection fraction

LONG Long-duration head-down bed-rest

LBNP Lower body negative pressure

MLE Maximum likelihood estimator

MEDES Institut de Médecine et de Physiologie Spatiales

MID Mid-duration head-down bed-rest

MRA Mineralocorticoid receptor antagonist

MMAM Modified moving average method

MUSIC MUerte Súbita en Insuficiencia Cardiaca (database)

MI Myocardial infarction

NYHA New York Heart Association

OCCL Occlusion recording

OT Orthostatic tolerance

OTT Orthostatic tolerance time

PCI Percutaneous coronary intervention

πCA Periodic component analysis

POST Post-HDBR period

PSD Power spectral density

PRE Pre-HDBR period

PCA Principal component analysis

P_{FA} Probability of false alarm

PFD Pump failure death

REC Recovery interval

RPA Repolarization alternans

RVE Resistive vibration exercise

RA Right atrium

RV Right ventricle

RMS Root mean square

SHORT Short-duration head-down bed-rest

SPECT Single photon emission computed tomography

SA Sinoatrial (node)

SR Sinus rhythm

SVG Spatial ventricular gradient

SM Spectral method

SCD Sudden cardiac death

TILT Head-up tilt interval

TWA T-wave alternans

TWAR T-wave alternans rate

VCG Vectorcardiogram

VF Ventricular fibrillation

VPC Ventricular premature contraction

VT Ventricular tachycardia

Chapter 1

Introduction

1.1 Motivation

Cardiovascular diseases (CVDs) remain the leading cause of death worldwide. According to data published in 2015, they are responsible for more than 4 million deaths in Europe (45.5% of all deaths) every year [1], accounting for 17.3 million cases worldwide, a number which is expected to rise up to $>$ 23.6 million by 2030 [2]. Among CVDs, ischemic (or coronary) heart

disease (IHD) and stroke are both the main single causes of cardiovascular-related death [1]. A great part of these deaths occur suddenly, shortly after the appearance of the first symptoms and generally as a consequence of malignant ventricular arrhythmias. This fatal outcome, known as sudden cardiac death (SCD), accounts for over 300,000 deaths per year in Europe, most victims being patients with structural heart disease [3]. In this context, implantable cardioverter defibrillators (ICDs) have been shown to be highly effective at terminating these life-threatening arrhythmias, eventually preventing SCD. However, in addition to the risk induced by the invasive procedure, the cost-effectiveness of this therapy is still low, and identifying patients who would benefit the most from device implantation remains a clinical problem.

These figures justify every effort in improving diagnosis, prevention, treatment and risk stratification of CVDs. Actually, this represents one of the major challenges that the European healthcare systems are facing nowadays, due to their social and economic costs.

Several non-invasive indices have been proposed for the assessment of the risk of developing ventricular arrhythmias. The left ventricular ejection fraction, obtained by echocardiographic analysis, is the most widely used in the clinical practice. In addition, the predictive value of some electrocardiographic indices, mainly based on the analysis of ventricular repolarizarion, such as QT interval/dispersion, has been proved [4], but it is still limited by their low specificity rates. T-wave alternans (TWA) has been postulated as one of the most promising non-invasive markers of electrical instability and ventricular vulnerability [5]. Its prognostic value has been widely assessed under different pathologies and, in the recent years, the analysis of TWA in ambulatory ECG recordings is yielding promising results. In this thesis, methodological advances are proposed to improve risk stratification based on ventricular repolarization indices, mainly TWA, which are robust to sporadic and sustained rhythm disturbances. Their clinical value was then assessed in both experimental and clinical databases.

1.2 The Heart

The *heart* is a muscular organ about the size of a fist, whose main function is to pump blood into the circulatory system. Its anatomy is actually divided into two separate, “mirrored” pumps, left and right, which supply the

systemic (or peripheral) and the *pulmonary* circulatory systems, respectively. Each of these pumps consists of two chambers: the *atrium* and the *ventricle*. The atria act as receiving chambers and help to move the blood into the ventricle. The ventricles supply the main pumping force to eject the blood either to the pulmonary circulation (right ventricle, RV) or throughout the systemic or peripheral circulation (left ventricle, LV) each cycle. Both pumps are separated by a muscular wall, called the *septum*, and direction of blood is controlled by two atrio-ventricular valves (*tricuspid* and *mitral* valves for right and left chambers, respectively) and the *pulmonary* and *aortic* valves, located between the ventricles and the arteries [6]. See Figure 1.1 for illustration.

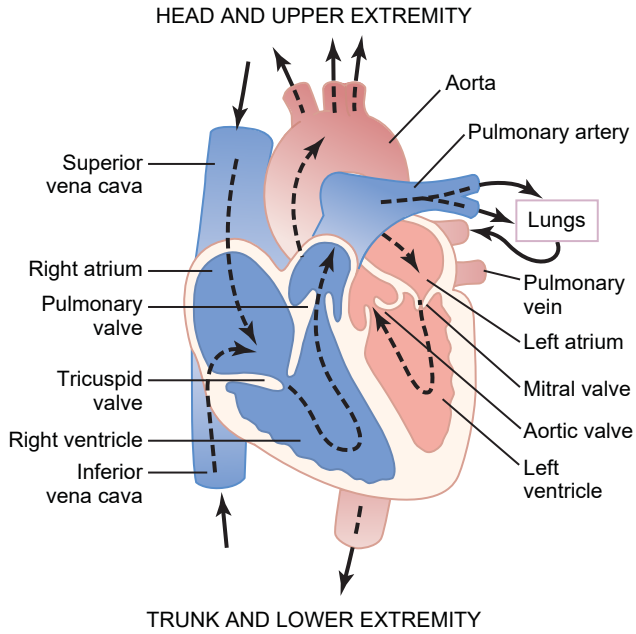

Figure 1.1: Structure of the heart, and course of blood through the heart chambers and heart valves. (Reproduced from [6]).

The wall of the cardiac muscle, called the *myocardium*, is composed by specialized muscle cells (*myocytes*) which are responsible of the rapid propagation of the electrical impulse throughout the conduction system and trigger the mechanical force during heart contraction, defining the cardiac cycle (heart beat). Each cardiac cycle starts with the spontaneous generation of an *action potential* (AP) in the *sinoatrial* (SA) node, located in the right atrium (RA), which is then propagated through to the ventricles.

This allows atrial contraction and, as a consequence, blood is pumped into the ventricles. Then, the stronger ventricular contraction ejects the blood into the body. This period is called *systole*. It is followed by a period of relaxation called *diastole*, during which the heart fills with blood until the next atrial systole [6].

1.2.1 Cardiac Electrophysiology

The heart is characterized by a specialized excitatory and conductive system, able to generate electrical impulses that induce cardiac contraction, and to propagate them cell to cell in a rapid and organized way throughout the heart (*depolarization* phase). Following depolarization, cardiac muscle returns to a resting state (*repolarization* phase) [6]. The transmembrane potential of each myocyte experimented changes during this cycle, which is called the *action potential*. Electrical activity of the heart can be characterized both from measurements at the cellular level, which are fundamental for a deeper understanding of the mechanisms behind cardiac disorders, and from measurements at the body surface (*electrocardiography*), reflecting the total extracellular activity of cardiac currents generated by potential changes across cardiac cells [7].

Cellular Electrical Activity

The AP of each cardiac cell is the result of ion charges moving in and out of the cell through ion channels. Under resting conditions, the inside of the cell has a more negative voltage than the outside, creating a negative transmembrane potential, defined as $V_m = V_{in} - V_{out}$. During depolarization, the transmembrane potential raises over this resting potential (from -90 to 20 mV) due to a rapid influx of sodium ions across the myocyte membrane. During repolarization, the membrane potential of the cell gradually returns to its resting value due to the opening of potassium channels [7]. The AP of a ventricular myocyte has five different phases (numbered 0-4) as illustrated in Figure 1.2:

Phase 4: The cell is at rest during diastole, and the transmembrane potential remains constant between -85 to -95 mV.

Phase 0: The opening of fast sodium (Na^+) channels entails an initial rapid upstroke that corresponds to the depolarization phase.

Fast sodium channels open and this originates a rapid influx of Na^+ ions into the cell. The activation of Na^+ channels triggers the AP and it is closely related to cardiac excitability.

Phase 1: The inactivation of fast Na^+ channels yields to an early and brief repolarization. Together with a net transient outward potassium (K^+) current, they are the responsible of the small downward deflection present in the AP (spike-and-dome morphology).

Phase 2: The influx of calcium (Ca^{2+}) through the L-type calcium channels compensates the repolarizing potassium currents, delaying repolarization and creating a slow-decaying plateau. This plateau prolongs the *AP duration* (APD).

Phase 3: The L-type calcium channels (I_{CaL}) start closing while potassium currents are open, leading the cell to its resting state (repolarization) [8].

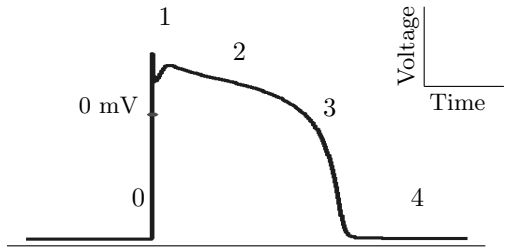

Figure 1.2: Action potential of a ventricular myocyte and its phases. (Reproduced from [8]).

Adjacent cardiac cells are connected by low-resistance gap junctions. When one cell depolarizes, depolarizing currents can pass through these junctions and depolarize adjacent cells. This process results in wavefront propagation of APs throughout the whole myocardium.

Electrical Activity of the Normal Heart

Cardiac contractions are controlled by the excitatory and conductive system of the heart. In the normal heart, a rhythmical impulse is generated in the

SA node, a mass of self-excitable cells located in the superior post-lateral wall of the RA, near the entry of the superior vena cava. The electrical impulse spreads throughout the atrial pathways to the *atrioventricular* (AV) node, where it suffers a delay that allows the atrial contraction to further increase the blood volume in the ventricles before the ventricular systole takes place. The impulse then passes the *bundle of His*, which lies in the *interventricular septum* and divides into right and left bundle branches, finally reaching the *Purkinje system* (Figure 1.3). The Purkinje system is a network of specialized conduction fibers which rapidly propagate the impulse to the inner layer of the cardiac muscle (*endocardium*), which is then propagated cell-to-cell towards the outer surface of the heart (*epicardium*) and back to the atrioventricular groove, in order to achieve a unified contraction within the ventricles [7].

However, ventricular repolarization is not an homogeneous process, consequence of a inhomogeneous distribution of ionic dynamics and different repolarization times. This originates spatial dispersion of repolarization among different regions of the myocardium (i.e., between base and apex, anterior and posterior side of the ventricles), between the two ventricles and even transmurally, (among endocardial, midmyocardial and epicardial cells), which has been widely documented [9]. While normal ranges of dispersion allow for an efficient contraction of the heart, an accentuated repolarization dispersion is associated to the risk of life-threatening arrhythmias [10–12].

Some cardiac cells have the intrinsic property of *automaticity* (i.e. they can generate an AP in the absence of external stimuli). The natural pacemaker of the normal heart is the SA node, as its cells are those with higher discharge rate. This natural rhythm, driven by the SA node, is known as the *sinus rhythm* (SR) [6]. The intrinsic *heart rate* (HR) of the SA node is about 100-120 beats/min in absence of the *autonomic nervous system* (ANS) influence [13]. The heart, however, is supplied with both the *sympathetic* and *parasympathetic* branches of the ANS, which regulate cardiovascular functions, including HR. Each of the branches is dominant under certain conditions: the sympathetic nervous system acts in an alarm situation and during exercise ("fight-or-flight" reaction), increasing HR and myocardial contractility; the parasympathetic nervous system, on the other hand, is the responsible of the so called "rest and digest" state predominant during resting conditions, decreasing HR and regulating respiration, among others.

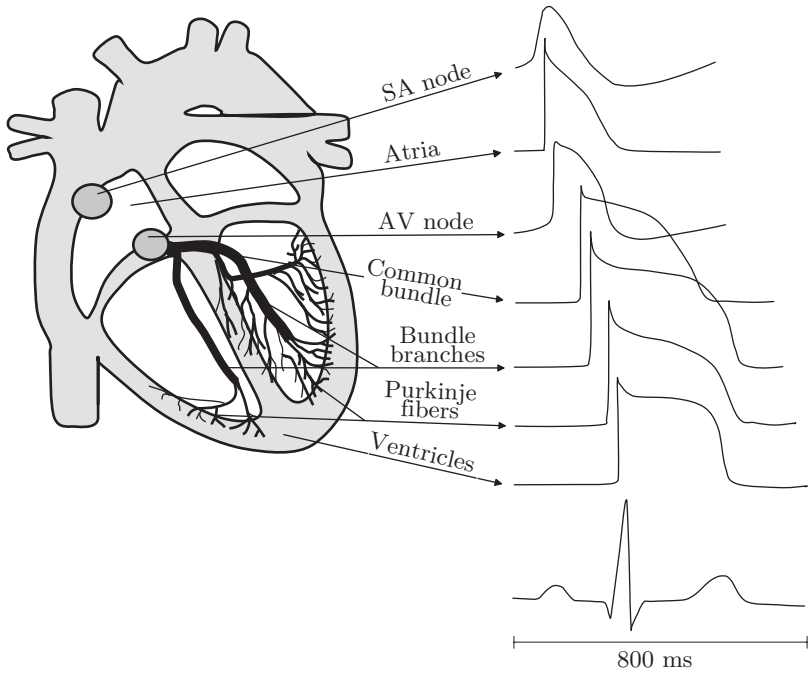

Figure 1.3: Specialized excitatory and conductive system of the heart. Morphology and timing of the action potentials from different regions of the heart and the related cardiac cycle of the electrocardiogram as measured on the body surface (Reproduced from [7]).

Occasionally, some parts of the myocardium can develop a more rapid discharge rate than that of the SA node in depolarization, taking the control of the cardiac beat generation. In this cases, the pacemaker, denominated *ectopic focus*, is somewhere else than the SA node and originates an abnormal sequence of muscle contraction that can cause an inefficient pumping of the heart [6].

1.3 Recording techniques

1.3.1 The Electrocardiogram Signal

The electrocardiographic signal or *electrocardiogram* (ECG) signal describes the electrical activity of the heart measured on the body surface, using electrodes that are placed on the skin. This activity is the resultant of the electrical activity of all cardiac cells at a given time, as observed in the body surface. The timing relationship between the different APs occurring at different regions of the heart and the resulting ECG recorded from an exploring electrode positioned on the chest is illustrated in Figure 1.3. For ECG acquisition, electrodes need to be positioned so that the spatio-temporal variations of electrical activity are sufficiently well-reflected.

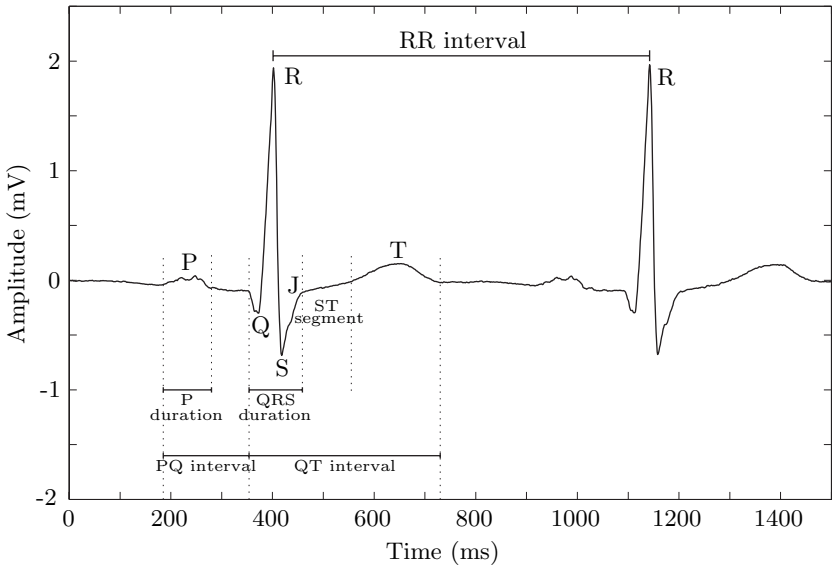

Figure 1.4: An ECG of two cardiac cycles with definition of main waves and most relevant time intervals (Reproduced from [7]).

Each cardiac cycle is reflected in the ECG as a sequence of positive and negative deflections or waves whose timing and morphology provide useful diagnostic information when disturbances in the electrical activity of the heart are manifested on it. These waves, associated to cardiac depolarization and repolarization, appear as a deviation from the baseline level or the *isoelectric line* of the ECG, which represents the resting state of all cardiac cells. The polarity and morphology of each individual wave depend on the position of the recording electrode. A depolarizing wavefront moving towards the electrode originates a positive deflection on the ECG, while a current moving away from the electrode originates a negative deflection. The opposite behaviour is observed during repolarization, since repolarization have an opposite polarity: a wavefront moving towards the electrode originates a negative deflection below the isoelectric wave whereas a positive deflection is generated if this wavefront moves away from the electrode. Depolarization waves in the ECG are generally steeper and peakier than those related to repolarization, which are smoother. Also the larger muscle mass of the ventricles originates much larger ventricular depolarization waves in comparison to atrial ones [7].

The amplitude and duration of the waves are defined considering as a reference level the isoelectric line of the ECG. The first positive deflection above the baseline level, with an amplitude normally lower than 300 μV and a duration shorter than 120 ms, is denoted as the *P wave* and reflects the initial atrial depolarization. Then, depolarization of right and left ventricles is reflected by the succession of a series of deflections (typically one to three), referred together as the *QRS complex*. In a typical beat from a healthy adult heart, the QRS lasts for about 70-110 ms and reaches an amplitude of about 1-2 mV. Atrial repolarization, which occurs simultaneously to ventricular depolarization cannot be discerned in the ECG as it is masked by the much higher amplitude of the QRS complex. There is a period during which ventricles remain in an active, depolarized state manifested as a nearly horizontal line between the end of the S wave (*J point*) and the onset of ventricular repolarization, denoted as the *ST segment*. Finally, the positive deflection originated in the ECG during ventricular repolarization is referred as the *T wave*, which is considerable longer (lasts for about 300 ms) and smoother than the QRS complex, as a consequence of the relatively slower repolarization phase of the myocardium in comparison to cardiac depolarization [7]. Figure 1.4 illustrates the typical waves and the most significant time intervals in a normal ECG during sinus rhythm.

1.3.2 The Lead System

Each ECG lead represents a different electrical axis onto which the electrical activity of the heart is projected. Therefore, each lead can be considered to represent a different spatial perspective of the heart's electrical activity. The ECG signal is typically recorded with a multiple lead configuration which includes unipolar or bipolar leads, or both. A so-called *unipolar* lead reflects the voltage variation of a single electrode and is measured in relation to a reference (commonly called the central terminal) whose voltage remains almost constant throughout the cardiac cycle. A *bipolar* lead reflects the voltage difference between two electrodes.

In the clinical practice, a number of lead configurations are used with standardized electrode positions, including the standard 12-lead ECG and the 3-lead orthogonal configuration. If these leads are appropriately placed, the ensemble of the different waveforms provides a robust understanding of the electrical activity throughout the heart, allowing the clinician to determine a number of pathologies through spatial correlation of events on specific leads. Actually, the choice of a particular lead system is guided by the type of clinical information desired and other practical considerations. For example, a few electrodes are usually used when only heart rhythm information is required, while ten electrodes (12-lead configuration) is preferred when wave's morphology needs to be analyzed [7]. Also depending on the purpose of the exploration, there are several specialised types of ECG. Some of them are: the resting ECG, the exercise stress test, the Holter ambulatory monitoring, the high-resolution ECG, the intensive care unit (ICU) monitoring and polysomnographic recordings, among others.

The Standard 12-lead ECG

The standard 12-lead ECG is the most extensively used setup in clinical routine, recorded using 10 electrodes positioned on the body surface. Based on the plane in which electrical activity is recorded, the 12 leads are divided in two groups of six: the six *frontal* leads (Figure 1.5, left) and the six *chest* lead, also referred as *precordial* leads (Figure 1.5, right).

The frontal leads can be sub-divided into two further configurations: the three *bipolar limb* leads and the *augmented unipolar limb* leads. The three bipolar limb leads, denoted as I, II and III, are obtained by measuring the

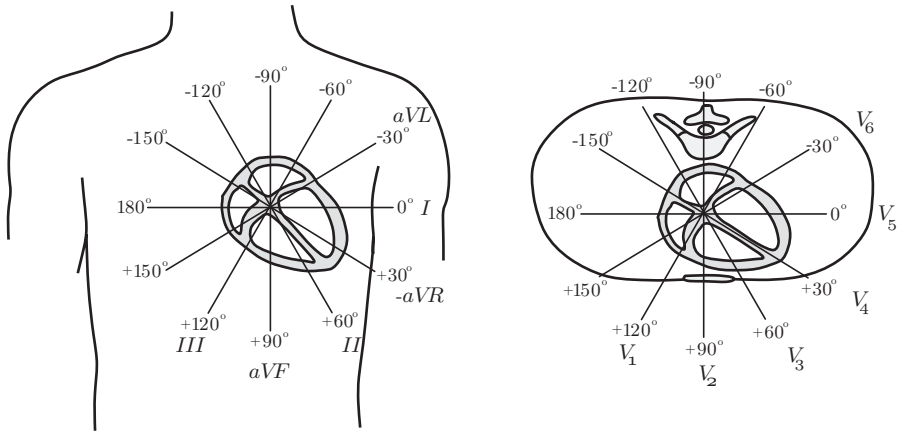

Figure 1.5: The direction of the six limb leads in the frontal plane (left) and the six precordial leads in the horizontal plane (Reproduced from [7]).

voltage difference between the left arm (V_{LA}), right arm (V_{RA}), and left leg (V_{LL}), according to the following combinations:

$$\mathrm{I} = V_{LA} - V_{RA} \tag{1.1}$$

$$\mathrm{II} = V_{LL} - V_{RA} \tag{1.2}$$

$$\mathrm{III} = V_{LL} - V_{LA} \tag{1.3}$$

The three electrode positions describe the equiangular "Einthoven's triangle" with the heart positioned at its center: Lead I looks directly to the heart from left hand, while lead II looks at the heart +60° clockwise from lead I and lead III, further +60° clockwise from lead II.

The augmented unipolar leads are denoted as aVF, aVL and aVR, and describe the directions which are shifted 30° from those of the bipolar leads using the same electrode configuration (Figure 1.5, left). They are defined as the voltage differences between one corner of the triangle and the average of the remaining two:

$$\mathrm{aVR} = V_{RA} - \frac{V_{LA} + V_{LL}}{2} \tag{1.4}$$

$$\mathrm{aVL} = V_{LA} - \frac{V_{RA} + V_{LL}}{2} \tag{1.5}$$

$$\mathrm{aVF} = V_{LL} - \frac{V_{LA} + V_{RA}}{2} \tag{1.6}$$

The six precordial leads, labeled from V1 to V6, are unipolar leads positioned on the front and the left side of the chest, and related to a central terminal ("Wilson central terminal") which is defined as the average of the voltages measured on the right and left arms and the left leg. Leads V1 and V2, positioned in the 4th intercostal space to the right and left of the sternum respectively, face the surface of the right ventricle. They are followed by the V3 to V6 leads positioned at equally spaciated intervals, the later positioned at the 5^{th} left intercostal space in the mid-axillary line: V3 and V4 face the anterior wall of the left ventricle, while V5 and V6 face the lateral wall of the left ventricle [7].

Orthogonal Leads

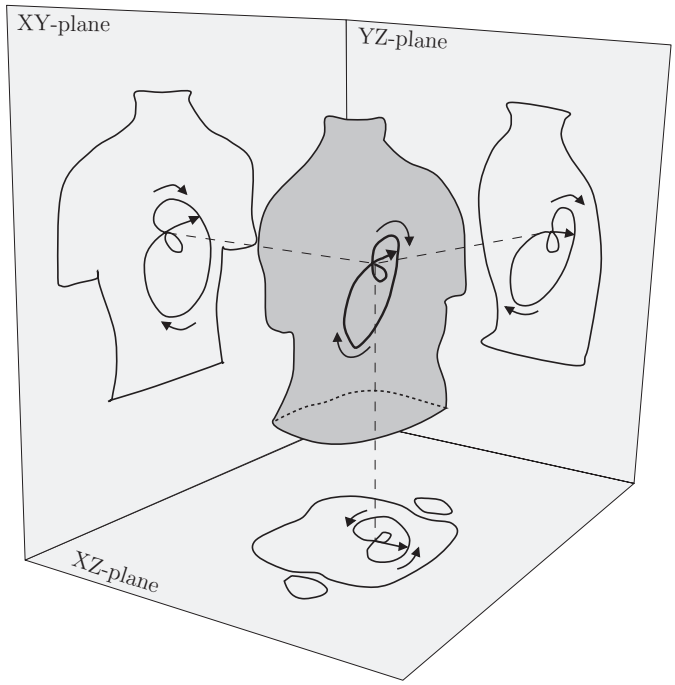

Figure 1.6: A vectorcardiographic loop and its projection onto the three orthogonal planes. The two arrows outside each loop indicate the direction in which the loop evolves (Reproduced from [7]).

The orthogonal lead system reflects the electrical activity of the heart in the right-left axis (lead X), the head-to-feet axis (lead Y) and the front-back axis (lead Z). This system, in addition to the ECG information acquired

from each individual lead, provides with additional information through the visualization of a three-dimensional loop together with the projection onto the $XY-$, $XZ-$ and $YZ-$ planes (Figure 1.6). Since a loop is traced out by the tip of the vector that describes the dominant direction of the electrical wavefront during the cardiac cycle, this recording is referred to as a *vectorcardiogram* (VCG) [7].

The most widely used orthogonal lead system, known as the Frank lead system after its inventor [14], is obtained as linear combinations of seven electrodes positioned on the chest, back, neck, and left foot. The resulting leads X, Y and Z view the heart from the left side, from below, and from the front.

1.3.3 The Intracardiac Electrogram Signal

The *intracardiac electrogram* (EGM) signal represents the local electrical activity of the heart recorded by multi-electrode catheters, directly in contact with the heart tissue. This kind of signals provide with more detailed information about wavefronts propagation, including the identification of the local *activation time* (time resolution), the *direction* and origin of the propagation and the localization of the discrete area of excited tissue that generates the recorded potentials (spatial resolution) [15].

Unipolar EGMs (Figure 1.7, left) represent the potential difference between the electrode in contact with the heart (the exploring electrode) and a reference distant electrode (the indifferent electrode, generally located on the patient's surface). When the wavefront moves towards the exploring electrode, it will result in a positive deflection on the EGM signal. On the contrary, when the wavefront moves away from the electrode, it will result in a negative deflection. The amplitude of the unipolar EGM decreases as the distance between the wavefront and the sensing electrode increases. It contains not only local information, characterized by a higher frequency content, but also far-field activity, less sharp but of higher amplitude [15].

Bipolar EGMs (Figure 1.7, right) are obtained as the difference between two close exploring electrodes (using the same reference). The amplitude of the bipolar EGM decreases even more rapidly with increasing distance than the unipolar amplitude and the spatial resolution increases as the distance between the two electrodes decreases. This kind of EGMs are less sensitive to far-field activity, as it is removed consequence of subtraction, allowing

for a better identification of local information with a higher signal-to-noise ratio. In contrast to unipolar EGMs, directionality of wavefront propagation can no be reliably inferred from signal morphology [15].

Unipolar EGMs recorded by decapolar catheters placed in the epicardial space, right and left ventricles and the coronary sinus will be used in this thesis.

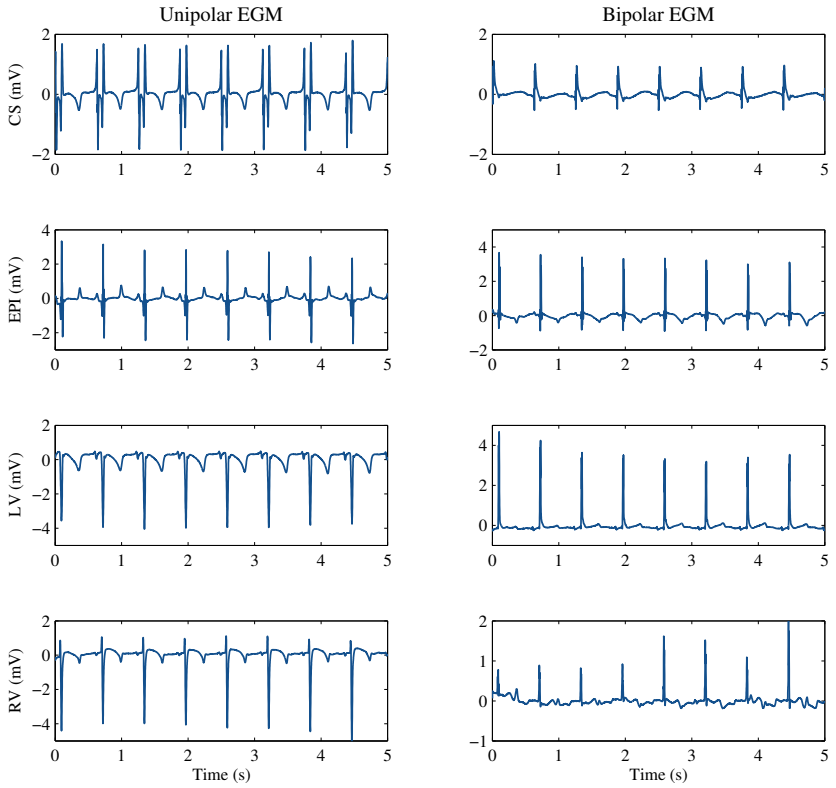

Figure 1.7: Example of unipolar (left) and bipolar (right) intracardiac electrogram signals recorded at four different anatomical locations: coronary sinus (CS), epicardial space (EPI), left and right ventricles (LV and RV).

1.4 Abnormal cardiac conditions and diseases studied in this thesis

1.4.1 Ventricular Arrhythmias and Electrical Disturbances

By definition, *ventricular arrhythmia* is any abnormal rapid heart rhythm that originates in the ventricles [16]. This term includes *ventricular premature contractions* (VPCs), *ventricular tachycardia* (VT) and *ventricular fibrillation* (VF).

Ventricular premature contraction: It is an extra, abnormal heart beat originated by an ectopic cardiac pacemaker located in the ventricle, that makes contract them too soon, out of sequence with the normal beats (Figure 1.8, (b)). The clinical significance of VPCs depends on their frequency, complexity, and hemodynamic response. Isolated VPCs in asymptomatic and healthy patients do not require treatment. Frequent VPCs can be a first sign of the progression towards more serious ventricular arrhythmias, like VT and VF in case of heart disease or a previous history of VT.

Ventricular tachycardia: It is a fast ($\geq$ 120 beats/min), regular beating of the ventricles, no longer controlled by the SA node, that may last for only a few seconds (by definition, at least 3 beats) or for much longer. This rhythm may cause severe shortness of breath, dizziness, or fainting (syncope). A few beats of VT often do not cause problems. However, episodes that last for more than a few seconds can be dangerous, as they can turn into VF.

Ventricular fibrillation: In this rhythm, the heart's electrical activity becomes disordered and ventricles contract in a rapid (sometimes reaches $\geq$ 300 beats/min), unsynchronized way, instead of pumpimg normally (Figure 1.8, (c)). This is the most serious cardiac rhythm disturbance, since the ventricles pump little or no blood, which can lead to SCD within a few minutes if not reverted to sinus rhythm.

Three main mechanisms that determine the onset and sustainability of these life-threatening arrhythmias have been identified. They are: a *vulnerable myocardium*, a *trigger* and external *modulators* [4].

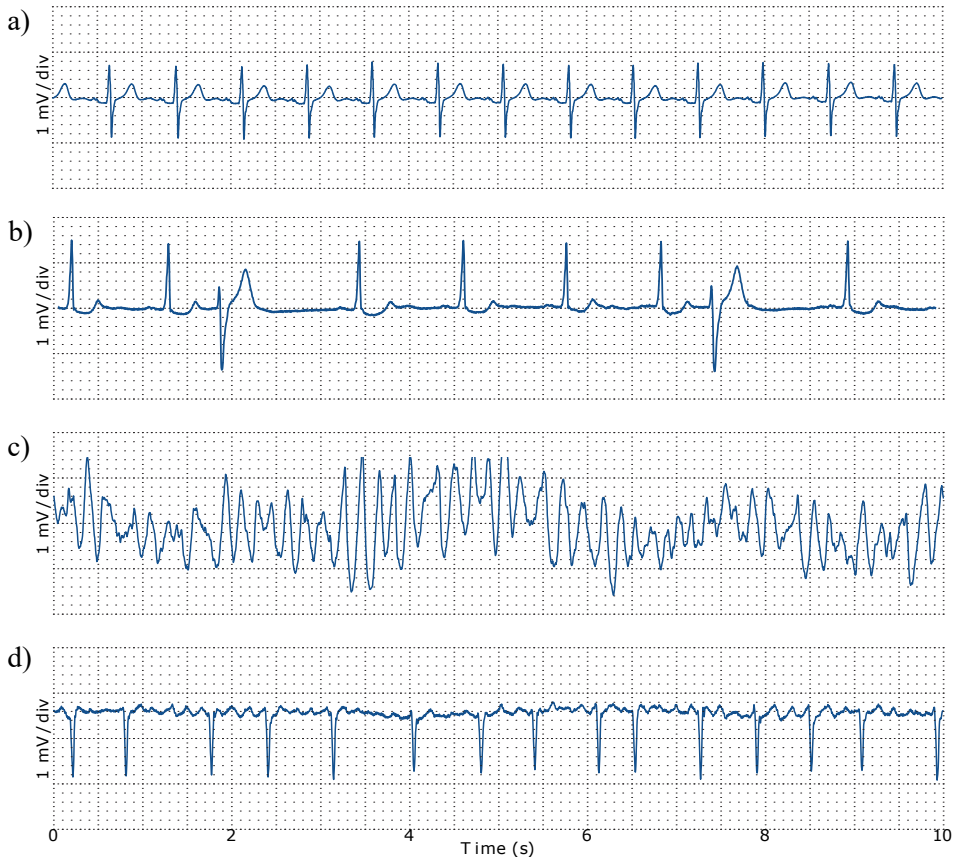

Figure 1.8: Examples of ECGs (a) in normal sinusal rhythm, (b) with a premature ventricular contraction followed by a compensatory pause (c) in ventricular fibrillation and (d) in atrial fibrillation (Reproduced and adapted from [7]).

A vulnerable myocardium is a substrate predisposed to arrhythmogenesis, which means that, when a triggering factor appears, it can easily lead to malignant arrhythmias, potentially ending in SCD. Increased dispersion of repolarization among cardiac cells or regions of the myocardium has been linked to ventricular vulnerability [17, 18]. Under normal conditions, electrical impulses are generated at the SA node, as described in section 1.2. Nevertheless, some ventricular cells have the ability of generating spontaneous APs in absence of any external stimulus (automaticity). Enhanced automaticity of ventricular cells can lead to an ectopic activation and, if it is maintained by the propagation of electrical activity in a circular path returning to the origin (*reentry*), it can degenerate into a sustained ventricular arrhythmia [16]. Finally, external modulators can alter the electrophysiological properties of the heart, and facilitate the arrhythmogenic properties of the myocardium and the appearance of triggering factors. Among them, the ANS is the most relevant one [19, 20].

Ventricular arrhythmias are present in most patients with CHF. Indeed, VPCs and episodes of asymptomatic, non-sustained VT are common, and their frequency increases as the severity of heart failure progresses. Sustained VT and its degeneration to VF are the main causes of SCD in patients with mild-to-moderate CHF (NYHA class II and III) [21, 22]. And only a small percentage of SCDs cases are due to bradycardia (<60 beats/min) [23].

1.4.2 Heart Failure

The heart pumps blood to the body in order to meet its oxygen and nutrients' demand. *Heart failure* (HF) means that the heart's pumping power is weaker than normal and blood moves through the heart at a slower rate. Consequently, in HF the *cardiac output*, which is defined as the amount of blood pumped by the heart every minute, is lower than in the normal heart. According to the last *ESC 2016 HF guidelines*, "HF is a clinical syndrome caused by a structural and/or functional cardiac abnormality, which results in a reduced cardiac output and/or elevated intracardiac pressure at rest. The current definition of HF is restricted to symptomatic stages, namely breathlessness, ankle swelling and fatigue, accompanied by other signs, such us elevated jugular pressure, pulmonary crackles and peripheral oedema" [22]. Usually, HF is a consequence of an underlying cardiac disease altering the cardiac output. The most common pre-existing precursors are myocardial abnormalities causing systolic and diastolic ventricular

dysfunctions, valvular dysfunction, abnormalities in pericardium and endocardium, heart rhythm and other conduction disorders. Patients who have had HF for some time are classified as *chronic heart failure* (CHF) patients, while the term *acute heart failure* (AHF) is used to refer to a rapid onset or worsening of HF symptoms, requiring for urgent evaluation, treatment and, typically, hospital admission [22]. Sometimes, the term *congestive* HF is used, for describing both CHF and AHF with evidence of fluid overload. Nonetheless, the historic terminology used to describe HF is based on the measurement of the *left ventricular ejection fraction* (LVEF), including HF patients with *preserved* ($\geq$50%), *mid-range* (40-49%) and *reduced* ($<$40%) LVEF [22]. Nevertheless, in this thesis patients will be consider to present a reduced LVEF if $\leq$35%, in agreement with prior studies using the same population.

The prevalence of HF, although dependent on the definition, reaches approximately the 1-2% of the adult population in developed countries, rising up to $\geq$10% in elderlies ($>$70 years) [24]. Recent data from hospitalized patients suggest that the incidence of this pathology may be decreasing, especially in the case of patients with reduced LVEF [25, 26]. Despite the last improvements in treatment and the evident increase in survival rates and reduced hospitalizations, the outcome for this pathology often remains unsatisfactory: most deaths have cardiovascular origin, mainly SCD and *pump failure* (worsening of HF) death (PFD) [27, 28]. Due to the wide aetiology of this disease, it lacks a single classification system to identify causes of HF, but a proper identification of these pathologies becomes crucial in order to adopt specific therapies.

Diagnosis of CHF is mainly based on three kinds of tests:

Blood test: *B-type natriuretic peptides* (BNP) are released in response to changes in pressure inside the heart and the degree of ventricular stretch. BNP levels are higher in patients with HF than in people who have normal heart function and BNP$\geq$ 35 pg/ml indicates abnormal cardiac function. However, there are other causes (atrial fibrillation, age, renal failure, among others) that raise BNP levels as well, so BNP tests are recommended to rule out HF, but further screening is needed to stablish diagnosis [22].

Electrocardiography: Abnomal ECG provides information on previous aetiology that can help also in therapy decision, and it increases the likelihood of HF diagnosis, but this test still has low specificity [29–32].

Cardiac imaging: *Echocardiography* is the most useful test to establish HF diagnosis due to its high accuracy, availability, safety and low cost. It provides direct information regarding chamber volumes, systolic and diastolic functions, wall thickness and valvular function, thus allowing the evaluation of LVEF [33–35]. Chest *X-ray* imaging, able to show pulmonary venous congestion or oedema, is also very helpful in the case of AHF [32, 36].

Symptoms and signs of HF are often unspecific, but are crucial in the evaluation of patient's response to the treatment. If they persist, this suggests that additional therapy is required. Severity of symptoms and exercise intolerance are defined according to the *New York Heart Association* (NYHA) functional classification [37]. Four functional classes are distinguished:

Class I: Patients have cardiac disease but without limitations of physical activity. Ordinary physical activity does not cause undue fatigue, palpitation, dyspnoea or anginal pain.

Class II: Patients have cardiac disease resulting in slight limitation of physical activity. They are comfortable at rest. Ordinary physical activity results in fatigue, palpitation, dyspnoea or anginal pain.

Class III: Patients have cardiac disease resulting in marked limitation of physical activity. They are comfortable at rest. Less than ordinary physical activity causes fatigue, palpitation, dyspnoea or anginal pain.

Class IV: Patients have cardiac disease resulting in inability to carry on any physical activity without discomfort. Symptoms of cardiac insufficiency or of the anginal syndrome may be present even at rest. If any physical activity is undertaken, discomfort is increased.

Therapy

Treatment of CHF is mainly oriented to improve the general clinical status as well as functional capacity and quality of life of diagnosed patients, preventing hospitalization and reducing mortality [22].

Pharmacological options include neuro-hormonal antagonists, as *angiotensin-converting enzyme inhibitors* (ACEIs) and beta-blockers, normally accompanied by diuretics or *mineralocorticoid/aldosterone receptor antagonists* (MRAs), if symptoms/signs of congestion are present. ACEIs, through the inhibition of the renin-angiotensin-aldosterone system, cause the relaxation of blood vessels and a decrease in blood volume, leading to lower blood pressure and oxygen demand from the heart. They have been shown to reduce both mortality and morbidity, especially in patients with reduced LVEF [38–40]. Beta-blockers, which can complement ACEIs, work by blocking the effects of epinephrine and norepinephrine receptors of the sympathetic nervous system, by slowing heart rate and thereby decreasing the heart's oxygen demand. The use of beta-blockers is highly recommended in the case of symptomatic patients, and it has been shown to reduce both hospitalization and death [41–44]. Finally, MRAs antagonize the action of aldosterone and other steroid hormone receptors with diuretic effect, reducing oedema and cardiac workload. They are recommended in case of persistent symptoms, despite being already treated with ACEIs and/or beta-blockers [45, 46].

In advanced stages of the disease or when the patient is persistently symptomatic, the above described medications are not effective enough. Another therapeutic alternative for CHF is the use of medical devices [22].

A great part of deaths in CHF patients are SCD, mainly consequence of ventricular arrhythmias [22, 23, 47, 48]. The human failing heart is characterized by a significant prolongation of the APD in comparison to the normal heart. If the prolongation of APD were homogeneous in all cardiac cells, this would not increase arrhythmogenity. However, this is not the case and enhanced differences in APD are present. These variations are the responsible of spatial inhomogeneities in repolarization and dispersion of refractoriness in the ventricles, underlying factors that lead to an increased vulnerability of the myocardial substrate [49]. In this case, *Implantable cardioverter-defibrillators* results effective in correcting ventricular arrhythmias and preventing bradycardia by restoring sinus rhythm [23, 50, 51]. While in patients with mild CHF (NYHA class II) this therapy has been shown to prevent about two deaths per year for every 100 implantations, this option is not recommended in end-stages of CHF, as the probability of pump failure death is higher [52]. On the other hand, *cardiac resynchronization therapy* (CRT) consists on a pacemaker implantation, which continuously monitors right and left ventricles and, in case of asynchronism in the contraction of both

chambers, an electrical impulse is applied to correct them. Both heart's efficiency and blood flow are increased. This kind of therapy is appropriate in patients with a severe-to-moderate stage of CHF [53, 54] with reduced LVEF and/or *left bundle branch block* (LBBB). A QRS duration $\geq$ 130 ms is generally used as the inclusion criterion for this kind of therapy.

1.4.3 Atrial Fibrillation

Atrial fibrillation (AF) is a supraventricular arrhytmia, characterized by the desynchronization of atrial electrical activity producing an irregular ventricular response. The asynchrony may be due to the appearance of secondary (ectopic) pacemaker activity and/or to areas of slow conduction that facilitate the persistence of reentrant activity. The atria beating at a much faster rate (300-600 beats/minute) makes the AV node discharge at irregular intervals, since only some of the impulses get through, causing a highly irregular rate of ventricular beats, often faster than the normal rate (120-160 beats/min). This ventricular response is mainly dependent on the electrophysiological properties of the AV node and other conducting tissues, the level of vagal and sympathetic tone, the presence or absence of accessory conduction pathways, and the effect of drugs [55].

AF is the most prevalent sustained arrhythmia encountered in clinical practice, with a prevalence of approximately 2-3% in the adult population, which increases with age, reaching rates up to the 10-17% in octogenarians [56,57]. It has become one of the most important health issues in developed countries as it is expected to double its incidence by 2030 [58,59]. AF is not only related to frequent symptoms and reduced quality of life [60] but also constitutes a major risk factor for stroke and mortality from cardiovascular and all causes [57, 59, 61].

Diagnosis of AF is based on ECG rhythm documentation. On the ECG, AF is clearly observable since consistent P waves are replaced with rapid oscillations or fibrillatory waves ("*f waves*") that vary in size, shape, and timing (consequence of the asynchronous depolarization of atrial tissue). The ECG in AF is also associated with an irregular, frequently rapid ventricular rate (consequence of the abnormal electrical conduction from the atria to the ventricles through the AV node), as illustrated in Figure 1.8 (d).

An AF episode can be symptomatic or asymptomatic, depending on its duration, ventricular rate, general health status and patient perceptions.

Symptoms are usually related to rapid heart rate and inefficient cardiac output due to loss of atrial contraction (up to 15-20% less than without the arrhythmia). These symptoms include palpitations, breathing insufficiency (dyspnea), chest pain and tiredness. It can also lead to situations of angina, shortness of breath and edema.

Mechanisms influencing atrial fibrillation

AF has a complex pathophysiology, with several mechanisms influencing initiation, maintenance and termination of AF episodes. Indeed, it has a heterogeneous clinical presentation: it may occur in the presence or absence of detectable structural heart disease or other apparent risk factors and related symptoms [57].

Structural remodelling: Structural heart disease, hypertension, diabetes, and also AF by itself induce a structural remodelling of the atria [62, 63]. In addition, inflammatory mechanisms have been also proposed as initiators of the arrhythmia [64]. As a consequence, electrical dissociation among different regions of the atria and conduction heterogeneities become present, which facilitate the re-entry and maintenance of AF.

Electrophysiological mechanisms: AF by itself causes progressive changes in atrial electrophysiology, by shortening the refractory period and the AF cycle length. It is well accepted that pulmonary veins play an important role in the initiation and maintenance of AF, since it is the most frequent area of generation. Three main hypothesis regarding the generation of atrial arrhythmias are postulated: (i) the multiple *wavelet* hypothesis, which states that AF is generated by various wavefronts propagated in a chaotic manner through the atria [65]; (ii) a *focal* hypothesis, where a focal source in the pulmonary veins lead to fibrillatory conduction and localized reentry [66]; (iii) the presence of a mother *rotor* defined as a stable, high-frequency rotating pattern that drives AF, have recently emerged as other potential mechanisms [67].

Genetic predisposition: Genetic factors, especially in early-onset AF, have been also associated to the presence of AF [68, 69].

Types of atrial fibrillation

Normally, AF progresses from short and isolated episodes to longer and more frequent attacks. According to the presentation, duration, and spontaneous termination of AF episodes, five different types of AF can be distinguished [57]:

First diagnosed AF: This type of AF occurs when the arrhythmia is diagnosed for the first time, irrespective of the duration of the episode or the presence and severity of related symptoms.

Paroxysmal AF: It is a self-terminating AF ending in most cases within 48 hours and, by definition, it may continue for up to 7 days.

Persistent AF: This type of AF lasts longer than 7 days, including cardioverted episodes, either with drugs or by direct electrical cardioversion. Persistent AF can be the first sign or can occur after some paroxysmal episodes.

Long-standing persistent AF: It is a continuous AF with a duration greater than one year, usually leading to permanent AF, in which cardioversion has failed or has not been attempted.

Permanent AF: This type of AF happens when cardioversion fails or the arrhythmia relapses within 48 hours.

Therapy

The major issues in the management of patients with AF are related to the arrhythmia itself but compromised with its prognostic impact, mainly oriented to stroke prevention, and these are not mutually exclusive. There are mainly two essential ways of handling the arrhythmia: *rhythm control*, i.e., to restore and maintain SR, or *rate control*, i.e., to accept AF to continue but ensuring that the ventricular rate is controlled. Regardless of the antiarrhythmic strategy, attention must be paid also to anticoagulation for prevention of ischaemic stroke in AF patients [55, 57].

The rate control is achieved with medications that increase the degree of block at the level of the AV node (beta-blockers, digoxin, calcium channel blockers or a combination), effectively decreasing the number of impulses that conduct down into the ventricles [70–72]. Restoration and maintenance

of SR, indicated to improve symptoms in AF patients who remain symptomatic under rate control therapy, can be achieved by various techniques, namely electrical and pharmacological cardioversion (amiodarone, sotalol, flecainide and propafenone, among others), catheter ablation, surgery and maze procedures [73–78].

Atrial Fibrillation in Chronic Heart Failure

AF and CHF frequently coexist. In particular, the prevalence of AF in patients with mild-to-moderate CHF (NYHA classes II and III), ranges from 10% to 15% [79].

A number of mechanisms have been reported [79], supporting both that CHF predispose to AF and that AF exacerbates CHF, often leading to PFD or SCD outcomes [57, 59]. In properly anticoagulated AF patients, it has been shown that most deaths were actually not related to stroke, thus raising the need for identifying other possible mechanisms and effective interventions to reduce mortality in AF [61]. In fact, recent data have pointed out the independent contribution of AF to SCD risk [80–83].

Many questions arise regarding the underlying mechanisms that associate AF, CHF and SCD risk and a better understanding is needed in order to adopt effective prediction and prevention strategies in this target population. Current therapeutic options are mainly oriented to an adequate control of ventricular rate and to restore and maintain sinus rhythm [22, 57, 84]. However, if risk stratification in each independent subgroup (AF or CHF) is challenging, identification of patients-at-risk in this target population that simultaneous suffer from the two diseases, becomes even more difficult. The major limitation is that the highly irregular ventricular response present during AF, makes the use of most electrocardiographic indices, such as QT interval, QT dynamics, Tpeak-to-end interval or TWA inappropriate, as they require the patient to be under a sinus rhythm condition to be properly assessed.

It is evident that the proper identification of pro-arrhythmic factors plays an important role in adopting specific therapeutic strategies. And this, together with an accurate risk stratification of patients, is crucial for improving the actual cost-effectiveness of described therapies, particularly low in the case of ICDs.

1.4.4 Coronary Heart Disease

Coronary heart disease (CHD), also referred as ischemic heart disease, is a pathological condition in which a fatty plaque builds up inside the coronary arteries, restricting blood flow to the heart. When plaque builds up in the arteries, the condition is called *atherosclerosis*. If the plaque ruptures, it can form a thrombus or blood clot. A large blood clot can mostly or completely block blood flow through a coronary artery. The condition in which the blood flow (and thus oxygen) is restricted or reduced in a part of the body is called ischemia. Myocardial ischemia is the name for decreased blood flow and oxygen to myocardial cells. A myocardial infarction (MI) occurs if the damaged heart tissue starts to die (necrosis) due to the lack of oxygen.

Over time, CHD can weaken the heart muscle and lead to HF. In addition, myocardial ischemia, and its degeneration to MI, are both conditions that can originate a vulnerable substrate to the development of ventricular arrhythmias.

The prevalence of CHD in the USA is around 6% in the adult population [85], increasing up to 25% in men and 16% in women among people between 60 and 79 years old [86]. It represents the number 1 cause of death in men and women worldwide and, although the mortality rate for this condition has gradually decayed over the last decades in western countries, it still causes about 20% of total deaths in Europe [86, 87].

Chest pain (angina pectoris) is the principal symptom related to CHD. It normally lasts minutes and can be radiated to the neck, jaw or arms. Chest pain, sometimes, can be accompanied by other less-specific symptoms, such as fatigue, faintness or nausea. Symptoms appear or become more severe with increased levels of exertion or emotional stress [86, 87].

Standard 12-lead stress ECG testing, by using exercise or pharmacological stress agents, has been established as the gold standard non-invasive test for the diagnosis of inducible ischemia [86]. Diagnostic endpoint for an ischemic ECG is ≥ 1 mm horizontal or down-sloping ST-T segment depression (at 0.06-0.08 ms after the J point) in one or more ECG leads [86, 88]. This test provides additional information with both diagnostic and prognostic relevance (hemodynamic response and HR recovery, symptoms and workload). It should be performed in absence of anti-ischemic drugs and ECG abnormalities at baseline.

When the ECG test results inconclusive (for example in the absence of symptoms or signs at maximum HR), non-invasive imaging test with pharmacological stress can be an alternative. Among imaging techniques, myocardial perfusion scintiography by *single photon emission computed tomography* (SPECT) and *cardiac magnetic resonance* (CMR) provides information related to myocardial blood flow and myocardial wall motion abnormalities, respectively.

Ischemia produces a series of alterations in myocardial tissue that are responsible for notable clinical and electrocardiographic features. Late repolarization of the ischemic zone is reflected by T-wave abnormalities on the ECG. At the cellular level, electrical properties of the myocardial cells affected by ischemia are altered: AP rest level is reduced and APD shortened. Those changes determine a voltage gradient between the normal and ischemic areas, originating an *injury current* flowing between these regions. It is manifested on the ECG as a ST-segment deviation (elevation/depression).

ST segment elevation in two or more contiguous leads during the acute phase of MI is the main sign to indicate for the need of an early reperfusion by a *percutaneous coronary intervention* (PCI).

1.4.5 Microgravity

The study and better understanding of ventricular repolarization and cardiac electrical disturbances are not only of great interest in the clinical practice. Ideed, control of autonomic and cardiovascular systems, even in the absence of disease, relay on a set of environmental conditions that, if changed, could produce malfunctioning. One of these conditions is gravity. Human space-flight represents a highly risky activity, due to both engineering and human elements that could fail during the different steps of the mission. As regards the human factor, risk assessment and identification of risk mitigation resources are the basis for minimizing potential medical disorders that could prevent mission success but, more important, put in danger the crew health [89].

It is well known that gravity plays an essential role in determining the distribution of hydrostatic pressure gradient and plasma volume within the cardiovascular system. In particular, a prolonged weightlessness condition results in a redistribution of body fluids from the lower half of the body towards upper districts, leading to cardiac deconditioning and inducing sig-

nificant changes in both autonomic and cardiovascular systems [90]. This results in orthostatic intolerance episodes once gravity is re-established, decrease in plasma volume and reduced aerobic capacity, together with bone and muscle loss. Potentially, cardiac electrical activity could also be affected by this process. Additional factors induced by space-flight, such as sudden pressure changes [91] or rapid onset and offset of +Gx or +Gz acceleration [92–94] could also present associated risks. The occurrence of serious cardiac rhythm disorders [95] and related diminished cardiac and vascular functions have been identified as primary cardiovascular risks of space-flight in the NASA Human Research Roadmap Program in 2005, currently under reevaluation process.

Indeed, cardiac rhythm disturbances have been observed among astronauts and cosmonauts since the Apollo 15 mission [96, 97], including one documented episode of non-sustained VT [98]. However, it is not clear whether these potentially critical events, as anecdotal reports, were due to pre-existing conditions or derived effects induced by weightlessness. During space-flights missions (up to 6 months), the incidence of SCD is about 1% per year [99]. It is very low, but still exists.

Nonetheless, some concern exists about the fact that prolonged exposure to microgravity might lead to cardiac electrical instability: bradycardia related to long-duration space-flights that could result in prolongation of the QT interval [100], the use of medications, alterations in the ANS [101–105], development of apoptosis in response to pathological, physiological, and/or genetic signals [106,107] resulting in cardiac atrophy [108], radiation exposure inducing structural changes [109], psychological stress [110]. Cardiac adaptation to all these factors, together with adrenalin/neurohormonal changes and stress related to space-flight, could also alter electrical conduction, increasing the inhomogeneity of electrical repolarization, and thus potentially increasing the risk of inducing cardiac rhythm disturbances.

Since research under real conditions of space-flights is of limited possibility, the head-down (-6 degrees) bed-rest (HDBR) model has been proved to be a reliable ground-based simulation analog for the most physiological effects of spaceflight [111]. This manoeuvre represents a model of chronic circulatory unloading, simulating sustained exposure to microgravity and offers a unique opportunity for studying the effects of prolonged space-flight on the cardiovascular system, as well as to test potential countermeasures (CM) to prevent its deconditioning. From 2001, the European Space

Agency (ESA) has led such HDBR studies, where subjects were placed on a bed with a 6° negative tilt for periods ranging from five days (short-term) to three months (long-term), resulting in a top level and valued programme.

1.5 Ventricular repolarization information from the ECG: indices of electrical instability

The assessment of ventricular repolarization based on this non-invasive test have been show to provide with valuable information for risk stratification performance [4]. Ventricular repolarization activity is reflected on the ECG throughout the T-wave. More precisely, the T-wave reflects these intrinsic heterogeneities of repolarizing currents, which depends on both the sequence of ventricular activations (conduction velocity) and the inhomogeneity in APD of cardiac myocytes. An accentuated APD is associated to many cardiac pathologies, such as ischemia or long QT syndrome, and instabilities in ventricular repolarization have been tightly linked to arrhythmia vulnerability [12].

Several ECG-derived indices have been proposed in the literature for the assessment of both spatial and temporal heterogeneities of ventricular repolarization. A brief description of proposed electrocardiographic indices of repolarization instability is presented below.

QT interval: As illustrated in Figure 1.4, it is measured from the onset of the QRS complex (Q-wave) to the end of the T-wave, and represents the total duration of ventricular depolarization and repolarization. Prolongued values of the QT interval can reflect conduction abnormalities during depolarization, like LBBB, and repolarization, and it has been consolidated as one of the most traditional ECG-derived indices for arrhythmic risk prediction [112–115].

QT dispersion: The QT interval varies from lead to lead, reflecting regional differences in repolarization. QT dispersion (QTd) is defined as the difference between the maximum and minimum QT intervals across leads and it has been proposed to quantify ventricular repolarization dispersion [115, 116]. However it has been shown to mainly reflect the different lead projections of the T-wave loop rather than any other type of dispersion [117]. Therefore, it is used marginally nowadays.

QT variability (QTV): QT interval presents spontaneous beat-to-beat fluctuations, reflecting temporal variations in ventricular depolarization and repolarization, originated by the direct action of ANS on the myocardium [118]. Increased repolarization variability has been associated to the risk of developing ventricular arrhythmias [118–120].

QT dynamics: The QT interval is greatly influenced by changes in heart rhythm [121], and it takes some time until reaching a steady state after HR changes. This adaptation time provides useful information for arrhythmic risk [122–125]. The slope of the relationship between the QT interval and the *RR* interval, a surrogate of the velocity in adaptation to HR, has been suggested also to indicate pro-arrhythmic risk, with higher slopes associated to higher risk [123, 126–128].

Tpeak-to-Tend (Tpe) interval and dynamics: The Tpe interval, measured from the peak to the end of the T-wave, reflects the time differences in completing ventricular repolarization at different regions [129]. This measurement has been linked to the development of ventricular arrhythmias in several pathological conditions [130–132]. Ventricular dispersion properties at different HRs are usually quantified by the so called APD restitution (APDR) curves, which represents the APD as a function of the *RR* interval for different sites of the myocardium. An increased dispersion of this APDR curve is associated to arrhythmia propensity [133, 134]. The relationship between the Tpe and the RR interval has been proposed as an indirect ECG surrogate of this APDR dispersion [135], and its clinical value has been evaluated in different clinical settings [136–139]

QRS-T angle: It is defined as a spatial angle between the spatial QRS vector and spatial T vector of the vectorcardiogram, measuring the difference in mean vectors of depolarization and repolarization [140]. An abnormally wide QRS-T angle has emerged as a prominent variable in stratifying cardiac death risk [141, 142].

T-wave alternans (TWA): Also known as repolarization alternans (RPA), it appears in the ECG as a consistent beat-to-beat alternation in the amplitude, duration or morphology of the ST segment and/or the T-wave [5]. It is presently regarded as a non-invasive risk marker of ventricular vulnerability and provides valuable information regarding SCD risk stratification [5, 143]. As it is one of the main topics of this

thesis, a more detailed review on TWA methodology is included in section 1.5.1.

1.5.1 T-Wave Alternans

While visible or macroscopic TWA had been first reported at the beginning of the 20th century and was considered as a rare finding [144], it was with the introduction of computerized electrocardiology when non-visible microvolt-level alternans could be detected. Since then, TWA has been considered a much more common phenomenon. It has been reported under several pathological conditions, including myocardial ischemia and infarction induced by coronary occlusion, HF, non-ischemic cardiomiopathy and other congenital diseases (Brugada syndrome and long QT syndrome) [5]. TWA emerges as a consequence of a beat-to-beat alternation in the APD at the myocyte level. It is known to reflect temporal and spatial heterogeneity of ventricular repolarization, associated to electrical instability. Therefore, it has been proposed as a non-invasive risk marker of ventricular vulnerability, providing valuable information regarding SCD risk stratification [5, 143].

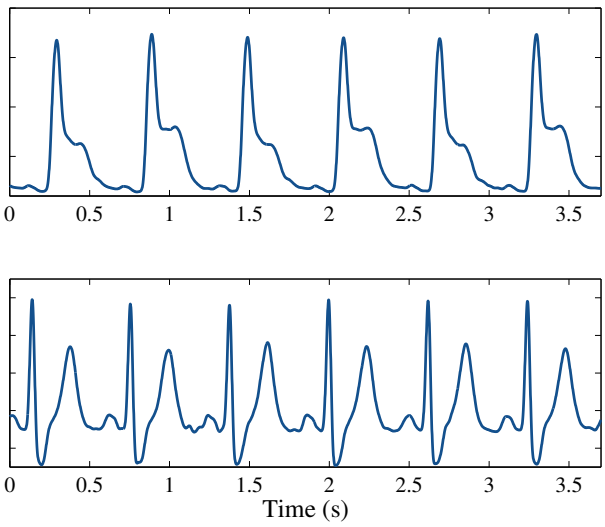

Figure 1.9: Two examples of ECG signals with TWA.

TWA tests are usually performed under a controlled HR increase, normally by pacing or exercise or pharmacological stress tests (a target heart rate range of 105-110 beats/min was determined for pathologic alternans

in adults). As microvolt-TWA can be even lower than the noise level, specially if it is assessed under exercise, TWA measurement is a challenging task. From the signal processing point of view, TWA analysis is based on two types of procedures: determining the presence or the absence of TWA in the ECG signal (i.e, a *detection* problem) and the quantification of TWA magnitude (i.e, a *estimation* problem), and a number of advanced signal processing methods have been proposed to do it [145].

The general scheme for TWA analysis consists of two main stages: ECG pre-processing, TWA detection and/or TWA magnitude estimation. The two most common methods used in the clinical practice or research are the *spectral method* (SM) [146] and the *modified moving average method* (MMAM) [147], as they are available in commercial equipment.

The SM is based on the classical Fourier analysis in which, after beat alignment to the QRS, the amplitude beat-to-beat series of consecutive ST-T complexes is generated and the short-term Fourier transform applied. Since the beat-to-beat series is generated by taking one measurement per beat, the frequency at 0.5 cycles per beat (cpb) represents the oscillation occurring every other beat, that is, the TWA frequency. Finally, the alternans power (in μV^2) is defined as the difference between the power at 0.5 cpb and the noise level, estimated as the power at an adjacent band (0.44-0.49 cpb). For detection, the alternans ratio (K-score) is calculated as the ratio of the alternans power divided by the standard deviation of the noise. TWA is considered significant if the K-score is $\geq$3 [146]. The TWA test using the spectral method is usually conducted during bicycle or treadmill exercise in order to reach an optimum heart rate [148].

The MMAM estimates the median ST-T complex patterns of odd and even beats using a recursive moving average. The moving average allows control of the influence of new incoming beats on the median templates with a non-linear limiting function (i.e., the fraction of morphology change that an incoming beat can contribute). TWA is estimated as the maximum difference between the odd and the even median complexes at any point. Abrupt changes due to noisy beats and extrasystoles are excluded and the effect of noise, movement and respiration is attenuated by filtering. However, the MMAM does not include detection stage and it rests sensitive to noise level changes, requiring visual validation [147]. The MMAM is mainly utilized in the analysis of TWA in ambulatory ECG recordings [149–152].

In this thesis, however, TWA analysis is based on the *Laplacian likelihood ratio method* (LLRM) [153], which has been reported to outperform the accuracy of the SM and MMAM in the presence of impulsive artifacts [154]. The LLRM is based on the signal processing theory for estimation and detection and uses a statistical model including alternans and physiological noise terms. Noise is modelled as a zero-mean Laplacian random variable, allowing for a more robust realistic description of noise present on real ECGs. The maximum likelihood estimator (MLE) and the generalized likelihood ratio test (GLRT) are used for TWA estimation and detection, respectively [153].

All these methods are usually applied in a *single-lead* basis, that is, considering each ECG lead independently. *Multi-lead* strategies have been proposed for taking advantage of the inter-lead redundancy of TWA and noise components, such as the methods based on principal component analysis (PCA) [155] or periodic component analysis (πCA) [156], thus leading to a more robust and sensitive analysis than lead-by-lead analysis. This two approaches include a *signal transformation* step before TWA detection and estimation, where a linear transformation is applied to the multi-lead ECG signal in order to emphasize the TWA content by exploiting the information available in all leads. The difference between PCA and πCA is on how the signal transformation is defined. PCA uses a maximum variance criterion to separate signal (alternans) and noise (non-alternans) into orthogonal subspaces. πCA, instead, uses a periodical criterion to separate alternans a non-alternans components by enhancing the 2-beat periodicity of the ECG signal, that corresponds with the TWA frequency. This last technique has been shown to be a more robust and sensitive tool, in comparison to both single-lead and PCA based techniques [156].

As the analysis of TWA based of πCA and together with the LLRM is the basis for chapters 2, 3, 4, a more detailed description of the two approaches will be included in next chapter.

1.6 Objectives and outline of the thesis

The main objective of this thesis is to propose methodological advances for the assessment of ventricular repolarization instability in invasive and non-invasive cardiac signals, to attain a better understanding of several pathological or abnormal conditions that may lead to an improvement in clinical

decisions, as those related to the prediction of malignant arrhythmias. In particular, methodological advances for the analysis of TWA under experimental conditions (chapters 2 and 3), and robust to sporadic (VPCs) and sustained (AF) rhythm disturbances (chapters 4 and 5, respectively) in CHF patients, are presented. The content of the rest of the thesis is organized as follows:

Chapter 2: This chapter includes a comprehensive characterization of TWA (prevalence, magnitude, time-course, and alternans waveform) induced by a porcine model of myocardial ischemia. Signals from both body surface ECG and intracardiac EGMs recorded from 4 different anatomical heart locations are analyzed following a multilead scheme based on πCA together with the LLRM, also presented in this chapter. Finally, under the hypothesis that a proper monitorization of in-vivo TWA from EGM signals could alert and prevent the onset of VT/VF episodes, an optimal intracardiac lead configuration that maximizes TWA rate detection is proposed. One manuscript with the research described in this chapter is under preparation.

Chapter 3: It is well known that microgravity exposure leads to cardiovascular deconditioning with potential impact in cardiac electrical activity. This raises the question of whether microgravity increases arrhythmia propensity and, consequently, SCD risk if cardiac repolarization is adversely influenced. In this chapter the effects of short- (5 days), mid- (21 days) and long- (60 days) exposure to simulated microgravity on TWA using the HDBR model are assessed. TWA is evaluated before, during and after the immobilization period, by the long-term averaging technique of ambulatory ECG Holter recordings [157]. In addition, an adapted short-term averaging approach for shorter, non-stationary ECG tracings obtained during two stress manoeuvres (head-up tilt-table and bicycle exercise tests) is proposed. Both approaches are based on the multilead analysis presented in chapter 2 but avoiding the detection stage, and the need for a threshold definition. Finally, changes in TWA indices induced by HDBR were quantified and discussed.

The research described in this chapter generated the following publications:

- **A Martín-Yebra**, V Monasterio, A Pellegrini, P Laguna, E Caiani, JP Martínez. Effect of Simulated Microgravity by Head-Down Bed-Rest

on T wave Alternans. *XXXIX International Conference on Computing in Cardiology*, pp. 377-380, Krakow (Poland), September 2012.

- **A Martín-Yebra**, E Caiani, V Monasterio, A Pellegrini, P Laguna, JP Martínez. T-Wave Alternans and Autonomic Nervous System Activity During Orthostatic Stress after 5 Days of Head-Down Bed-Rest. *Cardiovascular Oscillations (ESGCO), 2014 8th Conference of the European Study Group on;*, pp. 115-116, Fai della Paganella, (Italy), May 2014.
- **A Martín-Yebra**, EG Caiani, V Monasterio, A Pellegrini, P Laguna, JP Martínez. Evaluation of T-wave alternans activity under stress conditions after 5 days and 21 days of sedentary head-down bed-rest. *Physiological measurement*, 2015;(36):pp. 2041-2055.
- EG Caiani, **A Martín-Yebra**, F Landreani, J Bolea, P Laguna, P Vaïda. Weightlessness and cardiac rhythm disorders: current knowledge from space flight and bed-rest studies. *Frontiers in Astronomy and Space Sciences*, 2016;(3):27
- **A Martín-Yebra**, V Monasterio, P Laguna, JP Martínez, EG Caiani. Evaluation of changes in T-wave alternans induced by 60-days of immobilization by head-down bed-rest. *XLIV International Conference on Computing in Cardiology, 2017*. Accepted.

Chapter 4: The presence of one or more VPCs may alter repolarization dynamics, and they may introduce a phase reversal in the sequence of alternant T-wave morphologies [158]. This could hamper the estimation of TWA amplitude [159,160] and, consequently, its potential for risk stratification. In this chapter, a methodological improvement for the estimation of TWA amplitude in ambulatory ECGs, which deals with the possible phase reversal induced by the presence of VPCs in the alternans sequence is proposed. First, a simulation scenario was generated in order to evaluate the performance of the algorithm using synthetic signals. Then, the effect of the proposed method in the prognostic value of TWA amplitude was assessed in real ambulatory ECG recordings from patients with CHF. Finally, circadian TWA changes were evaluated as well as whether the prognostic value of TWA is sensitive to this circadian pattern. As a conclusion, the performance of the proposed methodology on the simulation study is discussed. Then, the improvement on the prognostic value of TWA for SCD and the circadian modulation on alternans activity are presented.

The research described in this chapter generated the following publications:

- **A Martín-Yebra**, EG Caiani, P Laguna, V Monasterio and JP Martínez. Circadian Modulation on T-wave Alternans Activity in Chronic Heart Failure Patients. *XLII International Conference on Computing in Cardiology, 2015*, pp. 845-848, Nice (France). September, 2015.
- **A Martín-Yebra**, V Monasterio, I Cygankiewicz, A Bayés-de-Luna, EG Caiani, P Laguna and JP Martínez. Post-Ventricular Premature Contraction Phase Correction Improves the Predictive Value of Average T-wave Alternans in Ambulatory ECG Recordings. *IEEE Transactions on Biomedical Engineering*, 2017; DOI: 10.1109/TBME.2017.2711645.

Chapter 5: The highly irregular ventricular response during AF makes innapropiate the use of the most common ECG-derived markers of ventricular repolarization heterogeneity, including TWA, in this particular condition as they require the patient to be in sinus rhythm to be properly assessed [161]. In this chapter, we investigated whether a non-invasive stratification of AF patients at risk of SCD is possible by assessing the ventricular repolarization in the electrocardiogram signal. Ventricular repolarization changes are assessed based on a selective heart rate bin averaging technique and new indices of repolarization variation are proposed. A clinical study demonstrates their prognostic values for SCD in a CHF population with AF.

The research described in this chapter generated the following publications:

- **A Martín-Yebra**, I Cygankiewicz, A Bayés-de-Luna, P Laguna, EG Caiani, JP Martínez. Index of T-wave Variation as a Predictor of Sudden Cardiac Death in Chronic Heart Failure Patients with Atrial Fibrillation. *XLIII International Conference on Computing in Cardiology, 2016*, pp. 5-8, Vancouver (Canada). September, 2016.
- **A Martín-Yebra**, P Laguna, I Cygankiewicz, A Bayés-de-Luna, EG Caiani, JP Martínez. Indices of Ventricular Repolarization Variation for Sudden Cardiac Death Prediction in Atrial Fibrillation Patients. Submitted to IEEE Transactions on Biomedical Engineering. *Under review.*

Also, this work was awarded with the following prizes:

- Finalist of the *Rosanna Degani Young Investigator Award*. Index of T-wave Variation as a Predictor of Sudden Cardiac Death in Chronic

Heart Failure Patients with Atrial Fibrillation. *XLIII International Conference on Computing in Cardiology*. Vancouver (Canada). September, 2016.

– *Mortara mobility fellowship*. Index of T-wave Variation as a Predictor of Sudden Cardiac Death in Chronic Heart Failure Patients with Atrial Fibrillation. *XLIII International Conference on Computing in Cardiology*. Vancouver (Canada). September, 2016.

Chapter 6: This chapter presents the main conclusions of the thesis and discusses future extensions of the work.

Chapter 2

Characterization of repolarization alternans in invasive and non-invasive cardiac signals during acute ischemia

2.1 Motivation

Although the mechanisms underlying TWA are not yet completely understood, this phenomenon has been linked to electrical instability and an increased vulnerability of the myocardium, predisposing to the development of ventricular arrhythmias (VT/VF) and, consequently, SCD. The presence of TWA has been documented under several clinical conditions, including HF, myocardial ischemia and post-MI patients [5].

Coronary occlusion by percutaneous coronary intervention (PCI) provides an excellent model to investigate the electrophysiological changes induced by acute ischemia, allowing the study of the initial minutes of the ischemic process and its progression towards tissue infarction. TWA from body surface ECG has been previously investigated during the first minutes of occlusion (<5 min) in patients undergoing PCI [153] and during long-lasting (40 min) occlusion using a porcine model of MI [162]. However, few works have characterized TWA or RPA on intracardiac EGMs, and normally limited to pacing-induced protocols [163–168].

As TWA provides information about ventricular vulnerability, we hypothesized that a proper detection and monitorization of in-vivo TWA. In EGM signals recorded by an implantable device, an ICD for example, could alert and prevent the onset of VT/VF episodes. Indeed, the presence of TWA on EGMs has been proposed as a short-term predictor of VT/VF [168–171], but this first requires a reliable detection and characterization of TWA in EGM signals.

The goal of the work presented in this first chapter, therefore, is twofold: (i) to characterize TWA (prevalence, magnitude, time-course with occlusion, and alternant waveform) from both body surface ECG and intracardiac EGM signals recorded from 4 different anatomical heart locations using a porcine model of myocardial ischemia induced by PCI (same model used in [167]); (ii) to search for the optimal intracardiac lead configuration clinically accessible by an implantable device in order to maximize the sensitivity for TWA detection. A multilead approach for TWA analysis, introduced in section 1.5.1, that combines the periodic component analysis (πCA) with the Laplacian Likelihood Ratio method (LLRM) was used.

2.2 Materials

ECG and EGM signals from a porcine model of acute ischemia are analyzed in this chapter. After being anesthetized and acutely instrumented, seventeen male Yorkshire swine (weight range 40-45 kg) underwent a PCI by the occlusion of the proximal *left circumflex artery* (LCX). The experiments were performed in the Animal Electrophysiology Laboratory of the Massachusetts General Hospital. The protocol was approved by the Hospital's Animal Care and Use Committee. The study was developed in collaboration with Prof. Armoundas and his group (Massachusetts General Hospital, Boston, USA).

Signal monitoring was initiated before starting the occlusion and lasted throughout the whole occlusion period, thus one *baseline* (BASE) and one *occlussion* (OCCL) recordig was available for each intervention. Standard ECG electrodes (leads II and V4) were placed on the animal's limbs and chest. Intracardiac EGMs were obtained from decapolar catheters, placed under fluoroscopic guidance in the (i) right ventricle (RV), the distal lead being at the RV apex, (ii) the coronary sinus (CS), the distal lead being at the distal CS, (iii) the left ventricle (LV), the proximal lead being at the LV apex and, finally, (iv) the epicardial space (EPI) in only 5 swines. A total of 12 intracardiac unipolar leads (3 in each of the RV, LV, EPI, and CS catheters), 4 far-field bipolar leads (1 per catheter, derived by subtracting nonadjacent pairs of unipolar leads with 2.7 to 3.6 cm spacing), 4 near-field bipolar leads (1 per catheter, derived by subtracting adjacent pairs of unipolar leads with $<$0.3 cm spacing) were available for each recording. An inferior vena cava catheter was inserted as a reference electrode for unipolar signals. Finally, an arterial line was used to monitor arterial blood pressure. All signals were recorded through a Prucka Cardiolab (General Electric) electrophysiology system that provided 16 high-fidelity analog output signals, then sampled at 1000 Hz by a multichannel 16-bit data acquisition card (National Instruments M-Series PCI6255). See [167] for more information about the experimental data.

2.3 Methods

As it was introduced in section 1.5.1, the general scheme for multilead TWA analysis consists of three main stages: ECG pre-processing, signal transformation and TWA detection/estimation.

2.3.1 Preprocessing

Signal preprocessing included QRS detection in surface ECG lead V4 using a wavelet-based ECG delineator [172]. Then, baseline wander was removed in each lead using a cubic spline interpolation technique [7]. The ECG was low-pass filtered (with cut-off frequency of 15 Hz) to remove noise out of TWA frequency range and down-sampled to 125 Hz to reduce the computational cost of TWA analysis. Finally, for each beat, an interval of 350 ms, 60 ms from QRS fidutial point was selected for TWA analysis, corresponding to the ventricular repolarization phase.

2.3.2 TWA analysis

In this chapter, TWA analysis is performed following a multilead scheme that processes all available leads based on periodic component analysis (πCA) [156]. πCA finds the optimal linear combination of all leads where the 2-beat periodicity of the ST-T complex (TWA periodicity) is maximized and projected into the first transformed lead. Then, the LLRM [153] was applied in that new combined lead to detect and estimate the TWA waveform in each segment. Combination of both approaches has been shown to outperform the classical single-lead SM [154, 156].

A detailed description of both methods is included in the following paragraphs.

Periodic Component analysis

Multilead analyisis takes the advantage of the redundancy of spatial and temporal information present in all available leads. Combining the information of all ECG leads by a linear transformation before TWA detection and estimation enhances the TWA content over noise, leading to an improved alternans-to-noise ratio (ANR) in the transformed signal. The periodic

component analysis technique searches for the optimal linear combination of the available leads which maximizes the desired periodicity in the combined lead [173, 174]. πCA-based scheme has been shown to provide a better ability to detect TWA than previously reported schemes (single-lead-based scheme and SM), with the potential to improve the prognostic value of TWA [156].

Being K the number of beats of the analysis window, N the number of samples within the ST-T complex and L the number of available ECG leads, the ST-T complex of the k^{th} beat in the l^{th} lead is denoted as $x_{k,l}(n)$.

Each ST-T complex can be modelled as:

$$x_{k,l}(n) = s_l(n) + \frac{1}{2}a_l(n)(-1)^k + v(n)_{k,l}, \tag{2.1}$$

where $s_l(n)$ is the background ST-T component present every beat, $a_l(n)$ is the alternant waveform, defined as the difference between even and odd beats, and $v_l(n)$ the additive random noise.

For each lead l, a vector $\boldsymbol{x}_l$ is built by concatenating the K consecutive ST-T complexes, and a data matrix $\mathbf{X}$ is then constructed whose rows are the vectors $\boldsymbol{x}_l^{\mathrm{T}}$ (dimension $L \times NK$). For TWA analysis, we are interested in combining the ECG leads in such a way that the 2-beat periodicity (TWA periodicity) is maximized in the resulting signal, $\boldsymbol{y}^{\mathrm{T}} = \mathbf{w}^{\mathrm{T}}\mathbf{X}$.

In a first step, the repetitive $\mathbf{s}_l$ component is cancelled by a detrending filter that computes the difference between each complex and the previous one:

$$x'_{k,l}(n) = x_{k,l}(n) - x_{k-1,l}(n), \qquad k = 1, \ldots, K-1; n = 0, \ldots, N-1. \tag{2.2}$$

Those *detrended* beats are arranged to form the data matrix $\mathbf{X}'$, concatenating the $K-1$ consecutive ST-T complexes $x'(n)$, with leads disposed as rows ($L \times N(K-1)$). In this way, background ECG is removed and only beat-to-beat T-wave variations and noise components are contained in $\mathbf{X}'$. This step avoids that πCA identifies the repetitive ECG component rather than the TWA component due to the higher power of the first one.

To maximize the m-beat periodicity of the signal, the desired transformation must minimize the following residual measure of periodicity (m=2 beats period):

$$\epsilon(\mathbf{w}, m) = \frac{\|\boldsymbol{y}'_{(m)} - \boldsymbol{y}'\|^2}{\|\boldsymbol{y}'\|^2}, \tag{2.3}$$

where $\boldsymbol{y'}^{\mathrm{T}} = \mathbf{w}^{\mathrm{T}}\mathbf{X'}$ and $\boldsymbol{y'}^{\mathrm{T}}_{(m)} = \mathbf{w}^{\mathrm{T}}\mathbf{X'}^{(m)}$. $\mathbf{X'}^{(m)}$ is the equivalent of $\mathbf{X'}$ after sliding the analysis window $m = 2$ beats forward.

By the Rayleigh-Ritz theorem of linear algebra, it can be shown that the weight $\mathbf{w}$ that minimizes 2.3 is given by the generalized eigenvector corresponding to the smallest generalized eigenvalue of the matrix pair ($\mathbf{A}_{\mathbf{X'}}(m)$,$\mathbf{R}_{\mathbf{X'}}$) [174], that is, the $\mathbf{w}$ associated to the smallest λ that accomplishes the following equation:

$$\mathbf{R}_{\mathbf{X'}}\mathbf{w} = \lambda\mathbf{A}_{\mathbf{X'}}(m)\mathbf{w}, \tag{2.4}$$

where $\mathbf{R}_{\mathbf{X'}}$ is the spatial correlation matrix of $\mathbf{X'}$, defined as:

$$\mathbf{R}_{\mathbf{X'}} = \frac{1}{(K-1)N}\mathbf{X'}\mathbf{X'}^{\mathrm{T}} \tag{2.5}$$

with K the number of beats in the analysis window and N the number of samples of each learning segment. In the same way, we defined $\mathbf{A}_{\mathbf{X'}}(m)$, the analogous spatial correlation matrix of the non-periodic components ($\mathbf{X'}^{(m)} - \mathbf{X'}$):

$$\mathbf{A}_{\mathbf{X'}}(m) = \frac{1}{(K-1)N}(\mathbf{X'}^{(m)} - \mathbf{X'})(\mathbf{X'}^{(m)} - \mathbf{X'})^{\mathrm{T}} \tag{2.6}$$

Finally, the πCA transformed lead, $\boldsymbol{y}^{\mathrm{T}} = \mathbf{w}^{\mathrm{T}}\mathbf{X}$, is computed applying the transformation to the original data $\mathbf{X}$. In the same way, $\boldsymbol{y'}^{\mathrm{T}} = \mathbf{w}^{\mathrm{T}}\mathbf{X'}$ is the πCA transformed lead with background ECG cancellation. That constructed ECG lead, contains the linear projection of the 2-beat periodic components of the ECG signal and it is the lead that will be used for TWA analysis. The n^{th} sample of the k^{th} beat of this πCA transformed lead is denoted as $y'_k(n)$. πCA transformation of a real ECG signal is illustrated in Figure 2.1.

Note that the optimal linear combination was computed for each analysis window of K beats, as it depends on how the alternant components and noise are distributed within the ECG leads.

Multilead TWA analysis was performed by combining ECG or EGM leads recorded at the same anatomical location (body surface ECG, CS, EPI, RV and LV), using a sliding signal window of K=32 beats.

Laplacian Likelihood Ratio Method

The LLRM uses a model-based approach where noise is modelled as a zero-mean Laplacian random variable. The maximum likelihood estima-

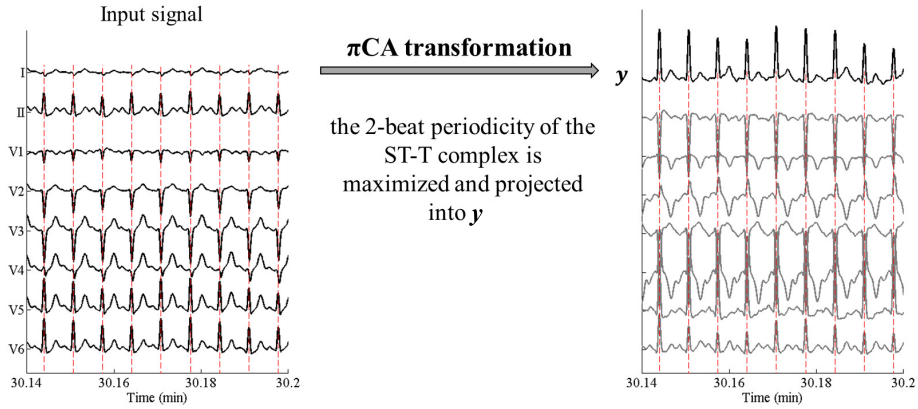

Figure 2.1: Eight independent leads of a real 12-lead ECG with TWA, non visible to the naked eye, and the resulted signal after πCA transformation. TWA is clearly enhanced in lead $\boldsymbol{y}$, the lead associated to the smallest generalized eigenvalue.

tor (MLE) and the generalized likelihood ratio test (GLRT) are used for TWA estimation and detection respectively [153]. Both detection and estimation are applied to the πCA transformed lead $\boldsymbol{y}$, after background ECG cancellation, i.e, using $\boldsymbol{y}'$.

Assuming noise as a zero-mean Laplacian distribution with unknown standard deviation σ_l, the MLE of the alternans waveform $\boldsymbol{a}_l$ is:

$$\hat{a}(n) = median\left(\left\{{y'}_k(n)(-1)^k\right\}_{k=1}^{K-1}\right) \qquad n = 0...N-1. \tag{2.7}$$

This $\mathbf{a}_l$ waveform describes how the TWA amplitude is distributed within the whole ST-T complex. Finally, the TWA amplitude is estimated as the root mean square (RMS) value of the altenans waveform:

$$Valt = \sqrt{\frac{1}{N}\sum_{n=0}^{N-1}\hat{a}^2(n)} \qquad (\mu V). \tag{2.8}$$

The GLRT statistic for the model is [153]:

$$Z = \frac{\sqrt{2}}{\hat{\sigma}}\sum_{n=0}^{N-1}\left(\sum_{k=1}^{K-1}\left|y'_k(n)\right| - \sum_{k=1}^{K-1}\left|y'_k(n) - \hat{a}(n)(-1)^k\right|\right) \tag{2.9}$$

where $\hat{\sigma}$ is the MLE of the standard deviation of the noise:

$$\hat{\sigma} = \frac{\sqrt{2}}{2NK}\sum_{n=1}^{N-1}\sum_{k=1}^{K-1}\|{y'}_k(n) - \hat{a}(n)(-1)^k\|_1. \tag{2.10}$$

The GLRT in 2.9 can be interpreted as an estimate of the ANR. In order to decide whether TWA is present or not, the GLRT statistic Z is compared to a decision threshold γ and TWA is considered to be present in the analyzed window if $Z \geq \gamma$. For a more detailed description of the model, the reader is referred to [145].

The probability of false alarm (P_{FA}) is defined as the probability of having a GLRT greater than γ when no TWA is present. In this case, we have set the detection threshold, γ, so that P_{FA} was 0.05, under the assumption that no TWA is likely to be found in BASE recordings. In other words, only the 5% of the Z statistic obtained in BASE recordings were above the threshold. This threshold was defined for each multilead analysis. Additionally, a minimum number of 32 beats was required to consider a significant TWA episode, in order to avoid spurious detections. Finally if TWA was detected, the TWA waveform was estimated in the first πCA transformed lead (the one maximizing the periodicity) using equation 2.7. When TWA was not detected, the TWA amplitude was considered to be zero.

2.3.3 Statistical analysis

Data are presented as median (25^{th};75^{th} percentiles), unless otherwise specified. In Figure 2.2 and Figure 2.5 data are represented as mean± standard deviation. Differences in the number of BASE and OCCL recordings with TWA were evaluated with the McNemar test. Non-parametric Wilcoxon signed rank paired test was applied to evaluate differences between BASE and OCCL due to the non-normality of the data. For all tests, the null hypothesis was rejected when p$\leq \alpha$, with $\alpha = 0.05$.

2.4 Results

Baseline recordings had a variable duration between 6.5 to 29.2 minutes (9.1 (7.8;12.3) minutes). In 11 interventions, balloon inflation lasted less than 22 minutes (from 4.5 to 21.5 min). In the remaining 6, occlusion was prolonged for more than 100 min (range 104.5 to 151 minutes), conforming the long-occlusion group. In this study, however, the TWA phenomenon was only characterized during the acute phase of ischemia (up to minute 30).

There was a significant increase in heart rate during the first minutes of occlusion compared to baseline records (RR=0.57±0.05 s in baseline vs RR=0.52±0.07 s during the first minute of occlusion, p=0.008, RR=0.53±0.07 s at minute 5 of occlusion, p=0.041, and RR=0.56±0.09 s at minute 10 of occlusion, NS). Figure 2.2 shows the time evolution of average RR interval along the occlusion period.

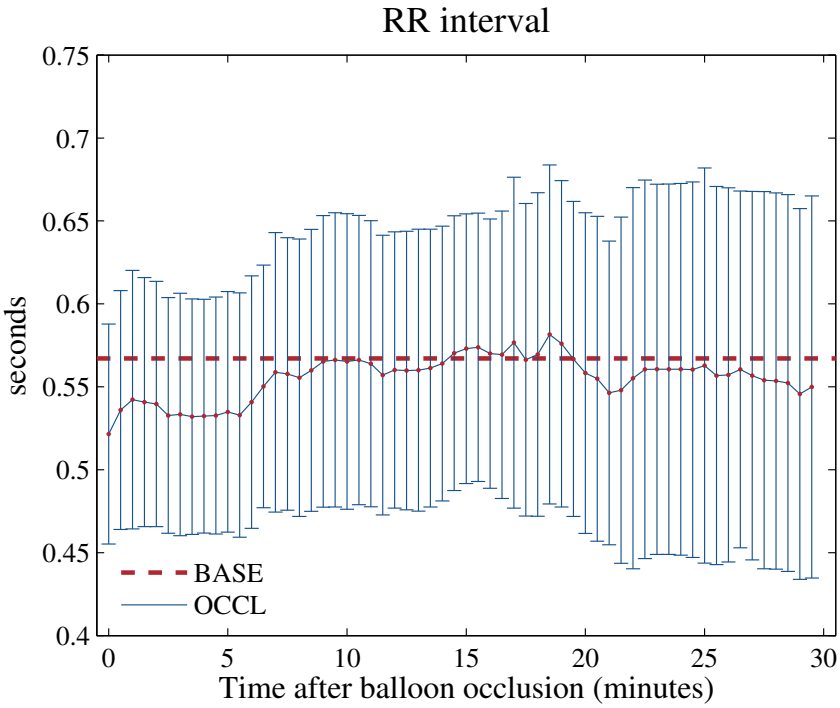

Figure 2.2: Time-course of the RR interval along the occlusion period (mean ± standard deviation). The red dashed line represents the average RR during BASE

2.4.1 Multilead TWA analysis by groups of leads

Body surface ECG

Leads V4 and II were the leads available for the body surface ECG group. After multilead TWA analysis in BASE and OCCL recordings, TWA episodes were detected in 14 out of 17 OCCL recordings (82.3%), but only in 3 BASE recordings (17.6%). In occlusion, maximum TWA amplitude ranged from 3.7 μV to 163.1 μV (32.0 (20.4;67.4) μV) and lasted for 6.2 (2.9;8.5) minutes on average. TWA episodes appeared 3.0 (1.7;6.9) minutes

Table 2.1: Number of records with TWA during baseline (BASE) and occlusion (OCCL) phases.

	BASE (%)	**OCCL** (%)
ECG	3 (17.6%)	14* (82.3%)
CS	3 (17.6%)	13* (76.5%)
EPI	1 (20%)	3 (60%)
RV	4 (23.5%)	11* (64.7%)
LV	2 (11.8%)	13* (76.5%)

*: p<0.05 BASE vs OCCL.

Table 2.2: Results of multilead TWA analysis by locations in occlusion recordings.

	TWA onset (min)	**TWA duration** (min)	**Maximum amplitude** (μV)
ECG	3.0 (1.7;6.9)	6.2 (2.9;8.5)	32.0 (20.4;67.4)
CS	5.1 (2.1;7.0)	4.5 (1.4;5.3)	188.9 (134.5;290.4)
EPI	3.9 (3.0;4.7)	0.9 (0.6;2.67)	91.42 (72.8;98.8)
RV	3.9 (2.9;14.9)	4.8 (2.6;8.6)	285.5 (125.7;419.4)
LV	3.4 (2.5;5.7)	5.5 (2.4;13.1)	409.6 (95.1;610.0)

after balloon inflation (range: second 7 and minute 24 of occlusion). In the BASE recordings, detected episodes had median maximum amplitudes of 17.7 (14.5;155.5) μV and a median episode durations of 60 (52;74) s.

Coronary Sinus

The three unipolar leads (two distal and one proximal) located on the coronary sinus conformed the CS group. After multilead analysis, TWA episodes were detected in 13 out of 17 OCCL recordings (76.5%), but only in 3 pigs during the baseline conditions (duration of 36, 37 and 170 s). In OCCL, the maximum amplitude of TWA ranged from 44.5 μV to 348.3 μV (188.9 (134.6;290.4) μV). The onset of TWA episodes ranged between 8 seconds

and 11.6 minutes after inflation (5.1 (2.1;7.0) minutes) and lasted for 4.5 (1.4;5.3) minutes.

Epicardial space

Unipolar EGM signals for this location of electrodes were recorded in only 5 out of 17 animals. In this case, 1 BASE recording had TWA detected during 31 seconds, with a maximal amplitude of 155.9 μV. Regarding to OCCL recordings, TWA was detected only in 3 out of 5 pigs (60%). The maximum detected TWA amplitude in each recording was 54.4, 106.3 and 91.2 μV. The onset of the episodes was at 2, 3.9 and 5.5 minutes after inflation, with a duration of 56 seconds, 4.40 minutes and 14 seconds, respectively.

Right Ventricle

Analyzing TWA in unipolar EGMs recorded on the right ventricle (two distal and one proximal leads), we found that 11 OCCL recordings presented TWA (64.7%). At BASE recordings, short TWA episodes (duration less than 1.5 minutes) were detected in 4 of them, with an amplitude of 474.13() μV. Maximum TWA detected amplitude in OCCL ranged from 98.2 to 1960 μV (285.5 (125.7;419.4) μV). The onset of TWA episodes was, on average, 3.9 (2.9;14.9) minutes after balloon inflation, with a duration ranging from 53 sec to 14.9 minutes (4.8 (2.6;8.6) minutes).

Left Ventricle

Finally, the multilead analysis of all left-ventricle intracardiac leads (two distal and one proximal) was performed to detect alternans. TWA was found in 13 out of 17 occlusion recordings (76.5%). In this group, TWA episodes lasted, on average, 5.5 (2.4;13.1) minutes, ranging from 1 to 21.5 minutes, with a median amplitude of 409.6 (95.1;610.0) μV. As for the onset of TWA episodes, they appeared between 10 sec and 23.7 minutes (3.4 (2.5;5.7) minutes) after balloon inflation. During baseline, only in 2 (11.8%) BASE recordings had TWA, during 43 and 144 s respectively.

TWA prevalence and characterization of TWA episodes by locations are summarized on Table 2.1 and Table 2.2, respectively.

2.4.2 Time-course analysis

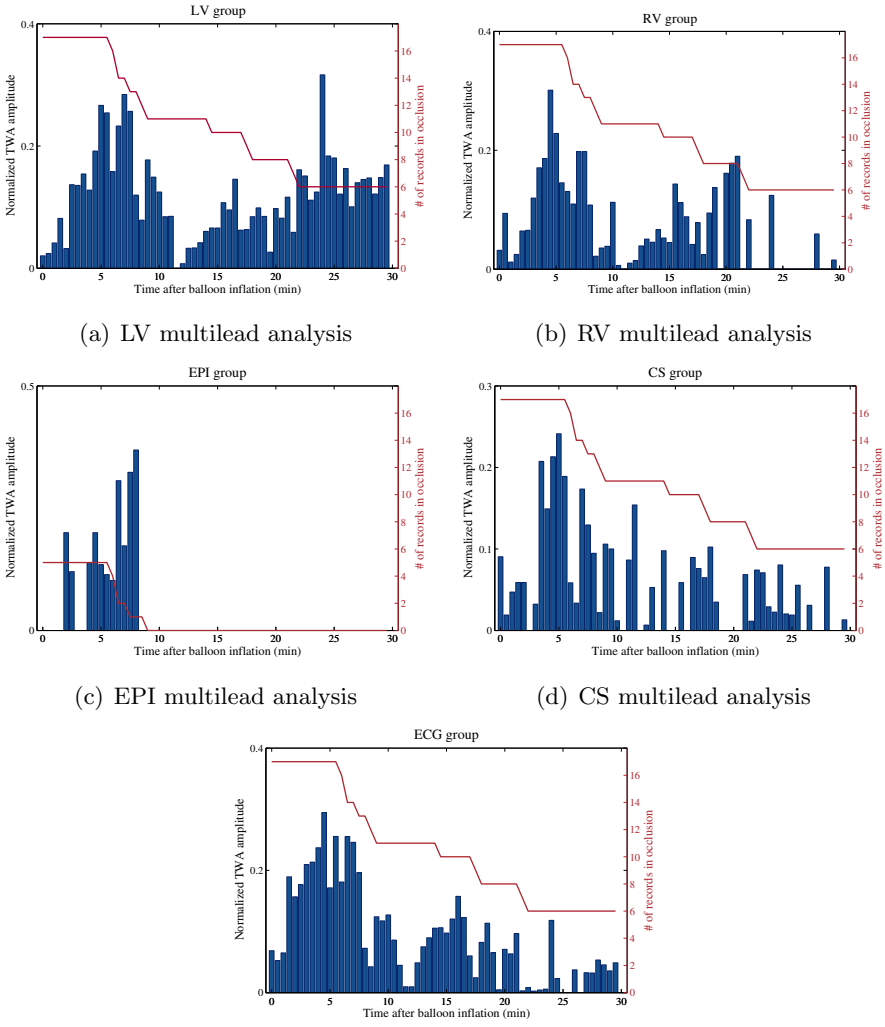

(a) LV multilead analysis

(b) RV multilead analysis

(c) EPI multilead analysis

(d) CS multilead analysis

(e) Body surface ECG multilead analysis

Figure 2.3: Time-course of normalized TWA amplitude along the occlusion period for each multilead study. The red line represents the total number of available recordings at any time.

Figure 2.3 shows the average time-course of normalized TWA amplitude during occlusion in all multilead studies. After averaging V_{alt} every 30 s, each individual time course was normalized respect to its maximum amplitude attained along the occlusion, so as the maximum is one in all the normalized time-courses. Then, all individual profiles were averaged to

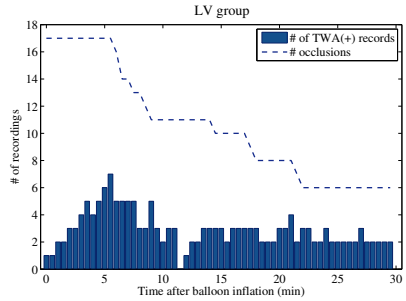

(a) LV multilead analysis

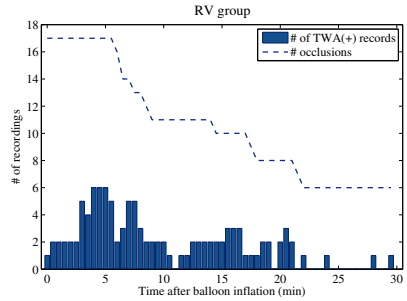

(b) RV multilead analysis

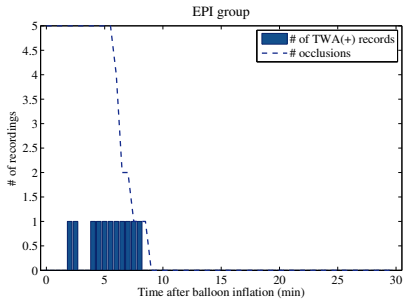

(c) EPI multilead analysis

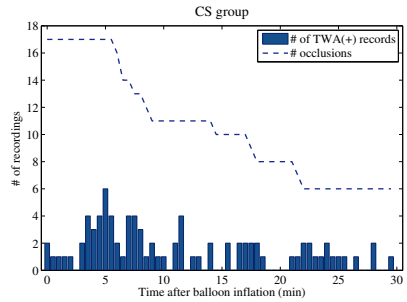

(d) CS multilead analysis

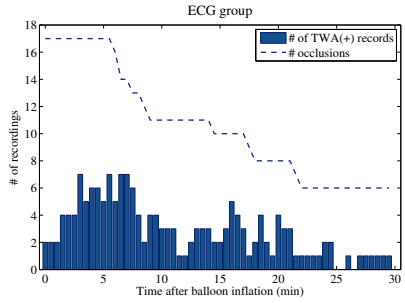

(e) Body surface ECG multilead analysis

Figure 2.4: Number of recordings with TWA at a given time after balloon inflation in each multilead study. The blue-dashed line represents the total number of recordings with occlusion at any time.

characterize the average TWA progression along the occlusion period. A two-peaked pattern can be observed in all locations: a first maximum is reached around 5 minutes after balloon inflation. Then, the mean amplitude decreases and grows again to attain a second peak around 15-17 minutes after the onset of occlusion (note that EPI records are all of them shorter than 9 minutes and, therefore, the second peak is not visible in this group).

The number of recordings with detected TWA at a given time instant along the occlusion is shown in Figure 2.4. The time-course presents a pattern similar to the one for amplitude: a first absolute maximum is achieved around minute 5 after the onset of occlusion. Afterwards, this number decreases and it usually remains stable with 1-4 recordings until 30 min of occlusion.

2.4.3 TWA waveform

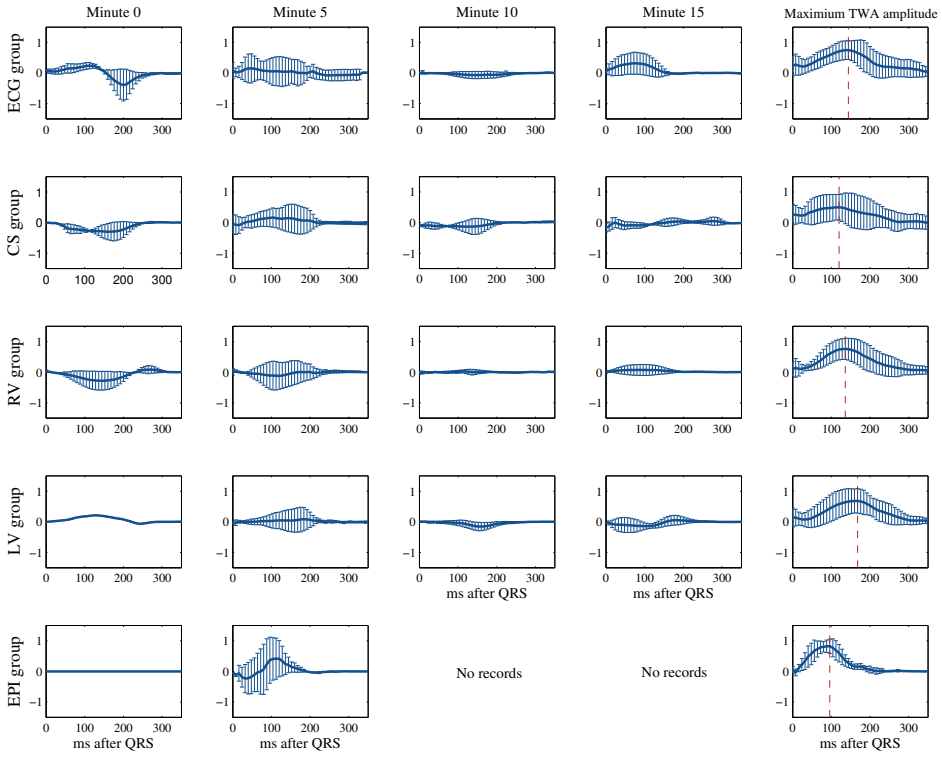

Figure 2.5: Evolution of the normalized TWA waveform along the occlusion period by groups of leads (from top to bottom, ECG, CS, RV, LV and EPI analyses, respectively), represented as mean ± standard deviation. Average TWA waveforms are represented from QRS fiducial point (milliseconds). The red dashed line indicates the position of peak amplitudes.

Figure 2.5 illustrates the evolution of the normalized TWA waveform (represented as mean ± standard deviation for each sample) measured at different time instants along the occlusion, and for each multilead analysis.

Average TWA waveform, represented from the QRS fiducial point up to the end of the T-wave, was computed at minute 0, 5, 10, and 15 of occlusion and at the time of maximum TWA detected amplitude. Before averaging, all TWA waveforms were normalized with respect to the maximum amplitude. To do that, the TWA waveform corresponding to the maximum detected V_{alt} within the occlusion recording was first identified. Then, all waveforms (i.e, at minute 0, 5, 10, 15 and maximum V_{alt}) were normalized with respect to the peak amplitude of the maximum one.

We observed that the TWA phenomenon at the maximum amplitude is distributed earlier within the repolarization phase in the epicardial space (Figure 2.5, last column). It is remarkable that the maximum amplitude in this case, 96 ms after QRS fiducial point, appears before than in the other locations. On the contrary, this peak appears later in EGMs from the left ventricle than in the rest of locations (168 ms after QRS point).

2.4.4 Sensitivity for TWA detection by groups of leads

The sensitivity of TWA detection in each group of leads was also evaluated. To do that, we need to define a *gold standard*. As there is no annotation available, we considered TWA present at certain instant (k beat) if it was detected by any of the 5 multilead analysis. That is, if the statistic $Z_g(k) \geq \gamma_g$ where $g = \{\text{ECG}, \text{CS}, \text{EPI}, \text{LV}, \text{RV}\}$, for at least one group, and this will be our *gold standard* (a logic OR of the 5 multilead detection analyses, 4 in the cases where EPI recordings were not available). The threshold γ_g was set to have a specificity rate of 95% in each group of leads, as explained in section 2.3. This way to select the *gold standard* relies on the hypothesis that intracardiac EGMs reliably detect TWA appearing locally, while TWA appearing in other zones may not be captured, in contrast to what happens in surface ECG.

The TWA rate (TWAR) was defined as the ratio between the total number of beats positive for TWA in our *gold-standard* and the total number of beats of the occlusion period. Additionally, the sensitivity ($\hat{Se}$) of each multilead group was estimated, using the previously defined threshold γ_g, as the ratio between the total number of beats positive for TWA and the total number of beats positive for TWA in our *gold-standard*.

Table 2.3 reports the TWAR and the $\hat{Se}$ of each multilead analysis obtained for each occlusion recording. Each occlusion recording had an average

Table 2.3: TWA rate (TWAR) and estimated sensitivity ($\hat{Se}$) obtained in each multilead analysis.

	OCCL		**ECG**	**CS**	**EPI**	**RV**	**LV**
ID	**beats**	**TWAR**(%)	$\hat{Se}$(%)	$\hat{Se}$(%)	$\hat{Se}$(%)	$\hat{Se}$(%)	$\hat{Se}$(%)
1	892	9.2	100	0	0	0	0
2	844	50.7	77.3	31.5	7.9	0	63.1
3	697	24.2	0	30.8	0	0	69.2
4	619	16.3	0	0	100	0	0
5	1029	53.7	100	0	96.9	97.8	52.1
6	1118	94.4	98.3	12.7	NR	89.1	34.4
7	1594	67.4	83.3	39.4	NR	86.4	98.4
8	2385	83.5	93.5	49.0	NR	83.4	82.8
9	1954	52.9	92.5	49.7	NR	51.2	58.3
10	2448	30.1	95.4	22.3	NR	43.3	66.3
11	3808	50.2	42.4	20.3	NR	4.9	97.1
12	2413	52.6	45.9	17.9	NR	8.7	84.8
13	2760	26.1	43.3	27.1	NR	16.1	74.8
14	2844	8.7	13.4	99.2	NR	18.6	22.3
15	825	0	-	-	NR	-	-
16	1360	19.0	27.9	72.1	NR	0	0
17	4181	44.4	58.9	77.0	NR	49.2	50.8
Record average		40.2	60.7	34.3	41.0	34.32	53.4
Gross Average		42.4	69.1	37.6	50.3	46.0	69.0

NR: No recording available

of 1869±1100 beats (total of 31771 beats). TWA was present in the 42.4% of the total beats during occlusion, with an average TWAR per recording of 40.2%. The multilead analysis of the ECG leads and the LV leads presented the best sensitivity (69.1% and 69.0%, respectively). On the contrary, the worst performance is obtained in the analysis of CS leads (37.6%). To note, the multilead ECG analysis had a $\hat{Se}$= 100% in two analyzed recordings, being higher than 90% in 6 of them. However, there were two recordings in which TWA was not detected using the ECG leads, while it was detected by the CS and LV analyses.

Finally, multilead analysis was compared to the analysis of individual leads in terms of $\hat{Se}$. In each anatomical location, single-lead TWA analysis was performed by individually processing the most distal and proximal unipolar EGM leads, as well as two bipolar EGM leads: one with a far-field configuration (subtracting two distant electrodes), and the other with a near-field configuration (from two adjacent electrodes).

Figure 2.6 shows $\hat{Se}$ rate of the multilead and single-lead TWA analysis. For each group of leads, the first bar corresponds to the multilead analysis,

followed by the single-lead analysis of the unipolar distal and unipolar proximal leads (denoted as 'ud' and 'up' respectively) and the two bipolar, near and far field configurations (denoted as 'bn' and 'bf', respectively). In the case of the ECG group, single-lead analysis of leads V4 and II are included. In all groups of leads except for the RV, multilead analysis clearly provided the best $\hat{Se}$. With respect to the RV leads, the highest $\hat{Se}$ is obtained when the proximal lead was analyzed ($\hat{Se}$ =49.0%), followed by the multilead analysis ($\hat{Se}$ =46.0%). The proximal lead is in all cases more sensitive than the distal one and the performance dramatically worsened when using the near-field bipolar lead.

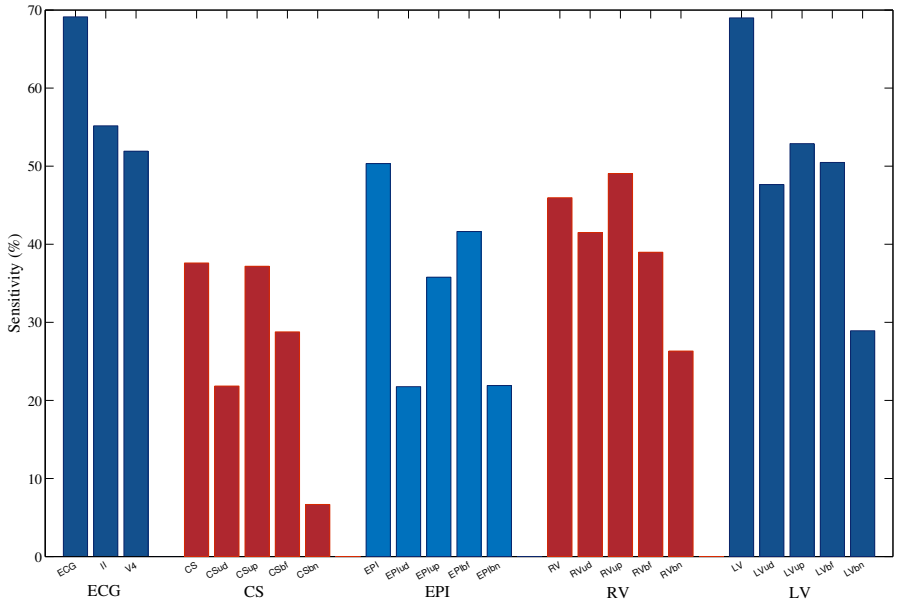

Figure 2.6: Sensitivity of multilead (first bar) and single-lead analysis (unipolar distal and proximal leads, followed by bipolar near-field and far-field leads) for each group of leads: ECG, CS, EPI, RV and LV.

2.4.5 Optimal intracardiac detection of TWA

Another objective of this study was to find an optimal intracardiac-lead configuration that maximizes the sensitivity of TWA detection, while using a minimum number of electrodes.

In order to do that, 3 electrodes from each clinical accessible locations, CS and RV, were processed using the multilead πCA method: the 2 most distal leads (denoted with subscripts: d, and d') and the most proximal one (denoted with subscript p) for each region. LV and EPI anatomical locations were considered not to be suitable for locating electrodes from implantable devices, as they would present derived risks, including blood clot formation. Sensitivity compared to the *gold standard* was evaluated for all possible lead combinations (from 1 to 6 electrodes) with the aim of minimizing the number of electrodes required to monitor TWA from an implantable device.

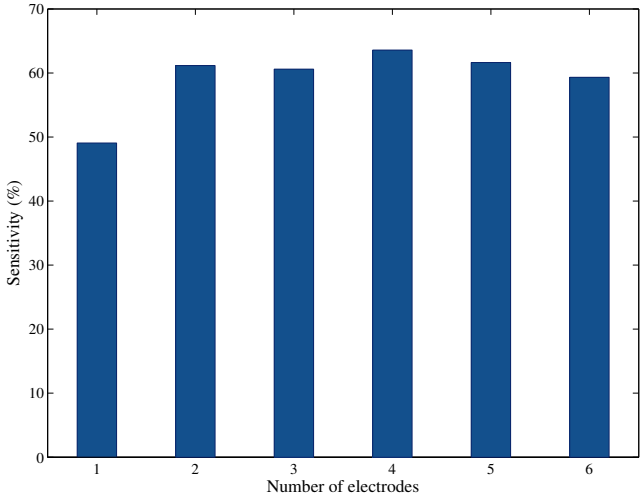

Figure 2.7: Optimal sensitivity ($\hat{Se}$) obtained for each combination of electrodes.

Table 2.4: Optimal combination of leads, $\hat{Se}$ and the median detected TWA amplitude, expressed as median (interquartile range), for the optimal combination of intracardiac leads using from 1 to 6 electrodes. Subscripts mean p=proximal lead, d=distal lead, d'=second most distal lead.

Number of leads	**Leads**	**Best $\hat{Se}$** (%)	**TWA amplitude** (μV)
1	RVp	49.1	51.0 (162.8)
2	RVd, CSp	61.2	117.0 (291.5)
3	RVd, RVp, CSp	60.6	132.2 (316.8)
4	RVd, RVd, CSp, CSd	63.6	210.3 (336.2)
5	RVp, RVd, RVd', CSp, CSd	61.6	221.6 (329.4)
6	RVp, RVd, RVd', CSp, CSd, CSd'	59.3	246.9 (317.9)

Figure 2.7 shows the best $\hat{Se}$ rate obtained for each optimal combination of electrodes, from 1 to 6. $\hat{Se}$ ranged from 49.1% using the optimal single electrode (lead RV proximal) to 63.6% when the optimal quadruplet were used. More detailed information including the optimal combination of leads, $\hat{Se}$ and the median detected TWA amplitude for each optimal combination of electrodes is reported on Table 2.4. Maximum $\hat{Se}$ is achieved using a 4-electrode configuration (63.6%). However, the difference with using 2 or 3 electrodes could be considered negligible (-2.4% and -3%, respectively), with the advantage that only 2 electrodes would be enough in to efficiently detect and monitor TWA. Therefore, combination of the distal RV lead together with the proximal CS lead (a far field configuration analysis) would be chosen as the optimal lead configuration.

2.5 Discussion

In the present chapter, we have performed a comprehensive study and characterization of TWA phenomenon from both body-surface ECG and intracardiac EGM signals using a porcine model of myocardial ischemia. A reliable characterization of TWA from EGM signals was required in order to investigate our second aim: finding an optimal intracardiac lead configuration for a continuous TWA in-vivo monitorization using an implantable device.

TWA during coronary occlusion has been previously characterized both in human and experimental hearts [153, 162, 175, 176] from surface ECG. However, the analysis of TWA from intracardiac signals has been limited to the study of pacing-induced alternans [163–168] and to the best of our knowledge, TWA dynamics on intracardiac signals during prolonged coronary artery occlusion has not been previously described in such detail.

Multilead TWA analysis has been performed by groups of leads recorded at different sites, including two body surface ECG leads (II and V4) and three unipolar EGM leads from 4 different anatomical locations (coronary sinus, epicardial space, right and left ventricles). TWA was detected in all but one occlusion recordings in at least one location. It was present in 14 out of 17 OCCL recordings when analyzing the ECG leads, in 13 recordings when CS and LV leads were processed while only 11 recordings presented TWA on the RV group of leads. Out of the 5 recordings for which epicardial leads were available, 3 of them had TWA.

In the ECG leads, TWA episodes were earlier detected, on average 3 minutes after the onset of occlusion, and lasted for a longer time than in the intracardiac leads. On the other hand, the TWA onset was most delayed in average in the CS group. Maximum TWA amplitudes were detected in LV leads, while TWA amplitude was minimal on the ECG group. This is in agreement with the larger signal amplitude of unipolar EGMs compared to body surface ECG. This results are concordant with what was reported in [167]. In that study, TWA phenomenon was investigated by using the commercial spectral method in a subset of 10 swine from our short-occlusion group (occlusion duration <22 min).

However, the evolution of TWA on the four intracardiac locations along the occlusion has been first characterized here. The two-peaked pattern observed on the average time course in all multilead analyses is concordant with what was previously observed from body-surface ECGs [162]. Interestingly, this biphasic behaviour also coincides with the two phases of increased arrhythmia incidence in a canine myocardial infarction model, previously reported in [177]. These two phases (named Ia and Ib) occur from 2 to 10 minutes after the onset of ischemia and after an arrhythmia-free interval, between minute 12 and 30. A similar time-course was also visible when evolution of alternans waveform along occlusion was studied: normalized amplitudes increased from the first minute to minute 5, being almost close to 0 at minute 10 with a slight increase after 15 min in all locations. When comparing the distribution of alternans at the instant of maximum amplitude within the repolarization phase, i.e, along the whole ST-T complex, it is interesting that TWA is distributed clearly earlier within the ST-T complex in the EPI leads, while it was most delayed at the left ventricle leads.

The results of this study confirmed the improved performance of multilead TWA analysis compared to single-lead analysis. We have also shown that TWA was better detected from the ECG group (highest $\hat{Se}$) than from the invasive EGMs. Among those, unipolar or far-field bipolar EGM leads, capturing far-field activity, are preferable rather than near-field configuration where exclusively local activity is recorded. This was also observed in [167].

Several studies have proposed the utility of TWA detection in EGM signals for VT/VF prediction [164,165,169–171]. Based on these observations, we aimed at finding an optimal lead configuration for TWA detection from

the two clinically suitable locations for ICD lead implantation: the right ventricle and the coronary sinus. Two distal and one proximal lead from each location were selected, and TWA detection of all possible combinations of 1 (single-lead analysis) to 6 leads was assessed. The best sensitivity was obtained using 4 electrodes ($\hat{Se}$=63.6%) but even 2 electrodes were enough for an efficient detection ($\hat{Se}$=61.2%) of TWA, significantly improving the optimal performance obtained when only one CS or RV lead was processed ($\hat{Se}$ = 49.1). Although these rates did not reach the $\hat{Se}$=69.1% obtained by the multilead analysis of the ECG leads, they are still comparable, with the potential clinical impact of TWA monitorization from an ICD device. Using the multilead strategy for TWA analysis, allowed us to optimize the number of leads required for a this porpouse, and only two electrodes will be required to obtain a $\hat{Se}$ >60%. In [167], however, a triangular lead configuration was instead required.

Despite further investigation will be needed for a deeper understanding of the association of TWA and imminent ventricular arrhythmias, detection of TWA from an ICD could potentially help to properly identify a vulnerable substrate prone to VT/VF, efficiently delivering therapy in those patients.

2.5.1 Limitations

Some limitations of the study need to be acknowledged. One limitation of this study is the lack of annotations for TWA presence. Therefore, in order to estimate and compare the sensitivity of each group of leads, we had to define a "*gold standard*" based on the detection made by our method, which may suppose an underestimation of the $\hat{Se}$ rate. On the other hand, the threshold, defined using baseline recordings where TWA is assumed not to be present, was set to obtain a specificity of 95%.

Another limitation relies on the absence of VF episodes during the occlusion period, which impeded the study of the association between the presence TWA and the occurrence of ventricular arrhythmias. Second, this study has characterized ischemia-induced TWA in intracardiac leads. However, TWA in non-ischemic conditions may have different characteristics, and should be studied specifically. Finally, myocardial ischemia was locally induced by the occlusion of the proximal LCX artery. Some of the results and conclusions of our study (in particular, the optimal sites for intracar-

diac TWA detection) may be different for other occlusion sites and ischemic areas.

2.6 Conclusions

In this chapter, temporal and spatial TWA dynamics during acute LCX coronary occlusion have been investigated from both, ECG and intracardiac EGM signals recorded at different anatomical locations. Although ECG leads presented the best sensitivity for TWA detection, an optimal combination of two unipolar leads located at the right ventricle and the coronary sinus can be an efficient solution for real-time TWA detection from an implantable device, such as an ICD.

Chapter 3

Assessment of repolarization instability induced by simulated microgravity by means of T-wave alternans

3.1 Motivation

Prolonged weightlessness condition leads to cardiovascular deconditioning, inducing changes in autonomic control of cardiovascular system [90]. This arises several alterations in the organism, as detailed in section 1.4.5, with potential impact also in cardiac electrical activity, and cardiac rhythm disturbances may be originated if cardiac repolarization is adversely influenced.

In particular, anecdotal data of cardiac arrhythmias and conduction disorders during spaceflight and higher incidence of VPCs [178], together with reports that long-duration spaceflight, but not short-duration ones, led to the prolongation of the QTc interval in crewmembers [100, 179], suggested that weightlessness can potentially increase arrhythmia susceptibility, and related SCD risk, in astronauts. More recently, spatial and temporal heterogeneity of ventricular repolarization induced by short (5-days) [180] and long duration (90-days) [181] head-down bed-rest (HDBR) were investigated. Both studies confirmed that HDBR induced a reversible increase in ECG repolarization heterogeneity by an increase in QRS-T angle accompanied by a decrease in the spatial ventricular gradient (SVG), thus supporting the hypothesis of increased ventricular arrhythmic risk. In addition, the T wave amplitude was found markedly reduced with HDBR.

Only one study [182] reported results relevant to TWA induced by 9 to 16 days of HDBR in 24 healthy males, concluding that this sustained immobilization head-down condition could lead to the development of sustained alternans. However, the heterogeneity of the observed subjects' response, and of the HDBR duration, did not allow drawing final conclusions about the potential negative effects of HDBR on cardiac electrical stability.

The general multilead scheme for TWA analysis presented in the previous chapter (section 2.3) included a TWA detection stage. This stage implies the definition of a threshold, which is not easily extrapolated among different studies, as it depends on multiple factors (number of leads, the analysis window or even the test condition). As an alternative, a new approach omitting the detection stage, suitable for the analysis of long-term ambulatory ECG recordings has been proposed in [157]. This study used the long-term averaging approach to longer periods for TWA quantification, under the hypothesis that it will produce a reliable measurement of average TWA activity, less sensitive to noise, in a fully automatic way. This appro-

ach presents the advantage of not requiring the posterior visual verification needed when other methodologies, such as the MMAM, are used.

Based on all previous observations, we hypothesized that HDBR induces reversible increase in ventricular repolarization heterogeneity that could be manifested by an increase on TWA, indicating an increased ventricular arrhythmic risk. The objective of this chapter is, therefore, to assess the effects of short- (5 days), mid- (21 days) and long- (60 days) duration HDBR on TWA. TWA will be evaluated before, during and after the immobilization period, by the long-term averaging technique of ECG Holter recordings (night period) and the short-term averaging of ECG tracings obtained during two stress manoeuvres (head-up tilt-table and bicycle exercise tests).

3.2 Materials

3.2.1 Head-down bed-rest experiments

ECG recordings acquired during short-duration (SHORT, five days), mid-duration (MID, twenty-one days) and long-duration (LONG, sixty days) HDBR studies conducted in the context of the ESA HDBR strategy were available for the present study. These campaigns have been hosted by two specialized centers: the German Aerospace Center (Deutsches Zentrum für Luft- und Raumfahrt e.V, DLR) in Cologne (Germany) and the Institut de Médecine et de Physiologie Spatiales (MEDES) in Toulouse (France).

An only-male population was recruited, after multiple screening and psychological tests, for two sedentary short-duration, two mid-duration and two long-duration HDBR campaigns. The choice of including only males was driven by ESA standardization plan. Subjects had no history of cardiovascular disease and were not taking medications of any kind. All volunteers provided written informed consent to participate in the study approved by the respective Ethical Committee for Human Research at both hosting institutions.

For SHORT and MID campaigns, the protocol was designed as a cross-over study: every subject repeated the HDBR two or three times, one with no intervention (control) and one or two with specific countermeasures (CMs) applied during HDBR, with a washout period (1.5 months for SHORT and 4 months for MID duration campaigns) between the end of

one repetition to the onset of the next one. The order of inclusion in the intervention group was randomly assigned to each subject. Due to the long washout period (> 2 years) required in the case of long-duration recruitments, a multi-group design (one control and one intervention group) was used in LONG campaigns.

The protocol for each campaign included some days of acclimation to the bed rest facility (referred as the PRE period). Those days of baseline data collection (BDC) are denoted as BDC-X, where X stands for the day before the beginning of the provoking manoeuvre (i.e, the uninterrupted HDBR period). During the HDBR, all subjects adhered to a monitored, strict 6° negative head-down tilt bed-rest, 24h a day for 5, 21 or 60 days in SHORT, MID and LONG campaigns, respectively. In this period, subjects were under a strictly controlled diet to prevent body weight changes and were awakened at 6:30 AM and prompted to start sleeping at 11:00 PM each day, with no napping allowed during the day. After completing the HDBR portion of the study, subjects remained in the facility for some additional days (referred as POST). Those days are denoted as R+0 to R+X, where R+0 is the day starting with termination of the immobilization period by the orthostatic tolerance (OT) test. During the PRE and POST periods, lying on bed during the day was not allowed. Figure 3.1 schematically shows the protocols of SHORT, MID and LONG campaigns. Decisions regarding the specific experimental protocol implemented for each campaign were driven by the ESA standardization plan, also based on the need to accommodate multiple experiments from different researchers.

Short-duration HDBR campaigns

One SHORT campaign (3 repetitions) was performed in MEDES facility (ESA acronym: BR-AG1), in which 12 subjects (age range 21-41 years) were enrolled. An additional SHORT campaign (3 repetitions) was organized in DLR (ESA acronym: SAG), including 10 subjects (age range 25-44 years). Applied interventions to be tested as CMs consisted in: (i) continuous 30 min or (ii) intermittent 6x5 min short-arm daily centrifugation periods in BR-AG1; and (i) 25-min of daily upright quiet standing and (ii) 25-min of locomotion replacement training in SAG.

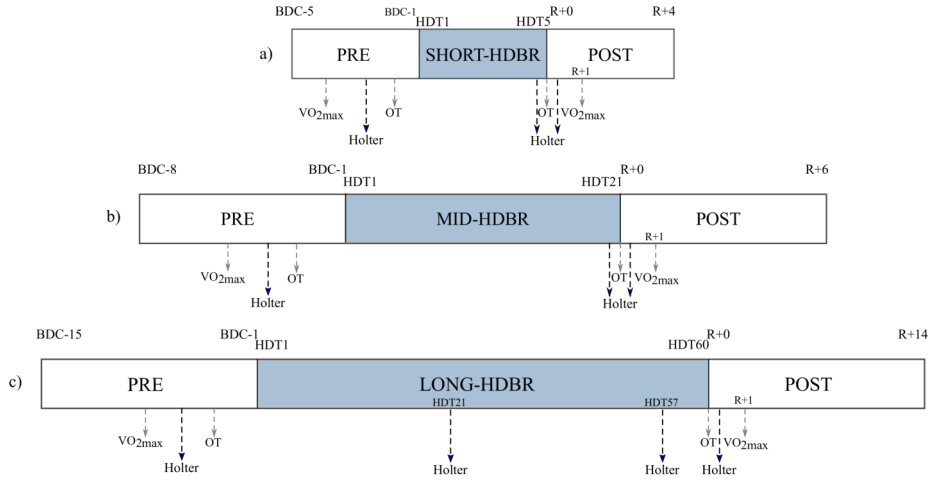

Figure 3.1: Schematic and timing of the OT and VO_{2max} tests and Holter recording acquisitions, for the (a) SHORT (b) MID and (c) LONG duration HDBR campaigns.

Mid-duration HDBR campaigns

One MID campaign (3 repetitions) was performed in MEDES facility (ESA acronym: MNX), in which 12 subjects (age range 20-44 years) were enrolled. An additional MID campaign (2 repetitions) was organized in DLR (ESA acronym: MEP), including 10 subjects (age range 23-42 years). Applied interventions to be tested as CMs consisted in: (i) resistive vibration exercise (RVE) and (ii) RVE + high protein intake (1.8 g/kg body weight/day+0.6 g/kg body weight/day of whey protein) and alkaline salt in MNX; (i) high protein intake (1.2 g/kg body weight/day+0.6 g/kg body weight/day of whey protein) and alkaline salt in MEP.

Long-duration HDBR campaigns

One LONG campaign was performed in DLR (ESA acronym: RSL), including 24 subjects (12 in control, 12 in the intervention group, age range 20-45 years). Applied intervention to be tested in this case consisted in reactive jumps in a sledge jump system, as a countermeasure for muscle and bone loss.

Table 3.1: Summary of ESA head-down bed-rest experiments included in this study.

HDBR	ESA acronym	Location	Participants	CM
SHORT	BR-AG1	MEDES	12(x3)	30' Continuous centrifugation 6x5' Intermittent centrifugation
SHORT	SAG	DLR	10(x3)	25' Passive exercise (Standing) 25' Active exercise
MID	MNX	MEDES	12(x3)	RVE RVE + protein intake
MID	MEP	DLR	10(x2)	Protein intake
LONG	RLS	DLR	24(x1)	Active exercise (jumps)

For the SHORT campaign, all 22 subjects in sedentary HDBR completed the experiments. For the MID, only 20 out of 22 subjects in sedentary HDBR completed the experiments (1 withdrawal in MNX and 1 in MEP). In LONG, one subject dropped out on BCD-4 for medical reasons not related to the study. In the study presented in this chapter, only the data obtained when the subjects were included in the sedentary control group will be analyzed for each campaign, to allow for comparison despite the different campaigns and adopted countermeasures. Therefore, the final study population is composed by 22 subjects in SHORT, 20 subjects in MID and 11 subjects in LONG. Anthropometric data of the final study population for each campaign is presented in Table 3.2.

Table 3.2: Anthropometric data of subjects participating in SHORT, MID and LONG duration HDBR campaigns.

	SHORT (n=22)	MID (n=20)	LONG (n=11)
Age (years)	31.6 (25.4;35.8)	32 (28.25;40)	27 (24;31.5)
Weight (Kg)	76.2 (73.6;80.4)	68.2 (63.9;76.8)	76.5 (68.6;83.3)
Height (m)	1.79 (1.75;1.82)	1.77 (1.74;1.83)	1.80 (1.78;1.83)

3.2.2 ECG acquisition

Twenty-four-hour Holter ECG recordings (H12+, Mortara Instrument Inc., Milwaukee, WI, 12 leads, 1000 Hz sampling frequency) were acquired at PRE, the last day of the HDBR period and at POST. In LONG, additional

Holter acquisitions recorded along the HDBR were also available. Additionally, ECG signal tracings acquired during orthostatic tolerance (OT) test by head-up tilt-table and during bicycle exercise test for maximum oxygen uptake (VO_{2max}) assessment, at both PRE and at POST periods (R+0 and/or R+1, as specified above) were also analyzed. The timing of the Holter recording acquisition, as well as of the OT and VO_{2max} tests for each subject and at each campaign is indicated in Figure 3.1.

Orthostatic tolerance test

At R+0, once the cardiovascular monitoring equipment was connected, the subjects first spent a period of at least 5 min in a supine position on a tilt board with their lower body enclosed in a lower body negative pressure (LBNP) chamber, which was not pressurized initially. Thereafter, the tilt angle was changed to +80° head-up tilt and maintained so far for 30 min in SHORT, and for 15 min in MID campaigns. After this time, if the orthostatic test was not yet ended, the pressure in the LBNP chamber was changed by -10 mmHg decrements at 3-min intervals until the test was terminated. Termination criteria included signs of pre-syncope (tunnel vision, pallor, sweating or malaise, sudden bradycardia, hypotension or undue lack of subject response to questions) and/or at the request of the subject (see [183] for more details). Orthostatic tolerance time (OTT) was defined as the time from head-up tilt until stop criteria was reached. At the end of the test, supine position was restored. The same protocol was performed during the ambulatory period (PRE) to assess OTT at baseline.

Exercise stress test

Maximum oxygen uptake (VO_{2max}) was determined during incremental dynamic leg exercise on a cycle ergometer (Ergometrics 800S, Ergoline, Bitz, Germany), before (PRE) and after HDBR (at R+1, after at least 26h from discontinuation of HDBR, except for the SHORT BR-AG1 campaign, in which it was performed at R+0, six hours after the OT test). Breathe-by-breathe VO_2 was recorded with an Oxycon Pro metabolic cart (E. Jaeger, Hochberg, Germany). VO_{2max} was determined during the subject selection. For each VO_2 recording, VO_{2max} was calculated to be the highest value in a 60 s moving average window. The subject exercised for steps of 5 min at power outputs estimated to require 25, 50 and 75% of VO_{2max}. Thereafter,

the power output was increased by +25 W every minute until exhaustion, i.e. when the required cycling cadence of >70 rpm was no longer maintained.

3.3 Methods

3.3.1 TWA analysis

Preprocessing

As in the previous study, preprocessing of ECG recordings included QRS detection and baseline wander removal in each lead using a cubic spline interpolation technique. Then, ECG was low-pass filtered and down-sampled to 125 Hz to reduce noise and the computational cost of TWA analysis. Finally, a segmentation of ventricular repolarization phase (ST-T complex) was done at each beat, by defining a fixed interval of 350 ms (reduced to 44 samples after decimation) after the end of the QRS complex.

Short-term averaging

Both OT and VO_{2max} tests are characterized by a transient stress-induced cardiac response, consequence of the passive head-up tilt or exercise, with the subsequent recovery phase (<40 min the whole test).

First, for the TWA analysis in the ECG recordings acquired during the OT and VO_{2max} tests, three specific intervals were selected for further processing:

for **OT test**: 1) baseline (BAS): the 4 minutes preceding the head-up tilt; 2) TILT: the first 4 minutes from head-up tilt; 3) recovery (REC): the first 4 minutes once supine position was restored at test termination.

for VO_{2max} **test**: 1) baseline (BAS): the 5 minutes preceding the start of the test, while the subject was already instrumented and sit on the cycloergometer but not pedaling; 2) EX1: the 5 minutes of exercise at 25% of workload; 3) EX2: from minute 5 to minute 10 of the test at 50% of workload. The analysis was limited up to a heart rate limit of 130 beats/min, to avoid the possible mechanical interference

at twice of the pedaling cadence (variable, but $\geq$ 70 rpm) in the ECG signal, which could induce mechanical alternant components at the TWA frequency [184].

Automatic TWA analysis was performed in 3 steps: (1) selection of signal segments suitable for automatic analysis, (2) estimation of the TWA amplitude in each segment and (3) computation of the index of average alternans activity that characterizes each analyzed interval.

The resulting preprocessed ECG signal was processed for automated TWA analysis in segments of 32 consecutive beats with a 50% overlap. To exclude from the analysis possible transients present in the signal, a stability criterion based on HR and baseline wander was defined. To be considered suitable for the automatic analysis, a segment must accomplish that (i) the difference between the maximum and minimum instantaneous HR in the segment is less than 20 beats/min and (ii) at least 80% of the beats fulfilled two conditions: the difference between the i^{th} and the $(i-1)^{th}$ RR intervals is less than 150 ms and with a difference between the baseline voltage measured at the PQ segment in that beat and the one measured in the preceding beat lower than 300 μV.

The method to estimate the TWA waveform is based on [157]. The 8 independent standard leads (V1 to V6, I and II) were linearly combined using πCA, in order to maximize the TWA content in the combined lead [156]. Then, the LLRM [153] was applied in the new combined lead to estimate the TWA waveform of each segment. For each k^{th} suitable signal segment, it gives a TWA waveform $\boldsymbol{y}_k$, denoted as

$$\boldsymbol{y}_k = [y_k(1), \ldots, y_k(N)]^{\mathrm{T}}, \tag{3.1}$$

with N the total number of samples within the ST-T complex. The TWA amplitude associated to the k^{th} segment, $V_{\mathrm{TWA}}(k)$ was defined as the absolute value of the mean of the TWA estimated waveform, $\boldsymbol{y}_k$.

Stress induced during both OT and VO_{2max} tests is known to reflect transients and noise on ECG signal tracings. This non-stationarity together with the limited duration of the tests could compromise the averaging performance. Consequently, we proposed an adapted short-term averaging approach for the analysis of TWA under this particular conditions.

To eliminate from the TWA amplitude the potential amount of noise and other non-alternant ECG components which could appear and interfere

in $V_{\mathrm{TWA}}(k)$ we defined a new measurement:

$$V'_{\mathrm{TWA}}(k) = V_{\mathrm{TWA}}(k) - V_{\mathrm{PWA}}(k), \tag{3.2}$$

where $V_{\mathrm{PWA}}(k)$ is the alternant component present in the P-wave of the ECG, and was computed similarly to $V_{\mathrm{TWA}}(k)$. Assuming noise as uniformly distributed within the whole beat, $V_{\mathrm{PWA}}(k)$ represents an estimate of the noise level in the TWA measurement. Therefore, $V'_{\mathrm{TWA}}(k)$ measures TWA amplitude over the noise level. See Figure 3.2 for illustration.

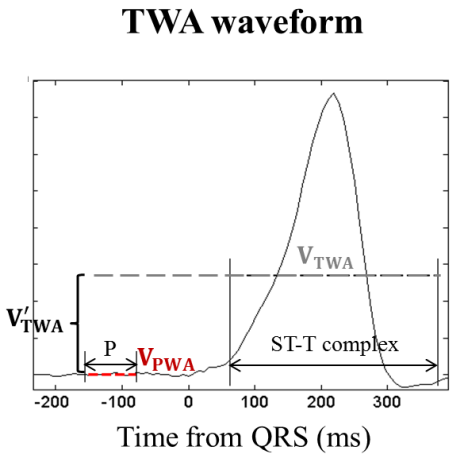

Figure 3.2: Illustration of an estimated TWA waveform and the measurement of V'_{TWA}.

Based on previous observations that HDBR induces modifications in the T-wave morphology, in particular by reducing the maximum T-wave amplitude and T-wave area [180,181], we introduced also a normalized measurement of TWA to take into account possible effects of these changes on TWA obtained at PRE and at POST bed-rest. The normalized TWA amplitude at each segment was defined as

$$V_{\mathrm{TWAn}}(k) = \frac{V'_{\mathrm{TWA}}(k)}{V_{\mathrm{T}}(k)}, \tag{3.3}$$

where $V_{\mathrm{T}}(k)$ represents the mean value of the first principal component in the ST-T complex computed by applying the PCA over the same 8 standard leads. Finally, the index of short-term average anternans (IAA^{ST}) and the index of short-term average normalized alternans ($IAAn^{\mathrm{ST}}$) were computed by averaging all suitable segments (all $V'_{\mathrm{TWA}}(k)$ and $V_{\mathrm{TWAn}}(k)$, respectively) at each defined interval.

Long-term averaging of Holter recordings

In order to avoid potential confounding effects (subjects were asked to complete several activities during the day), only the night period (23.00-06.00 h) was selected from the 24-hour Holter recording for the subsequent analysis. These ECG signals were processed in segments of L =128 consecutive beats (with 50% overlap). The stability criteria for segment's selection defined in the previous section was maintained. The TWA waveform associated to the k^{th} ECG segment, $\boldsymbol{y}_k$, was estimated following the same multilead approach.

The non-visible microvolt range of TWA, sometimes comparable to the noise level, makes the TWA estimation a challenging task. In those cases, the locally estimated alternans waveform $\boldsymbol{y}_k$ may have an important noise component that should be attenuated in order to properly measure TWA. At this point, a novel methodological step for the computation of the long-term averaging of TWA activity was included in the analysis, consisting on the phase alignment of all TWA estimated waveforms, associated to the K suitable ECG segments, before averaging. This step is needed since the estimated TWA waveform $\boldsymbol{y}_k$ may not have the same polarity, and therefore might cancel out if they are directly averaged.

First, a detrended version of each $\boldsymbol{y}_k$, denoted as $\boldsymbol{y}_{d,k}$ was computed, whose samples are:

$$y_{d,k}(n) = y_k(n) - (a_k + b_k n) \tag{3.4}$$

where the coefficients a_k and b_k were chosen as the ones with the best least-squares fit to the samples of $y_k(n)$. This step aims to eliminate any possible residual baseline component at the alternans frequency. Then, the correlation matrix of all suitable segments, $\mathbf{R}_{\mathbf{Y}_d}$, was estimated as

$$\mathbf{R}_{\mathbf{Y}_d} = \frac{1}{K}\mathbf{Y}_d\mathbf{Y}_d^{\mathrm{T}}, \tag{3.5}$$

being K the total number of suitable segments for the analysis and $\mathbf{Y}_d$ the data matrix built by concatenating all of them $\mathbf{Y}_d = \left[\boldsymbol{y}_{d,1}, \ldots, \boldsymbol{y}_{d,K}\right]$.

The dominant alternans waveform was obtained as the first principal component of the spatial correlation matrix [185], by solving the eigenvalue equation:

$$\mathbf{R}_{\mathbf{Y}_d}\mathbf{w}_1 = \lambda_1\mathbf{w}_1 \tag{3.6}$$

where λ_1 is the largest eigenvalue of $\mathbf{R}_{\mathbf{Y}_d}$ and $\mathbf{w}_1$ its corresponding eigenvector. At this point, the phase-aligned waveform, denoted as $\boldsymbol{y}_k^a$, was estimated as:

$$\boldsymbol{y}_k^a = \text{sign}\left(\boldsymbol{y}_{d,k}^{\mathrm{T}}\mathbf{w}_1\right)\boldsymbol{y}_k. \tag{3.7}$$

Consequently, $\boldsymbol{y}_k^a = \boldsymbol{y}_k$ if $\boldsymbol{y}_{d,k}^{\mathrm{T}}\mathbf{w}_1 \geq 0$ and $\boldsymbol{y}_k^a = -\boldsymbol{y}_k$ if $\boldsymbol{y}_{d,k}^{\mathrm{T}}\mathbf{w}_1 < 0$. In other words, if the waveform $\boldsymbol{y}_k$ has the same polarity as the dominant $\mathbf{w}_1$, it will remain unchanged, while if it has the opposite polarity, its sign will be changed. In this way, the method aligns the polarities of the estimated TWA waveforms, related to the phase of each alternans sequence, before averaging them.

Finally, the index of average alternans IAA was defined as the mean absolute value of the average of the phase-aligned waveforms $\boldsymbol{y}_k^a$:

$$IAA = \frac{1}{N}\sum_{n=1}^{N}\left|\frac{1}{K}\sum_{k=1}^{K} y_k^a\,(n)\right|. \tag{3.8}$$

As in the short-term analysis, the IAA normalized by the average T-wave amplitude of the recording was also computed ($IAAn$).

3.3.2 Power spectral analysis of heart rate variability in OT tests

For the ECG tracings recorded during the OT test, the instantaneous HR variability (HRV) series, $d_{\mathrm{HRV}}(n)$, was derived from the QRS detection marks obtained in the preprocessing stage as described in [186].

For HRV spectral analysis, three intervals of 3 min and 30 sec of duration were extracted according to the previously defined intervals for TWA analysis during OT test, but excluding HR abrupt transient changes due to head-up tilt: 1) baseline (BAS), from minute 4 up to 30 sec before the tilt; 2) TILT, from 30 sec after head-up tilt to min 4; 3) recovery (REC), from 30 sec after supine position was restored to minute 4 of recovery. For each interval, the power spectral density (PSD) of $d_{\mathrm{HRV}}(n)$ was computed by using the periodogram estimator. The power in the low frequency (0.04-0.15 Hz) and high frequency bands (0.15-0.4 Hz), P_{LF} and P_{HF} respectively, were obtained by integrating the power spectrum in the corresponding frequency bands. Then, the normalized P_{LFn} and the ratio $P_{\mathrm{LF}}/P_{\mathrm{HF}}$ were computed [187].

3.3.3 Statistical analysis

Data are presented as median and 25^{th} and 75^{th} percentiles (unless otherwise specified). Non-parametric Friedman test and Wilcoxon signed rank paired test with Bonferroni correction were applied for repeated measurements to evaluate differences among the different stages of the HDBR (among PRE, during HDBR and POST) in the analysis of Holter recordings.

To evaluate significance of changes induced by HDBR in the stress-induced manoeuvres (OT and VO_{2max} tests), non-parametric Wilcoxon signed rank paired test was applied between PRE and POST values. In addition, to evaluate significance of changes induced by the OT or by the VO_{2max} test, the same test was also applied with respect to the relevant BAS condition, for PRE and POST separately. To evaluate potential differences in the observed phenomena related to orthostatic deconditioning and on the effective application of the LBNP during the OT test, we subdivided the subjects into two subgroups, based on the OTT at POST:

> **LOW-OTT**, including subjects for SHORT with OTT≤30 min, and for MID and LONG with OTT≤15 min (i.e, no LBNP was needed to induce OT test termination);
>
> **HIGH-OTT**, including subjects for SHORT with OTT>30 min, and for MID and LONG >15 min (i.e, OT test termination after LBNP activation).

Comparisons between LOW-OTT and HIGH-OTT subgroups were performed using Mann-Whitney test.

For all tests, the null hypothesis was rejected when p≤ α, with $\alpha = 0.05$. In the case of multiple comparison, the corrected significance level, α_c, is defined as $\alpha_c = \alpha/N$, with N, the total number of comparisons.

3.4 Results

3.4.1 Orthostatic tolerance test

In the SHORT group, where LBNP was applied after the first 30 min of head-up tilt, OTT was significantly reduced between PRE and POST (38.7

Table 3.3: HRV parameters expressed as median (25^{th};75^{th} percentiles) computed at PRE and after five (SHORT), twenty-one (MID) and sixty days (LONG) of HDBR for each tilt interval (BAS, TILT and REC)

		PRE			POST		
		BAS	**TILT**	**REC**	**BAS**	**TILT**	**REC**
SHORT	P_{LF} (ms^{-2})	1146 (778;1321)	$1760^{\#}$ (1159;2553)	1229 (769;2867)	847^{*} (568;1125)	792^{*} (566;1652)	$1532^{\#}$ (891;1846)
	P_{HF} (ms^{-2})	456 (258;728)	$269^{\#}$ (143;422)	$555^{\#}$ (269;1632)	259^{*} (180;342)	$126^{\#*}$ (59;213)	$360^{\#}$ (199;560)
	P_{T} (ms^{-2})	1864 (1178;2542)	$2610^{\#}$ (1713;3536)	$2443^{\#}$ (1295;5234)	1323 (872;1674)	1869 (732;2599)	$2472^{\#}$ (1355;3024)
	P_{LFn}	0.70 (0.62;0.81)	$0.85^{\#}$ (0.80;0.93)	0.71 (0.60;0.80)	0.76^{*} (0.68;0.81)	$0.87^{\#}$ (0.84;0.93)	0.78^{*} (0.69;0.84)
	P_{LF}/P_{HF}	2.38 (1.61;4.27)	$5.62^{\#}$ (4.08;14.27)	2.43 (1.48;4.08)	3.17^{*} (2.12;4.30)	$6.84^{\#}$ (5.29;13.30)	3.58^{*} (2.23;5.39)
MID	P_{LF} (ms^{-2})	990 (579;1846)	$1625^{\#}$ (1003;3000)	1664 (971;2247)	817 (460;1399)	633^{*} (412;1656)	1142 (654;2628)
	P_{HF} (ms^{-2})	390 (230;588)	$240^{\#}$ (146;315)	$511^{\#}$ (310;812)	237 (153;366)	$84^{\#*}$ (31;216)	213 (110;489)
	P_{T} (ms^{-2})	1651 (1027;2592)	$2387^{\#}$ (1376;3609)	$2782^{\#}$ (1884;3564)	1629 (813;2482)	1121^{*} (629;2148)	1272 (1011;3637)
	P_{LFn}	0.73 (0.67;0.82)	$0.87^{\#}$ (0.84;0.92)	0.78 (0.70;0.82)	0.79 (0.67;0.85)	$0.90^{\#}$ (0.84;0.94)	0.82^{*} (0.74;0.88)
	P_{LF}/P_{HF}	2.68 (2.04;4.58)	$6.86^{\#}$ (5.21;12.25)	3.60 (2.35;4.54)	3.69 (2.04;5.96)	$9.16^{\#}$ (5.43;16.48)	4.67^{*} (2.84;709)
LONG	P_{LF} (ms^{-2})	1885 (1076;2373)	2508 (1520;4098)	1222 (866;2433)	1540 (579;2386)	895^{*} (421;1544)	746 (448;1902)
	P_{HF} (ms^{-2})	904 (438;2154)	$335^{\#}$ (168;740)	925 (491;1941)	320^{*} (195;574)	$161^{\#*}$ (134;196)	327^{*} (158;464)
	P_{T} (ms^{-2})	3438 (1797;4843)	3179 (2328;4918)	3015 (1497;5211)	2268^{*} (1096;3260)	2161^{*} (1169;2594)	1288^{*} (998;3061)
	P_{LFn}	0.65 (0.53;0.74)	$0.87^{\#}$ (0.79;0.92)	0.65 (0.56;0.76)	0.76^{*} (0.71;0.87)	$0.88^{\#}$ (0.79;0.95)	0.73 (0.58;0.79)
	P_{LF}/P_{HF}	1.82 (1.11;2.88)	$6.61^{\#}$ (3.80;10.99)	1.88 (1.28;3.30)	3.22^{*} (2.50;6.45)	$7.72^{\#}$ (3.76;17.29)	2.75 (1.40;3.88)

*: p <.05, PRE vs POST, #: p<.05 vs BAS

(36.18;43) vs 8.3 (5.37;32.5) minutes, p<0.001). In the MID group, where LBNP was applied after 15 min of head-up test, OTT after sedentary HDBR was dramatically reduced (24.1 (21;28.7) vs 13 (5.9;20.1) minutes, p<0.001). This decrease was even more accentuated in LONG, from 22.3 (18.9;24.8) minutes at PRE to 4.6 (3.2;12.4) minutes at POST, with OTTs lower than 4 minutes in 5 subjects.

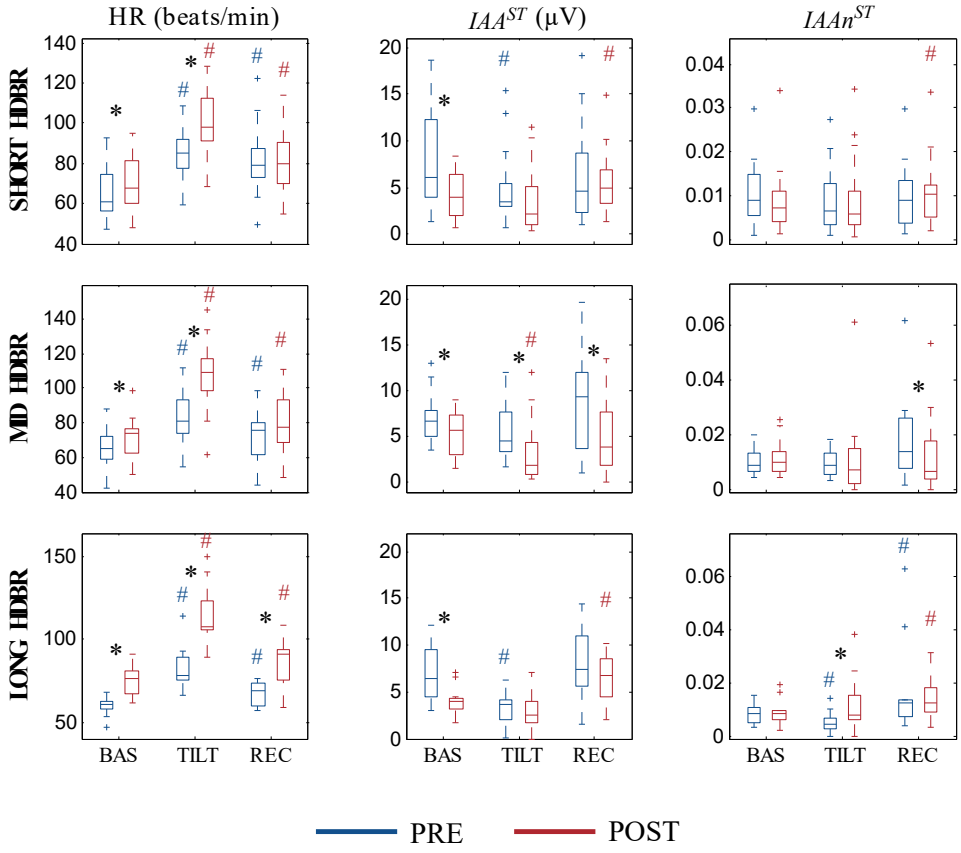

Figure 3.3: Cumulative results for HR and TWA indices, reported as absolute and normalized values, obtained in SHORT (top), in MID (middle) and LONG (bottom) campaigns during orthostatic tilt test before (blue) and after (red) HDBR (*: p<.05, PRE vs POST, #: p<.05 vs BAS).

Short-duration HDBR

In SHORT campaign, when comparing PRE vs POST, an increase in HR was found at BAS and at TILT at the end of the bed-rest. Despite this increment, a significant decrease in IAA^{ST} at BAS was present, while $IAAn^{\mathrm{ST}}$ did not change (Figure 3.3, top panels). From spectral analysis of HRV, P_{LF} and $P_{\mathrm{LF}}/P_{\mathrm{HF}}$ increased at POST during BAS and REC but not during TILT, evidencing a shift in the ANS balance towards sympathetic activation induced by HDBR in these two phases (Table 3.3).

When grouping subjects according to their OTT in LOW-OTT and HIGH-OTT subgroups, we observed that already at PRE three subjects terminated the OT test before LBNP was activated (OTT: 7.9, 22 and 24.3 min, respectively), thus showing earlier pre-syncopal symptoms even before HDBR. To avoid confusing effects, these subjects were excluded from the following comparison between subgroups. Accordingly, the LOW-$\text{OTT}_{\text{SHORT}}$ subgroup (OTT<30 min) was composed by 12 subjects, whereas the HIGH-$\text{OTT}_{\text{SHORT}}$ subgroup (OTT≥30 min) included the remaining 7 subjects.

When comparing these two subgroups at POST (Figure 3.4, columns 1 and 2) during TILT, higher values of IAA^{ST} and $IAAn^{\text{ST}}$, though not significant (p=0.056 and p=0.1, respectively), were observed in LOW-$\text{OTT}_{\text{SHORT}}$. This suggests that a lower orthostatic tolerance to head-up tilt manoeuvre could be related to an increased electrical instability measured in terms of higher TWA. Interestingly, in both PRE and POST during the recovery stage (REC), $IAAn^{\text{ST}}$ was significantly higher in those subjects with lower tolerance, i.e., the LOW-$\text{OTT}_{\text{SHORT}}$ subgroup compared to HIGH-$\text{OTT}_{\text{SHORT}}$ subgroup.

Regarding to HRV spectral analysis, before HDBR (Figure 3.4, columns 3 and 4), in LOW-$\text{OTT}_{\text{SHORT}}$, both P_{LFn} (0.68 (0.62;0.79) vs 0.91 (0.85;0.94) n.u., p=0.002) and $P_{\text{LF}}/P_{\text{HF}}$ (2.13 (1.68;4.11) vs 10.97 (5.58;15.92) n.u., p=0.002) significantly increased at TILT compared to BAS. This phenomenon was not observed in HIGH-$\text{OTT}_{\text{SHORT}}$, thus suggesting that sympathetic drive during orthostatic stimulation increased particularly in the LOW-$\text{OTT}_{\text{SHORT}}$ subgroup. Conversely, after HDBR, the increase in sympathetic response was visible in both subgroups (Figure 4 A, bottom).

Mid-duration HDBR

As in SHORT, a significant increase in HR was found at BAS and at TILT when comparing PRE vs POST, accompanied by a reduction in IAA^{ST} in BAS, TILT and REC (Figure 3.3, middle panels). However, when considering $IAAn^{\text{ST}}$, this reduction maintained its significance only at REC. Regarding HRV spectral analysis, P_{LF} and $P_{\text{LF}}/P_{\text{HF}}$ increased after HDBR at REC, evidencing higher sympathetic drive at POST during this phase (see Table 3.3).

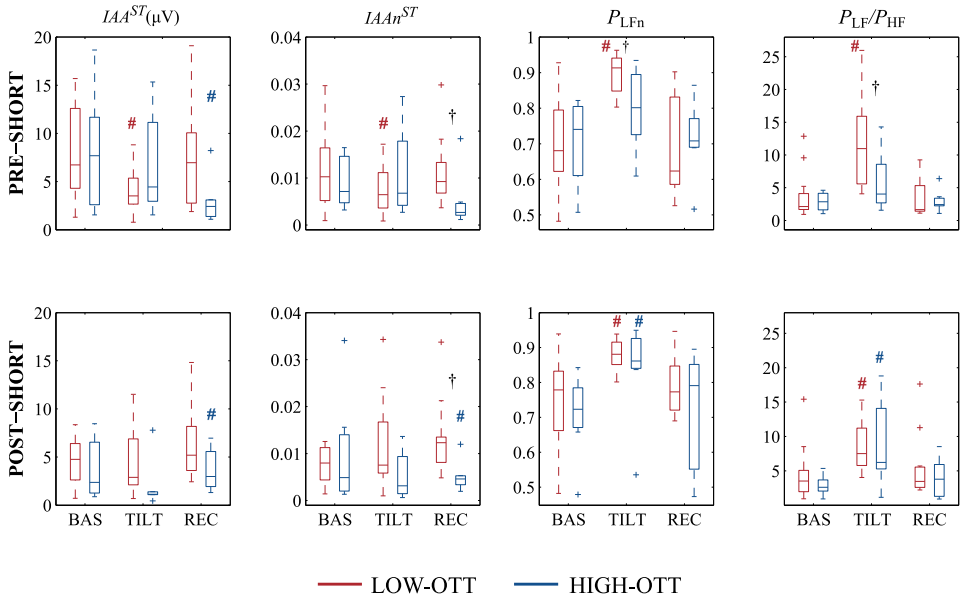

Figure 3.4: TWA and HRV indices computed for LOW-OTT_{SHORT} (red) and HIGH-OTT_{SHORT} (blue) groups, before and after the SHORT-HDBR (up and bottom panels, respectively).#: p<0.05, vs BAS. †: p<0.05, LOW-OTT_{SHORT} vs HIGH-OTT_{SHORT}.

Only one subject at PRE terminated the OT test before LBNP was activated (OTT: 12.1 min) and, as in the previous analysis, it was excluded for the following subgroups comparison. When considering LOW-OTT_{MID} (OTT<15 min) and HIGH-OTT_{MID} (OTTgeq15 min) subgroups, they included 10 and 8 subjects, respectively. From this comparison, neither IAA^{ST} nor $IAAn^{ST}$ differ between subgroups in this case. In both subgroups, P_{LF} and P_{LF}/P_{HF} increased during TILT when compared to BAS, suggesting that sympathetic ANS response with head-up tilt was present before and after HDBR.

Long-duration HDBR

After LONG HDBR, average HR was increased in all three analyzed intervals. While IAA^{ST} was decreased in BAS, no significant changes were found in the other two intervals. However, when normalized by T-wave amplitude, the head-up tilt manoeuvre elicited a significant increase in $IAAn^{ST}$ after the immobilization period (Figure 3.3, bottom panels). Regarding HRV

spectral analysis, a significant decrease in P_{HF} after HDBR together with a slight increase in P_{LFn} and the ratio $P_{\mathrm{LF}}/P_{\mathrm{HF}}$ during BAS, evidencing higher sympathetic drive at POST during this phase (see Table 3.3).

In this study group, two subjects did not end the OT test already at PRE (OTT: 12.75 and 9.9 minutes) and were excluded for comparison purposes. At POST, the LBNP was only applied in 3 out of the remaining 9 subjects, conforming the HIGH-OTT$_{\mathrm{LONG}}$ subgroup, while the other 6 subjects were in the LOW-OTT$_{\mathrm{LONG}}$ subgroup. However, no significant differences between both subgroups were found in terms of the studied repolarization and ANS variables.

3.4.2 Exercise stress test

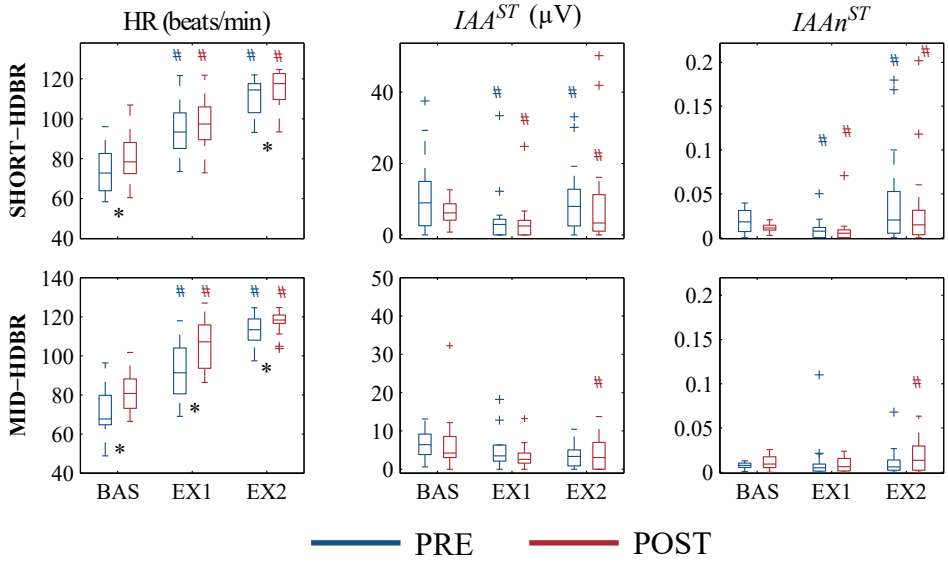

Figure 3.5: HR, IAA^{ST} and $IAAn^{\mathrm{ST}}$ distributions at each interval (BAS, EX1, EX2) of the VO_{2max} test, computed before (blue) and after (red) five days (top panels) and after twenty-one days (bottom panels) of HDBR. *: p<0.05, PRE vs POST. #: p<0.05, vs previous interval.

Due to technical problems, data during VO_{2max} test from both the PRE and POST were available for only 20 out of 22 subjects in SHORT. In MID, paired data from PRE and POST were available in only 18 subjects. In LONG, however, one PRE recording and four POST recordings had to be

discarded due to technical problems during acquisition and one additional POST recording missed. Consequently, only paired data from 6 subjects were finally available.

HDBR induced significant changes on aerobic power. In particular, maximum HR was increased from 179 (171;186) beats/min to 184 (175;187) beats/min in SHORT, from 183 (179;189) beats/min to 190 (180;195) beats/min in MID, but without significant changes in LONG. In addition, maximum VO_2 was diminished from 3187 (2739;3626) ml/min to 3115 (2766;3473) ml/min in SHORT, from 3355 (2507;3787) ml/min to 2564 (2234;3250) ml/min in MID and from 4078 (3664;4300) ml/min to 2700 (2647;2844) ml/min in LONG (Table 3.4).

Table 3.4: Results of aerobic capacity during VO_{2max} in SHORT, MID and LONG duration HDBR campaigns.

		HR_{max} (beats/min)	VO_{2max} (ml/min)	**TUE** (min)
SHORT	PRE	179	3187	18.5
		(171;186)	(2739;3626)	(17.8;19.9)
	POST	184*	3115*	19.2
		(175;187)	(2766;3473)	(17.9;19.9)
MID	PRE	183	3355	18.5
		(179;189)	(2507;3787)	(17.7;19.4)
	POST	190*	2564*	16.2*
		(180;195)	(2234;3250)	(15.2;17.1)
LONG	PRE	187	4078	13.6
		(182;192)	(3664;4300)	(12.7;14.2)
	POST	186	2700*	10.6*
		(178;196)	(2647;2844)	(8.8;10.8)

*: $p<0.05$ PRE vs POST
TUE: time up to exhaustion

Short-duration HDBR

Distribution of average HR and TWA indices are presented in Figure 3.5, upper panels. In both at PRE and at POST, HR increased progressively during the VO_{2max} test (EX1 vs BAS, EX2 vs EX1, $p<.001$), as expected. When compared to PRE values, HDBR induced an increase in HR, which was significant in BAS and EX2, though not in EX1. As regards TWA indices, both IAA^{ST} and $IAAn^{ST}$ showed a similar trend during the VO_{2max} test, with a reduction in EX1 compared to BAS and subsequent slight in-

crease in EX2. No significant differences between PRE and POST were evidenced.

Mid-duration HDBR

Results of average HR and TWA indices are presented in Figure 3.5, bottom panels. As in SHORT, HR progressively increased along the VO_{2max} test (EX1 vs BAS, EX2 vs EX1, p<.001). Compared to PRE, HR was significantly higher at POST in each stage of the test. Regarding TWA analysis, neither IAA^{ST}, nor $IAAn^{\mathrm{ST}}$ showed any difference induced by the test or by HDBR.

Long-duration HDBR

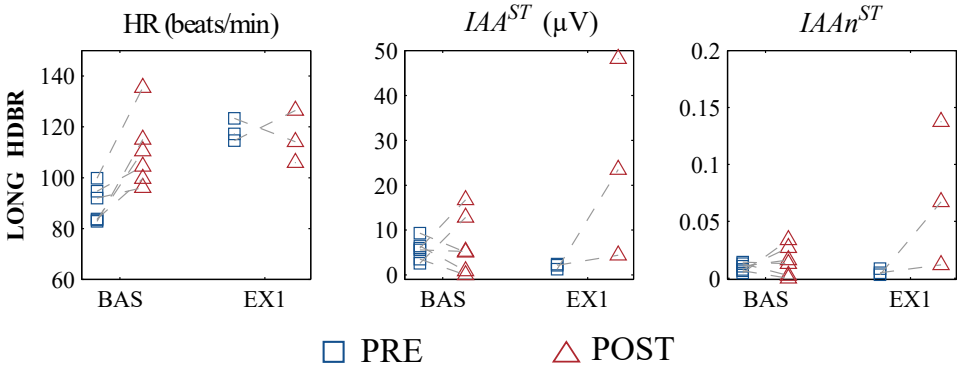

Figure 3.6: Distribution of HR, IAA^{ST} and $IAAn^{\mathrm{ST}}$ at each interval (BAS and EX1) of the VO_{2max} test, computed before (□) and after (△) sixty days of HDBR.

As observed in the previous campaigns, HDBR induced a significant increase in HR during BAS in all 6 subjects. Both at PRE and at POST, only 3 out of 6 subjects presented processable ECG segments with HR <130 beats/min in EX1, while no suitable segments in any subject were available during EX2, as all of them reached the maximum HR before, even at PRE. To note, this group of subjects presented a higher baseline HR already at PRE in comparison to SHORT and MID groups (87.9 (83.4;94.7) beats/min vs 72.8 (64;82.6) beats/min in SHORT and 67.7 (64.7;79.8) beats/min in MID). The reduced number of subjects and the final PRE-POST paired data, did not allow to make a reliable statistical analysis in this group. In-

dividual changes in BAS and EX1 from the final available tests are reported in Figure 3.6.

3.4.3 Long-term averaging of TWA activity

Data from all subjects (22 in SHORT, 20 in MID and 11 in LONG) were available for the long-term averaging of TWA. Distributions of average HR, IAA and $IAAn$ (in absolute values and normalized by T-wave amplitude) computed during the night period are included in Figure 3.7.

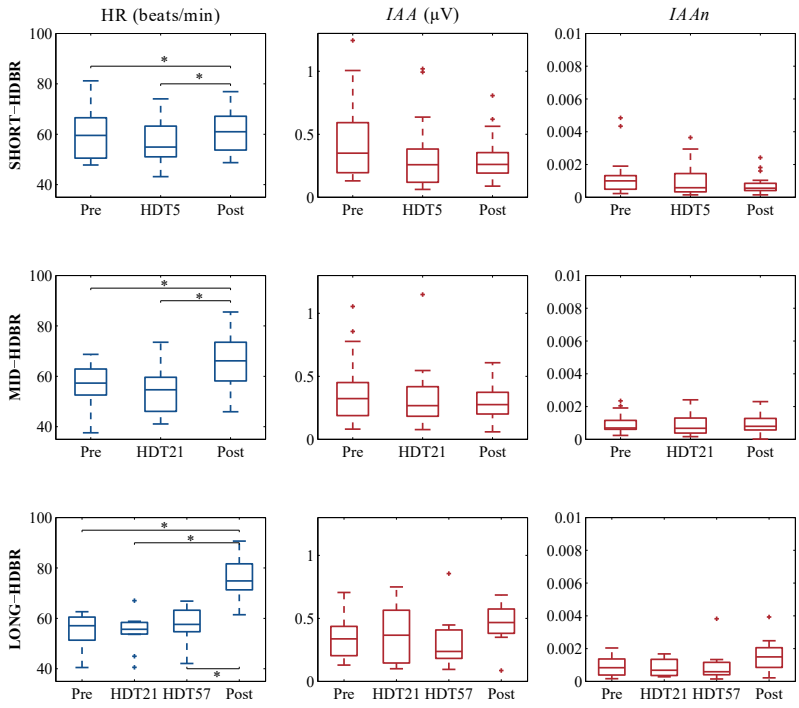

Figure 3.7: Distribution of average HR, IAA and $IAAn$ (normalized by T-wave amplitude) computed before (PRE), the last day of HDBR, and after (POST), in SHORT (top panels), MID (middle panels) and LONG (bottom panels) of HDBR. *: $p<0.05$.

Short-duration HDBR

A significant increase in average HR at POST was found both compared to PRE (59.5 (50.5;66.5) beats/min at PRE vs 70 (53.7;67.1) beats/min at POST, p=0.009, $\alpha_c = 0.0166$) and to HDT5 (54.9 (51.0;63.2), p=0.001, $\alpha_c = 0.0166$) although no significant differences along HDBR in IAA, neither in absolute nor in normalized amplitudes, were found (Figure 3.7, top panels).

Mid-duration HDBR

The same effect has been observed after 21 days of HDBR (Figure 3.7, middle panels). Average HR increased at POST compared to PRE (57.3 (52.6;62.9) beats/min at PRE vs 66.2 (58.2;73.5) beats/min at POST, p= 0.002, $\alpha_c = 0.0166$) and compared to HDT21 (54.6 (46.1;59.6) beats/min, p<0.001, $\alpha_c = 0.0166$) but no significant differences along HDBR in terms of TWA were found (IAA=0.323 (0.188;0.451) μV at PRE, IAA=0.275 (0.201;0.373) μV at POST, p=0.167, $\alpha_c = 0.0166$).

Long-duration HDBR

A significant increase in HR was found at POST compared to PRE (57.1 (50.8;60.6) beats/min vs 73.6 (70.8;81.6) beats/min, p=0.003, $\alpha_c = 0.0083$), HDT21 (55.7 (53.7;58.3)beats/min, p=0.003) and HDT57 (57.7 (54.7;63.3) beats/min, p=0.003, $\alpha_c = 0.0083$). A similar pattern was observed with TWA indices. The IAA showed an increasing trend at POST (0.467 (0.381; 0.574) μV) compared to PRE (0.337(0.204;0.437 μV) (p=0.2, $\alpha_c = 0.0083$) and the end of the HDBR (HDT57: 0.247 (0.188;0.454) μV, p=0.091, $\alpha_c = 0.0083$), tough not significant (Figure 3.7, bottom panels). These differences become even more accentuated when normalized by T-wave amplitude ($IAAn$: 0.15 (0.085;0.21)% at POST vs 0.08 (0.038;0.14)% at PRE, p=0.021, and 0.06 (0.040;0.012)% at HDT57, p=0.013, $\alpha_c = 0.0083$). Correlation with HR was R^2 =0.205 and R^2 =0.217, for IAA and $IAAn$, respectively.

3.5 Discussion

SHORT, MID and LONG duration sedentary HDBR induced a reduction in orthostatic tolerance, as well as a decrease in maximal oxygen uptake and reserve capacity to perform physical work, thus suggesting cardiovascular deconditioning after the immobilization period.

In this study, we were focused on the analysis of ventricular repolarization alterations induced by HDBR in terms of TWA activity. TWA was evaluated under two different conditions: (i) two non-stationary stress-inducing manoeuvres, as the OT by head-up tilt and the VO_{2max} by bicycle exercise, and (ii) at rest, during the night period. The methodological approach for TWA estimation based on averaging of the TWA estimated in short signal segments and avoiding a "hard detection" stage, has been adapted to the particular condition of non-stationary and noisy conditions. We have additionally introduced a normalization in TWA aplitude ($IAAn$), to evaluate whether changes in T-wave amplitude, known to be elicited by HDBR [180, 181], could also impact on TWA estimation. Those changes on T-wave have been related to the loss of fluids and hypovolemia, resulting in diminished plasma volume and shrinking of heart cavities [188].

Both OT and VO_{2max} tests lead to an increase in HR, sometimes required to elicit TWA. Despite previous observations that sedentary HDBR reversibly increases ECG repolarization heterogeneity and, consequently, pontentially ventricular arrhythmic risk [180, 181], we found an absence of a clear significant increase in terms of TWA indices, in both absolute values and normalized by T-wave amplitude, between PRE and POST 5, 21 and 60 days of HDBR under those particular conditions. Only after 60 days of HDBR the head-up tilt induced an increasing trend in $IAAn^{\mathrm{ST}}$. These results suggest that long-duration (up to 60 days) exposure to simulated microgravity was not able to alter the ventricular repolarization heterogeneity under stress conditions enough to the point of increasing TWA amplitude.

3.5.1 Orthostatic tolerance test

First, we evaluated TWA during OT test. We also performed spectral analysis of HRV to elucidate potential autonomic nervous system unbalance in relation to TWA. An apparent decrease between PRE and POST-HDBR in IAA^{ST} was visible in all campaigns (SHORT, MID and LONG) during BAS

interval. However, when considering $IAAn^{\mathrm{ST}}$, this effect disappeared, thus probably being related to a decrease of the amplitude of the whole T-wave at the surface ECG, in agreement to the results showing no effect of HDBR in terms of TWA during OT test.

We observed a decreasing trend in TWA when TILT was compared to BAS, significant only for SHORT and LONG at PRE and for MID at POST, together with a statistically significant increase in sympathetic tone (P_{LFn} and $P_{\mathrm{LF}}/P_{\mathrm{HF}}$) with respect to baseline values (BAS) during OT. In previous studies on Long QT syndrome patients, TWA has been shown to be provoked by emotional stress, suggesting that sympathetic stimulation may play an important role [189]. However, this sympathetic activation did not influence TWA amplitude in patients with structural heart disease or ventricular arrhythmias [190]. When considering normalized amplitudes ($IAAn^{\mathrm{ST}}$) this decrease at TILT became less evident and even nonsignificant. This different behaviour in TWA indices could be explained by the fact that sympathetic stimulation induces T-wave flattening with increasing tilt angles, as reported in [191], thus being compensated with the normalization step. Nevertheless, the relationship between these phenomena remains still controversial and further research would be needed to better elucidate the potential stabilization of repolarization with increased sympathetic tone in healthy subjects.

As regards spectral HRV analysis, the main effect of HDBR evaluated during the initial baseline condition was a decrease in absolute powers P_{LF} and P_{HF}, together with an increase in P_{LFn} and $P_{\mathrm{LF}}/P_{\mathrm{HF}}$ ratio, visible but not significant after 21 days of HDBR (MID). In previous studies, a decrease in absolute P_{LF} and P_{HF} power, but no changes in P_{LFn} and $P_{\mathrm{LF}}/P_{\mathrm{HF}}$ had been observed after 30 days of bed-rest during controlled breathing (0.25 Hz) [181]. Also in [192], a decrease in P_{HF} power with an increase in $P_{\mathrm{LF}}/P_{\mathrm{HF}}$ after a 14-day HDBR was reported. At POST, the head-up tilt induced and increase in P_{LFn} and $P_{\mathrm{LF}}/P_{\mathrm{HF}}$ with respect to baseline levels, together with a decrease in P_{HF} visible after 5, 21 and 60 days of HDBR, similar to what was previously reported in [193].

Interestingly, when we subdivided subjects according to the resistance to the head-up tilt manoeuvre at POST, in base to their OTT, higher TWA parameters during the recovery interval were observed in subjects with OTT<30 min (LOW-$\mathrm{OTT}_{\mathrm{SHORT}}$) after 5 days of HDBR, suggesting higher electrical instability associated to a more important orthostatic into-

lerance due to cardiac deconditioning. In addition, these subjects presented a significant increase with head-up tilt in both P_{LFn} and $P_{\mathrm{LF}}/P_{\mathrm{HF}}$ already before the HDBR, while in the HIGH-OTT$_{\mathrm{SHORT}}$ group this effect was not visible. Moreover, the increase in sympathetic tone observed during TILT was accompanied by a reduced $IAAn^{\mathrm{ST}}$, in agreement with previous studies on patients with syncopal and postural orthostatic tachycardia syndrome, in which the reaction of sympathetic tone to orthostasis was more severe compared to control subjects [194]. However, we could not confirm the such differences after 21 and 60 days of HDBR. This discrepancy could also be due to the different protocol, since LBNP was applied after only 15 min, instead of 30 min as in SHORT.

3.5.2 Exercise stress test

In addition to evaluating TWA during OT test, we performed a similar analysis during VO_{2max} test. Our findings from VO_{2max} test showed the expected increase in HR during the considered exercise phases (i.e., BAS, EX1, EX2) with higher values at POST compared to PRE, in agreement with the observed decrease in maximal oxygen uptake and reserve capacity. No HDBR-related increment in TWA was noticed, neither in absolute nor in normalized values, for all SHORT, MID and LONG. Unfortunately, the reduced number of tests finally available in the LONG campaign, in which effects of bed-rest were expected to be more pronounced, limited the drawing conclusions related to exercise induced stress on TWA. An additional LONG campaign is currently ongoing at MEDES facility and data from 10 more subjects is expected to be available by the end of the year to complete the study group.

Nevertheless, our results are not concordant with the only study assessing TWA PRE and POST-HDBR during incremental dynamic leg exercise on a cycle ergometer [182]. In that study, the number of subjects with positive TWA test, requiring TWA to be present at a HR higher than 110 beats/min, was found to increase after 9-16 days of HDBR. In particular, 4 out of 24 subjects (17%) were classified as positive already at PRE, becoming 10 out of 24 (41.7%) at POST. However, it has to be remarked that two positive subjects at PRE resulted negative at POST, without a clear explanation. A possible cause of discrepancy with Grenon et al. could be due to the fact that VO_{2max} test in our study was performed within 26 hours after the end of HDBR (R+1 day), while in [182] it was performed

within 6 hours after its conclusion. The fact that subjects had maintained in the upright position for a considerable period before the test could have mitigated some of the HDBR-induced effects.

To note, the protocols of these tests were not TWA specific but for aerobic power assessment. TWA test required a graded increase in heart rate, commonly during bicycle or treadmill exercise, up to an optimum HR range of 105-110 beats/min, which was determined for pathologic alternans in adults [5]. Usually, specific TWA tests try to keep the subject's HR as much time as possible within this range. However, this consideration was disregarded in the present VO_{2max} protocol. On the other hand, an additional control on the pedalling candence, prompting the subject to pedal at one third or two thirds of his heart rate, would had avoided the HR restriction (<130 beats/min), in order to avoid the possible mechanical-induced interference on TWA measurements [148, 195].

3.5.3 Long-term averaging of TWA activity

Finally, electrical instability in ventricular repolarization was assessed by the long-term averaging of TWA activity during the night hours. The selection of the night period was motivated by the fact that subjects were asked to perform numerous experimental tests during the day period (especially in PRE and POST periods) that could induce confounding effects. While no statistically significant changes after 5 and 21 days of HDBR were found, an increasing tendency in IAA at POST with respect to both PRE and the end of the 60-day immobilization period (HDT57) was observed in LONG, although it did not reach statistical significance. These changes were more evident when IAA was normalized by changes on T-wave amplitude. This increase in TWA could have been induced by the same pattern observable on average HR. However, a low correlation between both parameters was obtained. Previous reports on which ventricular repolarization heterogeneity was assessed using different repolarization indices (QTc, spatial QRS-T angle, ventricular gradient, among others) has been shown to be reversibly altered after short and long-duration HDBR studies [180, 181]. All these observations might be an indicative of initial electrical instability on the myocardial substrate induced by log-term HDBR.

Anyway, data available in the LONG-duration campaign was limited in terms of study subjects, especially during VO_{2max} test, which did not allow

to draw final conclusions in this study group. Results need to be confirmed in a larger population. An additional LONG campaign, currently on going in MEDES facility, will provide data from 10 additional subjects, which are expected to be available by the end of the year.

3.6 Conclusion

The absence of significant changes between PRE and POST-HDBR in TWA indices suggests that a 60-day exposure to simulated microgravity is not enough to induce significant changes in healthy myocardial substrate up to the point of reflecting electrical instability in terms of TWA on the surface ECG. Nevertheless, the increasing tendency observed after 60 days of immobilization period might be indicative of initial alterations in the repolarization phase. From the clinical perspective, reduced gravitational stimulus during HDBR experiments, could also provide interesting information which could be taken into account in immobilized or bedridden patients.

Chapter 4

Improvement of T-wave alternans predictive value in ambulatory recordings by dealing with the effect of ventricular premature contractions

4.1 Motivation

In clinical research, TWA tests are usually performed under controlled heart rate conditions, typically by exercise-induced stress. The most widely used methods are the SM or the MMAM described in section 1.5.1, as these are the two alternatives commercially available, resulting in a TWA-positive, -negative or -indeterminate test. In the clinical practice, an important percentage of indeterminate TWA tests is reported (between 20% and 40%) [196–198]. The main causes of an indeterminate result are excessive noise, lack of capacity to reach a target heart rate of 105 to 110 beats/min, non-sustained TWA (<1 minute) or the presence of ventricular ectopic activity, which may directly interfere with the frequency content of alternans [199]. Therefore, from the signal processing viewpoint, robust algorithms able to overcome these limitations are required in order to guarantee the clinical value of TWA. The LLRM [153], as an alternative to the mentioned SM and MMAM, has been shown to outperform the accuracy of these methods in the presence of impulsive artifacts, as the ones produced in the beat-to-beat amplitude series by VPCs or electrode motion [154].

In the recent years, the analysis of TWA in ambulatory ECG recordings has become a matter of increasing interest, yielding promising results [149–152, 200, 201]. In particular, the long-term averaging of TWA activity in 24-hour Holter recordings has been shown to be an independent predictor of SCD in CHF patients [157]. In that study, the same averaging approach presented in the previous chapter was used, avoiding the need for visual verification required by other methodologies, as in the case of MMAM [149–151]. The method for TWA analysis in [157] discards unstable segments, defined in terms of instantaneous heart rate changes, abrupt baseline wander and the percentage of ectopic beats. Indeed, segments with a low percentage of abnormal beats were still included in the analysis, as the LLRM for TWA estimation is able to cope with a small number of abnormal beats. However, the presence of one or more VPCs may alter repolarization dynamics, and they may introduce a phase reversal in the sequence of alternant T-wave morphologies [158], which could hamper the estimation of TWA amplitude [159, 160] and, consequently, its potential for risk stratification.

In this chapter, we propose a method to improve the estimation of TWA amplitude in ambulatory ECGs, by dealing with the possible phase reversal induced by the presence of VPCs in the alternans sequence. First, a simulation scenario was generated in order to evaluate the performance of the algorithm using synthetic signals. Then, the effect of the proposed method in the prognostic value of TWA amplitude was assessed in real ambulatory ECG recordings from patients with CHF. Finally, circadian TWA changes were evaluated as well as whether the prognostic value of TWA is sensitive to this circadian pattern.

4.2 Materials

4.2.1 Simulated data

Series of 2080 beats were created by replicating one beat extracted from an actual Holter recording (sampling frequency 200Hz), with synthetic TWA. This TWA was generated by adding and subtracting in even and odd beats respectively a given waveform (modelled as a Hamming window, with peak amplitudes varying from 0 to 300 μV in steps of 50 μV) to the repolarization phase of the beat (i.e, the ST-T complex). Moreover, three real sources of noise -electrode motion (em), muscular activity (ma) and baseline wander (bw), obtained from the Physionet MIT-BIH Noise Stress Test Database (NSTDB) [202]– and synthetic white Gaussian noise (gn) were independently added to the simulated ECG in order to create a more realistic scenario.

For each simulated TWA amplitude, baseline wander segments properly scaled to present different standard deviations, σ_{bw} , varying from 0 to 800 μV, in 100 μV steps, were added to the synthetic ECG. These baseline wander segments were randomly selected form one of the 2 available leads of the NSTDB. The same procedure was replicated for the ma and em noises, with σ_{ma} and σ_{em} ranging from 0 to 200 μV, in 25 μV steps, and for the synthetic Gaussian noise (σ_{gn} varying from 0 to 100 μV).

A total of 100 realizations were generated for each combination of noise and TWA amplitudes in order to have a reliable characterization of the method's performance. For each realization, VPCs were randomly allocated along the 2080-beat sequence. The phase of the alternans sequence in the next beat after each one labelled as VPC was randomly selected, with a

0.5 probability of a phase shift. Additionally, the effect of the presence of ectopic beats in the TWA estimation was also evaluated for low, medium and high levels of noise, varying the percentage of VPCs included in the sequence from 0 to the 20%.

4.2.2 Ambulatory ECG recordings

A total of 992 consecutive patients with symptomatic CHF corresponding to NYHA classes II and III were enrolled in the multicenter MUSIC (MUerte Súbita en Insuficiencia Cardiaca) study, a prospective study designed to assess risk predictors for cardiovascular mortality in ambulatory CHF patients [203]. Patients were enrolled from the specialized CHF clinics of eight University Hospitals between April 2003 and December 2004. The original MUSIC study included patients with both reduced and preserved LVEF. Patients with preserved LVEF were included if they had CHF symptoms, a prior hospitalization for CHF or objective CHF signs confirmed by chest X-ray and/or echocardiography. Patients were excluded if they had recent acute coronary syndrome or severe valvular disease amenable for surgical repair. Patients with other concomitant diseases expected to reduce life-expectancy were also excluded. Originally, patients in sinus rhythm, atrial fibrillation, atrial flutter and in pacemaker rhythm were included. The clinical data for the overall population were already reported in [203].

The 24-hour Holter ECG recordings of 651 patients (187 females) in sinus rhythm, aged 18-89 years (62.9±11.9 years) were analysed in the present study. ECG signals were acquired by using SpiderView records (ELA Medical, Sorin Group, Paris, France) and two or three (96.8%) orthogonal leads (X, Y, Z) sampled at 200 Hz were available for each subject. Most patients (82.3%) were in NYHA class II. Ischemic etiology of CHF was present in 50.2% of patients. Mean LVEF was 36.9±13.8% (range 10-70%), and half of patients (54.7%) presented LVEF$\leq$35%. Intraventricular conduction delay, defined as QRS duration geq0.12s, was present in 292 patients. Some relevant patient characteristics are summarized on Table 4.1.

Patients were followed up every 6 months during 48 months. Whithin the study population, there were a total of 55 victims of SCD, 59 of other cardiac causes, 26 non-cardiac deaths and 511 survivors. SCD, defined as (i) a witnessed death occurring within 60 minutes from the onset of new symptoms unless a cause other than cardiac failure was obvious, (ii) an unwitnes-

Table 4.1: Characteristics of patients. Data are presented as mean±standard deviation and as absolute frequencies (percentages).

	Overall population (n=651)	**SCD group** (n=55)	**Non-SCD group** (n=596)
Age (years)	62.9±11.9	64.54±10.72	62.81±12
Gender (males)	464 (71.3%)	46 (83.6%)	418* (70.1%)
LVEF $\leq$ 35%	356 (54.7%)	40 (72.7%)	316* (53.0%)
NYHA class III	115 (17.7%)	16 (29.1%)	99* (16.6%)
Diabetes	244 (37.5%)	24 (43.6%)	220 (36.9%)
Beta-blockers	455 (69.9%)	39 (70.9%)	416 (69.7%)
Amiodarone	61 (9.4%)	6 (10.9%)	55 (9.2%)
ARB or ACE inhibitors	576 (88.5%)	45 (81.8%)	531 (89.1%)
QRS duration $\geq$ 120 ms	292 (44.9%)	30 (54.6%)	262 (44.0%)

LVEF: Left ventricular ejection fraction; NYHA: New York Heart Association; ARB: angiotensin receptor blocker; ACE: angiotensin-converting enzyme.
*: p$\leq$0.05 SCD vs Non-SCD groups

sed death ($\leq$ 24 hours) in the absence of pre-existing progressive circulatory failure or other causes of death, or (iii) death during attempted resuscitation, was considered as an independent endpoint in this study. Endpoints were reviewed and classified by the MUSIC Study Endpoint Committee. The study protocol was approved by institutional investigator committees and all patients gave written informed consent [203].

4.3 Methods

4.3.1 Preprocessing

Preprocessing of ECG recordings included heart beat detection and classification (including identification of VPCs) using the Aristotle ECG analysis software [204] and linear high pass filtering (0.5 Hz cut-off frequency) for baseline wander attenuation. Then, the ECG signal was low-pass filtered (15 Hz cut-off frequency) to remove noise out of TWA frequency range, and down-sampled to 100 Hz. Finally, a segmentation of ventricular repolarization phase (ST-T complex) was done at each beat, by defining a fixed interval of 300 ms (30 samples after decimation) after the end of the QRS complex (80 ms after QRS fiducial point).

Analogously to the study presented in the previous chapter (section 3.3.1), ECG signals were processed in segments of L =128 consecutive beats (with 50% overlap). Segments were deemed valid for automatic analysis if at least 80% of their beats fulfilled two conditions: (i) they were labelled as normal beats and (ii) there was a difference lower than 200 μV between the baseline voltage measured at the PQ segment in that beat and the one measured in the preceding beat.

Moreover, an additional criterion based on instantaneous HR changes was applied to ensure heart rhythm stability in the segments accepted for TWA analysis: only 128-beat segments where the difference between the maximum and minimum RR interval, ΔRR^N, was lower than 300 ms were included (considering only RR intervals defined between normal-labelled beats). Thus, with this criterion the RR intervals related to VPCs are not considered to decide whether the segment is included or not.

4.3.2 TWA estimation

The method to estimate the TWA waveform is based on [157]. For each k^{th} signal segment, it gives a TWA signal $\boldsymbol{y}_k$, denoted as

$$\boldsymbol{y}_k = [y_k(1), \ldots, y_k(N)]^T, \tag{4.1}$$

with N the total number of samples within the ST-T complex. The three orthogonal leads are linearly combined using πCA, in order to maximize the TWA content in the combined lead [156]. Then, the LLRM [153] was applied in that new combined lead to estimate the TWA waveform of each segment ($\boldsymbol{y}_k$). The original method in [156] disregarded the possible phase shift in the TWA produced by the presence of any VPC (a maximum of 20% of VPCs was allowed).

4.3.3 VPC processing

The possible phase shift following a VPC influences TWA estimation. Two examples of TWA sequences without and with a phase shift after the VPC are shown in Figure 4.1. As the LLRM has been demonstrated to be robust enough to the presence of impulsive noise [145], in the original method [157] segments with a low percentage of VPC were accepted for TWA analysis and processed in the same way as segments with all normal beats. However,

if the ectopic activity produces a phase shift in the sequence of repolarization waveforms during a TWA episode, TWA could be undetected and its amplitude could be underestimated. To avoid this problem, we introduced an additional processing step when VPCs are present in the segment, consisting on controlling the phase of the alternans sequence after the ectopic beat.

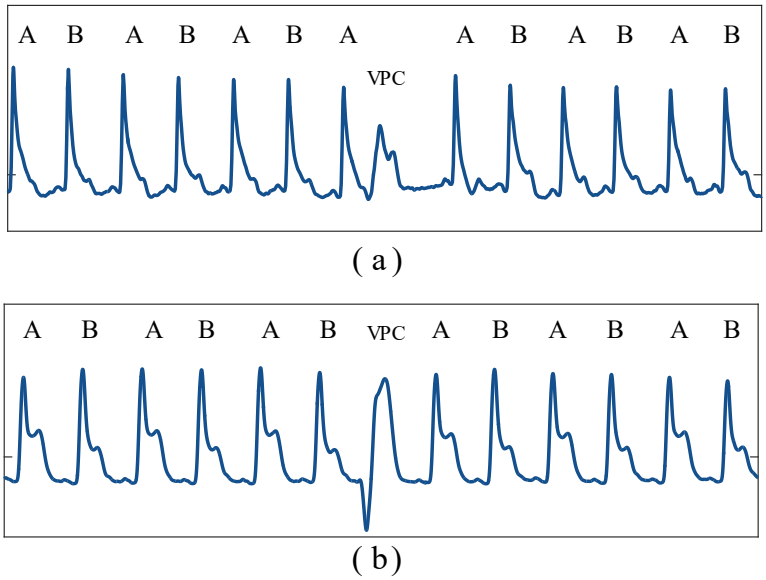

Figure 4.1: Two TWA sequences including a VPC extracted from real ECG signals of patients undergoing a percutaneous transluminal coronary angiography (PTCA): in (a) the alternans sequence maintains the phase after the VPC while in (b) there is a phase shift after the VPC.

Let us consider a VPC within a segment of L beats with TWA. If more than one consecutive VPC appear, the whole sequence of VPCs is considered as a single VPC for the purpose of the algorithm described in this section.

In the following, we will consider, without loss of generality, that an alternant pattern $ABAB \dots AB$ is present in the signal. Note that if no TWA is present, A and B beats are expected to be similar.

If the ectopic beat lies in an odd position within the series, the sequence of beats before the abnormal beat can be represented as $S_{pre} = \{ABAB \dots AB\}$. As the abnormal beat may, or may not, reset the phase, the alternant sequence after the ectopic (S_{post}) can be either $S_{post1} = \{ABABAB...\}$ or $S_{post2} = \{BABABA...\}$. On the contrary, if the ecto-

pic beat is in an even position, the sequence of beats previous to the VPC will end in an A beat (i.e. $S_{pre} = \{ABAB...ABA\}$) and, again, there are two possible continuations of the series after the VPC: $S_{post1} = \{ABABAB...\}$ or $S_{post2} = \{BABABA...\}$.

The proposed approach consists on determining what is the relative phase of the S_{post} sequence of beats with respect to the S_{pre} sequence, discarding the abnormal beat, and properly concatenating S_{post} at the end of S_{pre}. If needed, the first beat of the post-VPC series is also eliminated to keep the continuity of the alternans phase in the resulting series. As an illustrative example, Figure 4.2 shows two possible scenarios where S_{pre} and S_{post} are in phase (a) and out of phase (b). In the latter situation, both the ectopic and the following beat need to be discarded in order to preserve the phase of the alternans in the final sequence.

To determine the relative phase between the two subsequences (S_{pre} and S_{post}), the following procedure is applied:

1. The TWA waveform of each subsequence ($\boldsymbol{y}_{k,pre}$ and $\boldsymbol{y}_{k,post}$ in S_{pre} and S_{post}, respectively) was estimated using the LLR method [153], i.e. as the median of the demodulated differences (alternative sign change) between the consecutive ST-T complexes included in each subsequence.

2. If the mean values of $\boldsymbol{y}_{k,pre}$ and $\boldsymbol{y}_{k,post}$, defined as

$$\bar{y}_{k,pre} = \frac{1}{N} \sum_{n=1}^{N} y_{k,pre}(n) \tag{4.2}$$

$$\bar{y}_{k,post} = \frac{1}{N} \sum_{n=1}^{N} y_{k,post}(n), \tag{4.3}$$

   respectively, are both positive or both negative (same sign), this indicates that TWA has the same polarity in both subsequences and, consequently, both of them start with the same phase. On the contrary, if $\bar{y}_{k,pre}$ and $\bar{y}_{k,post}$ have opposite signs, this indicates that both sequences start out-of-phase. Therefore, if the S_{pre} has an even number of beats and both sequences start in phase, only the VPC beat is discarded before concatenation (Figure 4.2 (a)). The same procedure is applied when the S_{pre} has an odd number of beats and S_{post} starts at the opposite phase. In the remaining two cases, both the VPC and the next beat are discarded before concatenation, in order to keep continuity of the TWA phase.

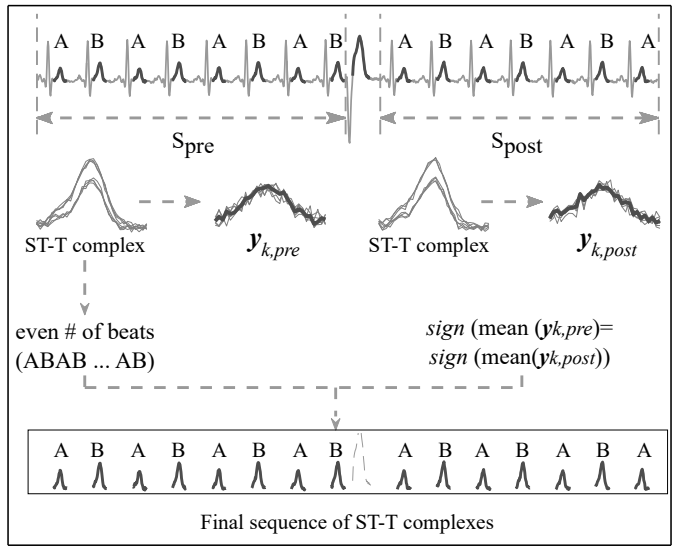

(a) $\boldsymbol{y}_{k,pre}$ and $\boldsymbol{y}_{k,post}$ with the same phase

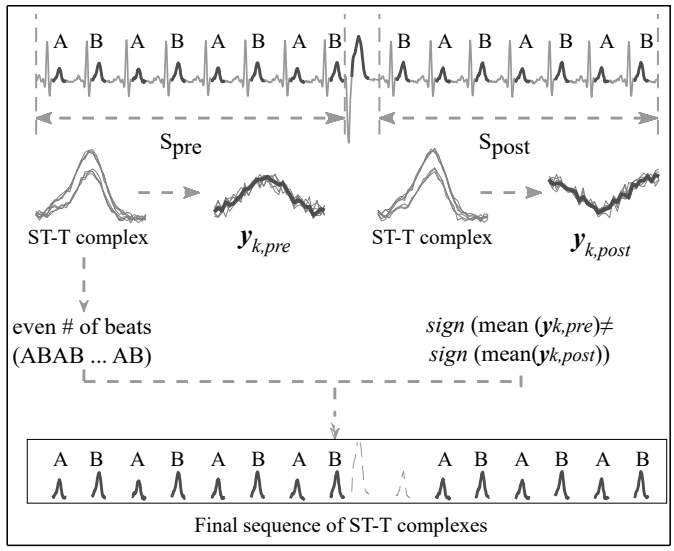

(b) $\boldsymbol{y}_{k,pre}$ and $\boldsymbol{y}_{k,post}$ with opposite phase

Figure 4.2: Two examples of synthetic TWA sequences including the presence of one VPC, and the processing applied for the estimation of the alternans waveform. (a) S_{pre} and S_{post} sub-sequences start at the same phase ($\bar{y}_{k,pre} > 0$ and $\bar{y}_{k,post} > 0$) and the VPC is in an odd position: only the VPC is excluded in the final sequence considered for the estimation of TWA waveform. (b) S_{pre} and S_{post} sub-sequences start with the opposite phase ($\bar{y}_{k,pre} > 0$ and $\bar{y}_{k,post} < 0$) and the VPC is in an odd position: both the VPC and the following beat are excluded in this case.

If there are M >1 non-consecutive abnormal beats in one ECG signal segment, M+1 subsequences can be defined. In this case, the same described approach is followed to concatenate the sequence of beats after each VPC to the previous sequence until all VPCs have been processed. Subsequences of just one or two beats are discarded.

Note that in the absence of TWA, the procedure can be applied in the same way, even if the estimated phases are related to other beat-to-beat variability components rather than TWA.

4.3.4 Alternans waveform estimation

Finally, the TWA waveform of the k^{th} segment, $\boldsymbol{y}_k$, was expressed as the median of the demodulated differences between ST-T complexes of even and odd beats [153], after the phase correction is applied to the data.

4.3.5 Phase alignment of alternans waveforms

TWA waveforms, $\boldsymbol{y}_k$, may not have the same polarity and, therefore, might cancel out when averaging. Thus, before final averaging, phase-alignment step is needed. As described in the previous chapter (see section 3.3.1), this phase-aligned waveform, denoted as $\boldsymbol{y}_k^a$, was estimated as:

$$\boldsymbol{y}_k^a = \text{sign}\left(\boldsymbol{y}_{d,k}^{\text{T}}\mathbf{w}_1\right)\boldsymbol{y}_k. \tag{4.4}$$

where $\boldsymbol{y}_{d,k}$ is a detrended version of $\boldsymbol{y}_k$ and $\mathbf{w}_1$ is the dominant waveform, obtained by a classical PCA analysis (see section 3.3.1 for a detailed description).

Finally, the index of average alternans including the VPC processing IAA_{VP} was defined as the mean absolute value of the average of the phase-aligned waveforms $\boldsymbol{y}_k^a$:

$$IAA_{\text{VP}} = \frac{1}{N}\sum_{n=1}^{N}\left|\frac{1}{K}\sum_{k=1}^{K} y_k^a\left(n\right)\right| \tag{4.5}$$

4.3.6 Statistical analysis

Data are presented as mean ± standard deviation for continuous variables and as number (percentage) for categorical variables, unless otherwise specified. Comparisons between SCD and non-SCD groups were evaluated by the two-tailed MannWhitney and Fisher exact tests for quantitative and categorical data, respectively. Non-parametric Friedman test and Wilcoxon signed rank paired test with Bonferroni correction were applied to evaluate differences among time intervals in circadian analysis. Prognostic value of TWA indices in predicting SCD was determined with univariate Cox proportional hazards analysis. Survival analysis was performed by using Kaplan-Meier estimator and comparison of cumulative events by log-rank test. For all tests, the null hypothesis was rejected when p$\leq \alpha$, with $\alpha = 0.05$. In the case of multiple comparison, the corrected significance level, α_c, is defined as $\alpha_c = \alpha/N$, with $N =$ the total number of comparisons.

4.4 Results

4.4.1 Simulation study

The effect of VPCs and the possible phase resetting of the alternans sequence in the estimation of the IAA index were evaluated using synthetic signals. Figure 4.3 shows examples of simulated beat sequences with artificial TWA and four additive noises: Gaussian noise, baseline wander, muscular activity and electrode motion.

For each TWA level, noise type, noise level and VPC probability, 100 different realizations were generated, randomizing the presence of the VPCs along the whole beat sequence, as well as the posterior phase resetting of the alternans sequence. Figure 4.4 shows the mean and standard deviation of the estimated IAA index, computed including the VPC processing and phase alignment (IAA_{VP}, blue line) and when these steps are not included, i.e. analyzing raw beat segments (IAA_{nVP}, grey dashed line), under different levels of noise (σ_{gn}, σ_{bw}, σ_{em} and σ_{ma}), for a VPC probability of 2%. Each curve is associated to a different TWA simulated amplitude. From top to bottom, peak amplitudes of alternans waveform were set to 300, 250, 200, 150, 100, 50 and 0 microvolts, which corresponds to average alternans

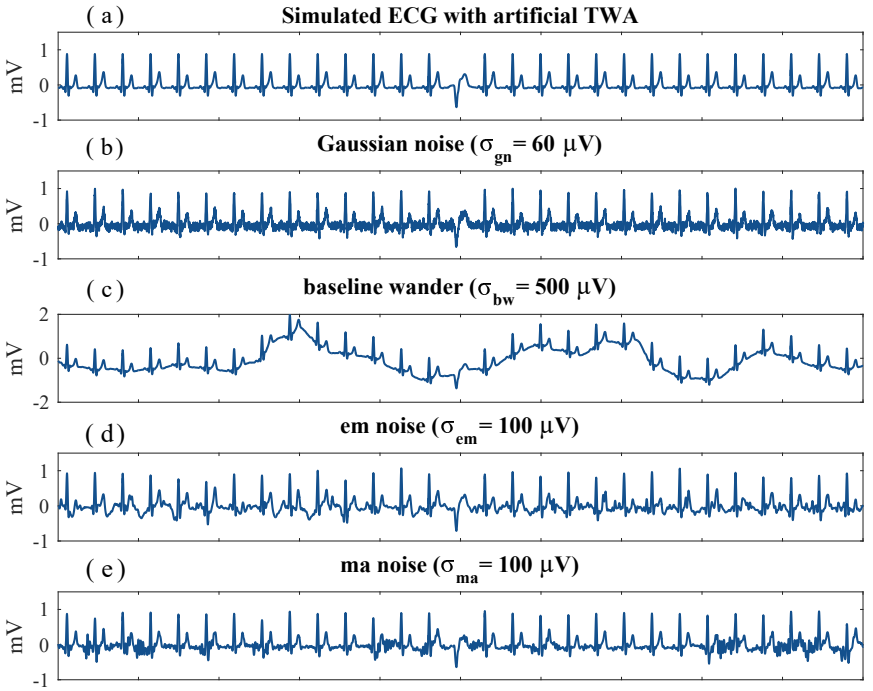

Figure 4.3: Simulated ECGs with added artificial TWA (a) and corrupted by different noises: Gaussian noise (b), baseline wander (c), electrode motion (d) and muscular activity (e).

amplitudes (IAA_{sim}) of 159.8, 133.2, 106.6, 79.9, 53.3, 26.6 and 0 microvolts, respectively.

Additionally, the effect of the number of VPCs present in the segment was also evaluated. For low, medium and high noise levels, the IAA was estimated by varying the probability of having a VPC from 0 to 20% (Figure 4.5). Peak alternans amplitudes from 0 to 200 μV in steps of 50 μV are represented (corresponding to IAA_{sim} of 0, 26.6, 53.3, 79.9 and 106.6 μV).

4.4.2 Ambulatory ECG

Holter ECG signals from CHF patients were processed using the same methodology. We computed both IAA_{VP} and IAA_{nVP} indices, as a measurement of the average TWA amplitude for the 24h recording, and compared the associated prognostic values. Patients were classified as TWA(+) or TWA(-) based on a risk threshold (TWA(+) if $IAA \geq th_{risk}$, TWA(-) otherwise). This th_{risk} threshold was defined as the third quartile of the total distribu-

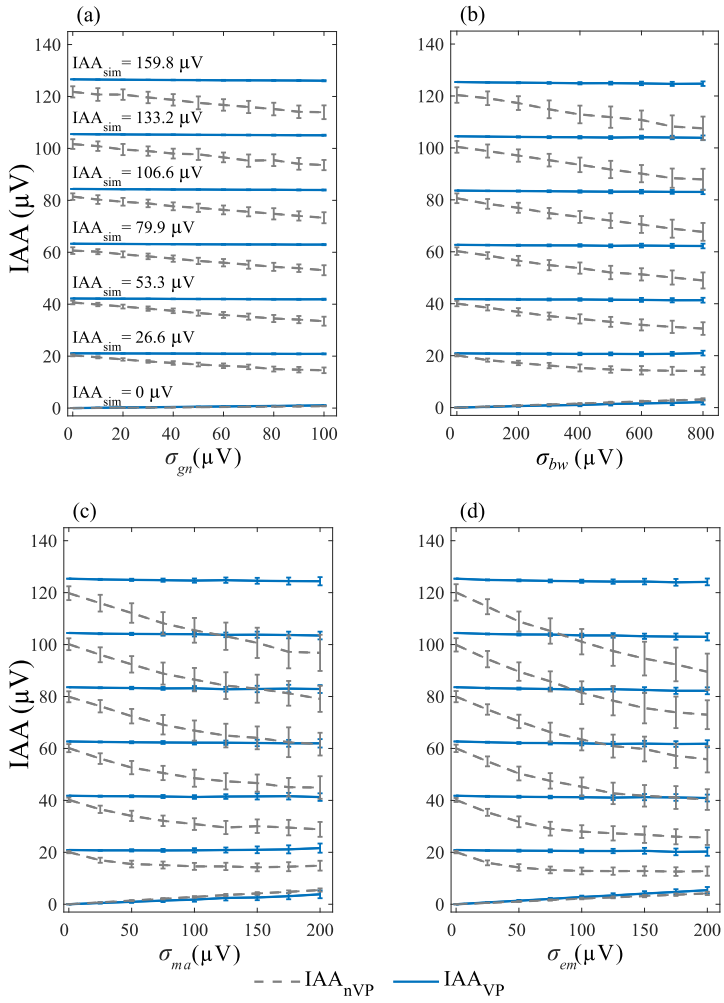

Figure 4.4: IAA estimation on synthetic signals with different noises types and levels (σ_{gn}, σ_{bw}, σ_{ma} and σ_{em} in panels (a), (b), (c) and (d), respectively) when the probability of VPCs is limited up to the 2%. Results are represented as mean std of 100 realizations for each combination of σ and alternans amplitude. From top to bottom, the curves represent the measured IAA with both methods when the simulated mean TWA amplitude (IAA_{sim}) was, respectively of 159.8, 133.2, 106.6, 79.9, 53.3, 26.6 and 0 μV (corresponding with the alternans peak amplitudes of 300, 250, 200, 150, 100, 50 and 0 μV). Blue line corresponds to the IAA estimated with the ectopic protection and phase alignment (IAA_{VP}) and grey dashed line represents the IAA estimation without any protection (IAA_{nVP}).

tion of IAA indices. Accordingly, the TWA(+) group is composed by the 25% of patients (n=163) with the largest IAA values each time. See Table 4.2 for the distribution of SCD events in the TWA(-) and TWA(+) groups.

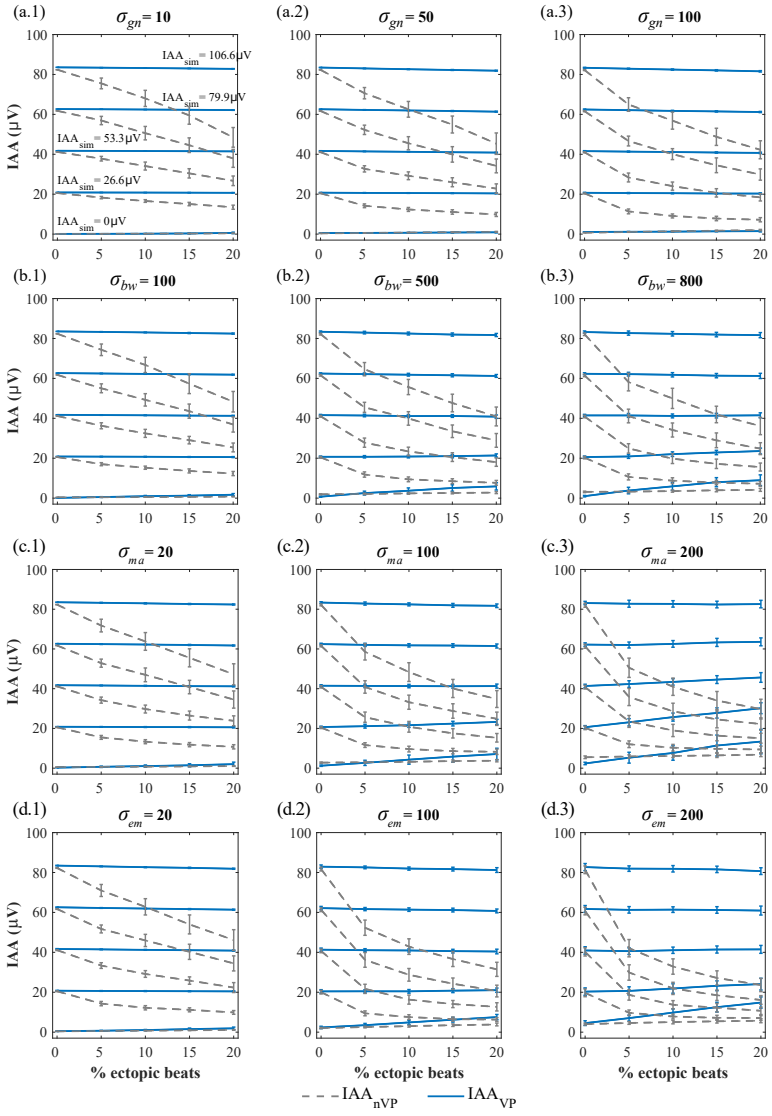

Figure 4.5: Effect of the number of VPCs present in the segment on IAA estimation for a low (left column), medium (middle column) and high (right column) levels of noise, from top to bottom σ_{gn}, σ_{bw}, σ_{ma} and σ_{em}. Results are represented as mean std of 100 realizations, where blue line corresponds to the IAA estimated with the VPC processing and phase alignment (IAA_{VP}) and grey dashed line represents the IAA estimation without any protection (IAA_{nVP}). In each panel, from top to bottom, the curves represent the measured IAA with both methods when the simulated mean TWA amplitude (IAA_{sim}) was, respectively of 106.6, 79.9, 53.3, 26.6 and 0 μV (corresponding with the alternans peak amplitudes of 200, 150, 100, 50 and 0 μV).

Finally, we evaluated the effect of including additional VPCs in the processing and we assessed the prognostic value of IAA indices in SCD prediction by performing a univariate Cox proportional hazards analysis. Results are summarized on Table 4.3. We started by including in the analysis only those VPC-free segments with $\Delta RR^N < 300$ ms, i.e. stable rhythm segments containing only normal beats. TWA(+) outcome was not associated with SCD. By sequentially adding segments containing a maximum of 1, 2 and 3 VPCs, TWA(+) outcome according to IAA_{VP} was in all cases successfully associated to SCD when the ectopic processing was included in the processing. In contrast, no association was found between IAA_{nVP} and SCD, except when a maximum of 1 VPC was allowed, being the hazard ratio in all cases lower than the one obtained with the ectopic processing (IAA_{VP}). Hazard ratios were increased by 17%, 19%, 29% when including 1, 2 and 3 VPCs, respectively. Finally, when all segments with $\Delta RR^N < 300$ ms regardless of the number of VPCs were included in the analysis, neither IAA_{nVP}, nor IAA_{VP} preserved the alternans predictive value (see Table 4.3).

Table 4.2: Number of SCD events included in TWA(-) and TWA(+) groups as a results of the analysis with the ectopic processing (IAA_{VP}) and without any protection (IAA_{nVP}). Data are expressed as absolute frequencies and percentages whithin TWA groups. Significant differences between the number of SCD events in TWA(-) and TWA(+) groups are indicated by *(p<.05) and **(p<.005).

	$\boldsymbol{IAA}_{\mathrm{nVP}}$		$\boldsymbol{IAA}_{\mathrm{VP}}$	
	TWA(-) (n=488)	**TWA(+)** (n=163)	**TWA(-)** (n=488)	**TWA(+)** (n=163)
ΔRR^N <300 with no VPCs	37 (7.6%)	18 (11.0%)	-	-
ΔRR^N <300 with ≤1 VPC	34 (7.0%)	21* (12.9%)	32 (6.6%)	23** (14.1%)
ΔRR^N <300 with ≤2 VPCs	36 (7.4%)	19 (11.7%)	34 (7.0%)	21* (12.9%)
ΔRR^N <300 with ≤3 VPCs	37 (7.6%)	18 (11.0%)	34 (7.0%)	21* (12.9%)
ΔRR^N <300	36 (7.4%)	19 (11.7%)	37 (7.6%)	18 (11.0%)

Table 4.3: Association of IAA indices with sudden cardiac death computed in patients with chronic heart failure. Results from the analysis with the ectopic processing (IAA_{VP}) and without any protection (IAA_{nVP}) are included. Hazard ratios significantly greater than 1 are indicated in bold.

	Average # of segments	**Risk threshold** (th_{risk})	**Hazard ratio** (95% CI)	**p-value**
ΔRR^N <300 with 0 VPC	527±414	th_{risk}^{nVP}=1.394 μV	1.590 (0.901,2.808)	0.11
ΔRR^N <300 with ≤1 VPC	669±448	th_{risk}^{nVP}=1.381 μV	**2.030** (1.174,3.509)	**0.011**
		th_{risk}^{VP}=1.470 μV	**2.386** (1.391,4.092)	**0.002**
ΔRR^N <300 with ≤2 VPCs	749±455	th_{risk}^{nVP}=1.354 μV	1.708 (0.977,2.987)	0.060
		th_{risk}^{VP}=1.544 μV	**2.026** (1.172,3.502)	**0.011**
ΔRR^N <300 with ≤3 VPCs	804±458	th_{risk}^{nVP}=1.339 μV	1.582 (0.898,2.786)	0.112
		th_{risk}^{VP}=1.649 μV	**2.035** (1.177,3.518)	**0.011**
ΔRR^N <300	1018±423	th_{risk}^{nVP}=1.509 μV	1.657 (0.950,2.889)	0.075
		th_{risk}^{VP}=2.282 μV	1.502 (0.885,2.638)	0.157

Finally, survival probability curves for the most significant predictive indices are shown on Figure 4.6. Results associated to both IAA_{nVP} and IAA_{VP} indices are included in grey and blue lines, respectively.

Circadian analysis of IAA_{VP}

Several studies have reported differences in repolarization dynamics between day and night, as well as in the incidence of SCD events [205–207]. In this section, circadian TWA changes in the 24-h hour Holter recordings from our CHF population were assessed. In addition, we evaluated whether the prognostic value of IAA_{VP} is sensitive to this circadian pattern. To do that, the IAA_{VP} was measured in consecutive 6-hour intervals (00.00-06.00

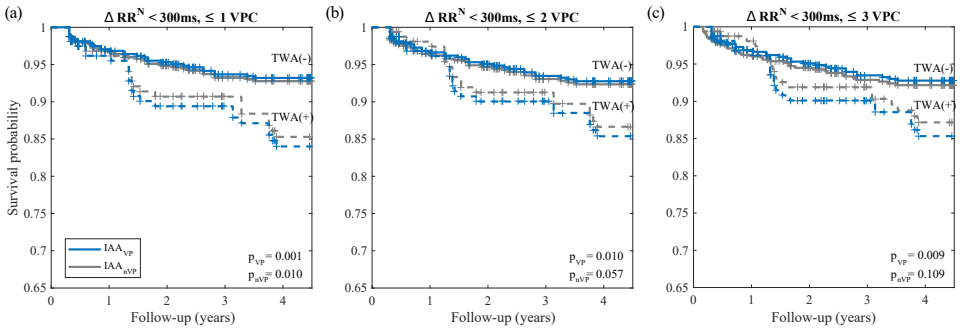

Figure 4.6: Survival probability curves of sudden cardiac death associated to IAA_{nVP} (grey lines) and IAA_{VP} (blue) in the chronic heart failure population. Each panel includes results corresponding to different selection criteria: (a) segments with $\Delta RR^N < 300$ ms with a maximum of 1 VPC allowed; (b) segments with $\Delta RR^N < 300$ ms with a maximum of 2 VPCs and (c) segments with $\Delta RR^N < 300$ ms with a maximum of 3 VPCs.

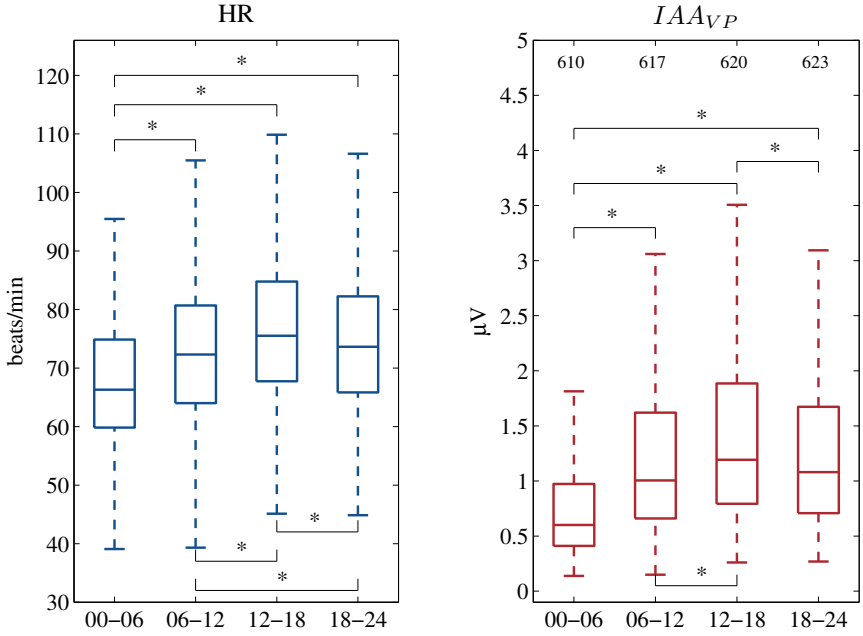

Figure 4.7: Distribution of HR and IAA_{VP} indices for each day interval. Number of records in which IAA_{VP} could be computed at each day period is indicated on left panel above the boxes.*: p<0.001, $\alpha_c = 0.0083$

h; 06.00-12.00 h; 12.00-18.00 h; 18.00-24.00 h) denoted, respectively, as $IAA_{\mathrm{VP}}^{00\text{-}06}$, $IAA_{\mathrm{VP}}^{06\text{-}12}$, $IAA_{\mathrm{VP}}^{12\text{-}18}$ and $IAA_{\mathrm{VP}}^{18\text{-}24}$.

According to the results presented in the previous section, this analysis was performed only considering the index that led to the best stratification performance, that is, including segments with ΔRR^N <300 ms and ≤1 VPCs.

The distributions of HR and IAA_{VP} for the four defined intervals are presented in Figure 4.7. Significant differences were found between the night and all daytime periods. IAA_{VP} was minimal during the night period, reaching its maximum value for the interval defined from 12.00 to 18.00 h ($IAA_{\mathrm{VP}}^{\text{00-06}}$=0.60 (0.41;0.97) $IAA_{\mathrm{VP}}^{\text{12-18}}$= 1.19 (0.79;1.89) μV, p<0.001, $\alpha_c = 0.0083$). It should be noticed here that not all recordings presented processable data for the total 24 hours, and consequently the index could not be computed for each interval in all subjects (number of available recordings for each day period are indicated in Figure 4.7, top of right panel).

The same trend was observed when considering average HR. However, only a weak correlation was found between IAA_{VP} and average HR (R^2 =0.038, p<0.001). The computation of the IAA_{VP} index for each time interval was also computed by restricting to ECG segments with average HR within an specific range from X-10 to X beats/min, denoted as $IAA_{\mathrm{VP}}^{\mathrm{X}}$, where X = $\{70, 80, 90, 100\}$). Results shown similar pattern of variation along the day for each HR range (Figure 4.9). Additionally, an increasing tendency from IAA_{VP}^{70} to IAA_{VP}^{100} in all day periods, was evidenced.

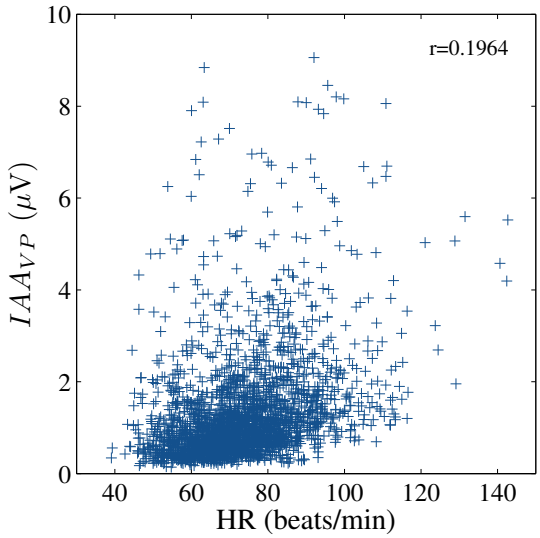

Figure 4.8: Scatterplot of IAA_{VP} versus HR.

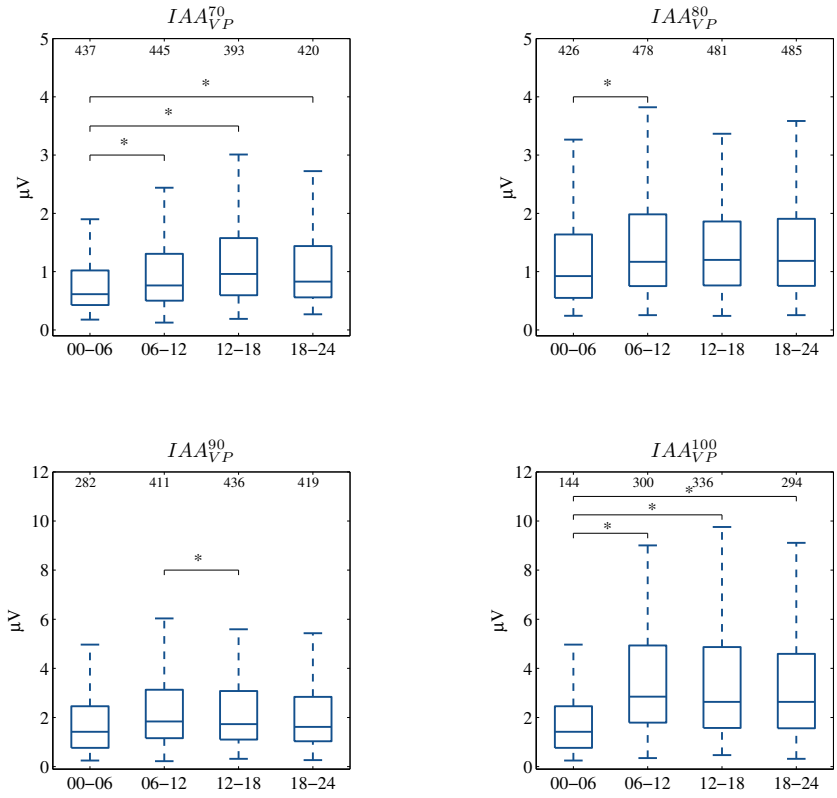

Figure 4.9: Distribution of IAA_{VP} HR-restricted indices at each day interval considering segments with average HR from 70 to 100 beats/min. Number of records in which IAA_{VP} could be computed at each day period is indicated above the boxes. *: p<0.001, $\alpha_c = 0.0083$

In order to evaluate the effect of the circadian pattern on the prognostic value, we replicated the Cox proportional analysis associated to the each index computed for each day interval. Patients at risk were defined according to a risk threshold which, as in the previous study, was set at the third quartile of the total distribution. Results are summarized in Table 4.4. By setting a cut point $IAA_{\mathrm{VP}}^{06\text{-}12}$=1.621 μV, the index computed during the morning hours was still successfully associate to SCD.

Table 4.4: Association of IAA_{VP} indices with SCD death.

	Hazard ratio (95% CI)	**p-value**
$IAA_{\mathrm{VP}}^{\text{00-06}} \geq 0.973$	1.45 (0.784, 2.690)	0.236
$IAA_{\mathrm{VP}}^{\text{06-12}} \geq 1.621$	**1.96 (1.114, 3.429)**	**0.019**
$IAA_{\mathrm{VP}}^{\text{12-18}} \geq 1.886$	1.60 (0.891, 2.856)	0.116
$IAA_{\mathrm{VP}}^{\text{18-24}} \geq 1.973$	1.69 (0.934, 3.048)	0.083

4.5 Discussion

In this chapter, we have proposed a method to improve the quantification of TWA activity in long-term ambulatory recordings by overcoming the presence of VPCs and the possible associated phase shifts in the alternans sequence, as well as other sources of noise that could lead to the underestimation of TWA amplitude.

TWA testing, usually performed in the clinical setting in stress tests, provides a positive, negative or indeterminate test result [199]. However, the rate of indeterminate tests remains high (up to 40%) [196–198] and the analysis of TWA on ambulatory ECG recordings has recently emerged as an alternative [149–152, 200, 201]. In particular, fully-automatic long-term averaging of TWA activity in 24h-ECG recordings has been already shown to be an independent predictor of SCD [157]. In that study, TWA estimation is based on the LLRM, which has been proved to be more robust than other methods to the presence of impulsive noise [145, 154], as the one produced in the beat-to-beat series when isolated abnormal beats (VPCs) are present in the analyzed segment. However, both unaltered and reversed phase of the alternans sequence following a premature beat have been described in the literature [158, 208] and this potential phase resetting can have a relevant impact on TWA estimation [147, 159, 209]. In particular, if the phase reversal occurs in the central beat of the segment, it can lead to measure a zero-voltage alternans when spectral analysis is used [160]. In order to overcome this limitation, the new approach presented in this work included an additional phase reversal control after the presence of any VPC, ensuring the phase continuity if alternans is present in the segment. For that purpose, the VPC and, if needed, the following beat are discarded before

estimating TWA magnitude in the segment. As a note, this methodology requires prior beat classification and VPC identification.

Additionally, all estimated alternans waveforms were aligned in sign, using a correlation criteria, before IAA estimation.

4.5.1 Simulation study

First, the accuracy of TWA estimation was assessed using synthetic ECG signals with added synthetic TWA and in the presence of four different types of noise: white Gaussian noise, baseline wander, muscular activity and electrode motion. According to the simulation results, with a fixed VPC probability per beat of 2%, the estimation accuracy is clearly higher when the ectopic processing and phase alignment were included (i.e, IAA_{VP}) than when this step is not included (IAA_{nVP}). Note that even in the absence of noise, TWA amplitudes are slightly underestimated as a consequence of the pre-processing baseline removal linear filter. Results evidenced also that TWA amplitude was markedly underestimated and had a larger variance when the VPC processing was not applied, being this bias larger as the noise level increased for a given TWA level. Moreover, both bias and variance were larger as the simulated TWA amplitude increased, but still both parameters, and especially the variance, were greatly reduced when the processing of ectopic beats and phase control were included.

Secondly, the impact of the number of VPCs on the TWA estimation was also evaluated. In this case, IAA_{VP} values remained essentially unchanged as the VPC probability increased for low and medium levels of noise. However, both parameters, bias and variance, significantly increased for IAA_{nVP} even when a very low percentage of VPCs ($\tilde{5}\%$) was allowed with low noise levels, regardless of the noise type.

A similar pattern of degradation for any *gn*, *bw* and *ma* noises was observed. Still, both methods appeared to be sensitive to high *ma* and *em* noise levels (>100 μV) and >5% of VPCs probability. Actually, this led to an over-estimation of IAA_{VP} with greater variances, in the absence of TWA, most probably due to noise components overlapping the TWA bandwidth, thus being interpreted as TWA. Even so, results confirm that the new approach represents a robust alternative for TWA estimation against the presence of moderate levels of noise and VPCs and the possible subsequent alternans phase reversal.

Nonetheless, in this simulation study only the effect of the possible phase resetting in the alternans sequence after the VPC has been taken into consideration, disregarding other possible induced changes in TWA morphology and amplitude, which were assumed unaltered. It is known that in real ECG signals the presence of a VPC, in addition to the possible phase resetting of alternans sequence, has also a derived effect in subsequent repolarizations, and changes in T wave morphology after VPCs have been studied [210–212]. Consequently, other possible variations in the sequence of TWA amplitudes, that could interfere in TWA measurement, could be also present in real ECGs.

4.5.2 Ambulatory ECG recordings

From a clinical perspective, with this work we have also demonstrated that the inclusion of the VPC processing in the TWA estimation led to an enhanced predictive value of the average TWA activity in the examined CHF population. That is, hazard ratios associated to the classification obtained for IAA_{VP}, including the VPC processing step, were always increased with respect to those based on IAA_{nVP}.

The motivation for using the long-term average of alternans activity in ambulatory ECGs was to provide with a reliable and robust measurement of TWA in a fully automatic way, but this requires for some additional restrictions in order to consider only suitable ECG segments to be included in the automatic analysis. In particular in this study, segments were considered suitable for the automatic analysis based on instantaneous RR-interval changes associated to "Normal" labelled beats present in the segment, and only those segments with instantaneous changes lower than 300 ms were included ($\Delta RR^N < 300$ ms). Nevertheless, from a physiological view-point, it becomes necessary to limit the maximum presence of VPCs as it would not make sense to measure TWA if many VPCs were included. Segments with more than 20% of abnormal beats were directly excluded from the analysis.

Moreover, the sequential inclusion of ECG segments with a controlled number of VPCs evidenced how the presence of VPCs affected the prognostic value of the index. Using the most restrictive criterion, that is, discarding segments containing any number of VPCs, led to the loss of predictability of the IAA_{nVP}. This could be explained by the low number of segments that

had fulfilled this requirement, consequently compromising the long-term average TWA estimation.

However, as this restriction was relaxed and segments with one VPC were included, TWA(+) outcome obtained for both IAA_{nVP} and IAA_{VP} was successfully associated to SCD, with more than a 2-fold increased risk in TWA(+) classified patients than in TWA(-), providing the best stratification performance. The inclusion of segments with 2 and 3 VPCs in the analysis decreased the hazard ratio, but still with significant association with SCD outcome for IAA_{VP}. However, when the ectopic protection was not included, then IAA_{nVP} lost its predictive value. Still in the last case, when no limitation in the number of VPCs was imposed ($\Delta RR^N < 300$ ms), the predictive value of IAA_{nVP} and IAA_{VP} was lost.

Actually, the presence of m VPCs in a 128-beat segment, originates m+1 shorter subsequences within it, which, as m increases, could compromise the local TWA estimation (i.e. $\boldsymbol{y}_{k,pre}$ and $\boldsymbol{y}_{k,post}$) used for the posterior decision in the concatenation of subsequences. This fact can be especially critical if it is the case that the S_{post} alternans sequence is also altered by the abnormal beat, being more sensitive as the number of VPCs included in the segment increases. This may also explain why the inclusion of all segments with more than 3 VPCs did not add additional prognostic value with respect to the other scenarios. Some studies have already revealed an increment in TWA amplitude after the occurrence of one isolated VPC just in some patients [158, 208], but the effect of more than one VPC within a short period of time (<128 beats) needs to be investigated.

Finally, higher th_{risk} values associated to the IAA_{VP} (th^{VP}_{risk}) were obtained with respect to th^{nVP}_{risk}, as reported on Table 4.3. This is in agreement with the the fact that IAA_{nVP} underestimates TWA amplitude with respect to IAA_{VP} as shown in the simulation study (see Figures 4.5 and 4.6). The use of a 75^{th} percentile of the total distribution of TWA measurements for the definition of the th_{risk}, already utilized in [157], is commonly adopted when a technique is first tested on a population [213,214]. Nevertheless, the applicability of the cut-points derived in this study still require additional prospective evaluation.

Circadian analysis

TWA activity was significantly higher during the day periods than during the night. Moreover, average TWA activity computed during the morning (from 06.00 to 12.00 h) period was associated with the risk of SCD in CHF patients. Interestingly, it coincides with the period of most elevated risk for SCD, whose distribution has been reported to present a primary peak of incidence from 7 to 11 a.m. and a secondary peak from 5 to 7 p.m. [207]. It should be remarked that the $IAA_{\mathrm{VP}}^{06-12}$ index would considerably reduce the required time for ECG monitoring from 24 to 6 hours, which could imply some practical advantages in the clinical practice.

Moreover, the increasing trend observed in IAA_{VP} when computed in segments with increased HR is also consistent with the fact that TWA amplitudes for the same subject rise with instantaneous HR. The HR-restriction of IAA_{VP} indices presented the same pattern for IAA_{VP}^{70} and IAA_{VP}^{100}, being similar when considering IAA_{VP}^{80} and IAA_{VP}^{90}. However, only a weak correlation was found between average HR and IAA_{VP} along the day. This suggests the influence of other HR-independent factors in IAA_{VP}, which are known to be also determinant for TWA and related to higher cardiac electrical instability. Changes in autonomic neurotransmitters, with and increased activity of sympathetic nervous system during the day, especially more prominent at waking time, could be other determinant factors that significantly influence TWA [151]. Also, fluctuations in symptomatic and silent myocardial ischemia episodes, well-known to be linked to TWA phenomenon, have been reported to present this similar behavior [215]. This supports the hypothesis that TWA modulation along the day could be actually due to a circadian effect.

4.6 Conclusion

The proposed methodology for computing the index of average alternans, deals with the presence of ventricular premature contractions and with the possible induction of phase resetting in the alternans sequence. The simulation study showed that it represents an accurate and noise-robust solution for quantifying TWA. Moreover, the analysis of ambulatory ECGs of mild-to-moderate CHF patients demonstrated the enhancement in the predictive value of IAA for SCD stratification by analyzing segments with limited

number of VPCs. In addition, results suggest that a circadian pattern modulates the IAA_{VP} index, and that the time of the day should be considered for SCD risk prediction.

Chapter 5

Quantification of ventricular repolarization instabilty in ambulatory recordings for SCD-risk stratification in CHF patients with AF

5.1 Motivation

As introduced in section 1.4.3, AF is the most common arrhythmia and it has become one of the most important public health issues in developed countries, together with CHF. Both pathological conditions are highly associated to poor outcomes, including SCD. Actually, recent data reported that AF can increase the risk of ventricular arrhythmias [80–83] leading to SCD more often than to stroke. However, the mechanisms that associate AF, CHF and SCD risk are still unclear and a deeper understanding is required to adopt effective predictive and therapeutic strategies in this target population. ICD implantation, which protects from SCD by terminating ventricular tachyarrhythmias, can be an alternative, but it results difficult to identify those patients who may benefit the most from this therapy, especially in the AF subgroup.

The most common ECG-derived markers (see section 1.5 for a detailed description), including QT-interval duration and dynamics, the Tpe interval or TWA to name some of them, require the patient to be in sinus rhythm to be properly assessed [161]. It is the highly irregular ventricular response during AF, mainly influenced by the properties of the AV node and atrial electrophysiology, that makes the use of those indices not appropriate in this particular condition.

In this chapter, we hypothesized that a non-invasive stratification of AF patients at risk of SCD is possible by assessing ventricular repolarization in the electrocardiogram signal. For that purpose, a new method to quantify ventricular repolarization changes based on a selective heart rate bin averaging technique is presented. New indices of repolarization variation are proposed and their prognostic values for SCD evaluated in a CHF population with AF.

5.2 Materials

The potential clinical value of the proposed indices was evaluated in a cohort of 171 patients with permanent AF enrolled in the MUSIC study, already introduced in section 4.2.2. Some relevant patient characteristics of the AF subgroup are summarized on Table 5.1. Within the study population, a total of 19 patients were victims of SCD, 24 of other cardiac causes, 20 of non-cardiac deaths and 108 were survivors after 48 months of follow-up.

Table 5.1: Characteristics of atrial fibrillation patients. Data are presented as mean±standard deviation and as absolute frequencies (percentages).

	Overall population (n=171)	**SCD group** (n=19)	**Non-SCD group** (n=152)
Age (years)	68.9±10.4	69.2±10.5	68.9±10.4
Gender (males)	128 (74.8%)	16 (84.2%)	112 (73.7%)
LVEF $\leq$ 35%	87 (50.9%)	14 (73.7%)	73* (48.0%)
NYHA class III	49 (28.6%)	5 (26.3%)	44 (28.9%)
Diabetes	50 (29.2%)	6 (31.6%)	44 (28.9%)
Ischemic etiology	46 (26.9%)	10 (52.6%)	36* (23.7%)
Beta-blockers	100 (58.5%)	9 (47.3%)	91 (59.9%)
Amiodarone	25 (14.6%)	2 (10.5%)	23 (15.1%)
Digoxin	106 (62.0%)	11 (57.9%)	95 (62.5%)
QRSd $\geq$ 120 ms	71 (41.5%)	11 (57.9%)	60 (39.5%)

*p$\leq$0.05 SCD vs Non-SCD groups
LVEF: Left ventricular ejection fraction
NYHA: New York Heart Association; QRSd: QRS duration.

5.3 Methods

5.3.1 Preprocessing

Preprocessing of ECG recordings included detection and labelling of ventricular complexes using the Aristotle ECG analysis software [204]. The RR interval associated to the i^{th} beat was defined as the difference between the R-wave positions of the i^{th} and $(i-1)^{th}$ beats, as illustrated in Figure 5.1. Then, after high-pass linear filtering of baseline wander, the ECG was low-pass filtered (with cut-off frequency of 15 Hz) in order to remove noise out of T-wave frequency range and down-sampled by a factor of 2. From the 3 orthogonal leads, the vector-magnitude of the VCG signal was also computed.

5.3.2 Selective beat averaging

We proposed the use of a concept similar to selective beat averaging technique [216] to compute the average T-wave variation waveform in consecutive beats defined by bins of stable RR. The algorithm proceeds as follows:

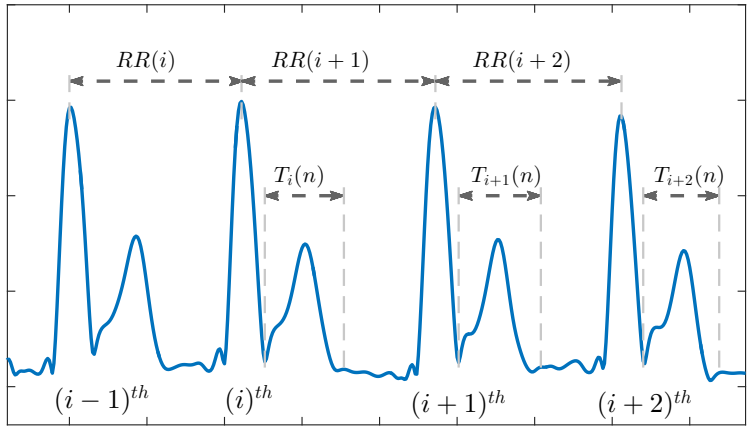

Figure 5.1: Illustration of the vectormagnitude of an ECG signal with main explicative intervals.

1. After automatic identification, ventricular $QRS-T$ complexes were grouped based on their associated RR interval. To do that, we first define S as the set of all triplets of consecutive beats within the Holter recording: $(i, i+1, i+2)$, for any initial beat i. We then subdivide the considered range of RRs (initially between $minRR = 300$ ms and $maxRR = 1600$ ms) into K bins, denoted as I_k, $(k = 1, \cdots, K)$. For each bin, an associated subset S_k is defined as containing those triplets in S whose first element i is included in I_k, and whose difference between consecutive RR intervals (i.e, between $RR(i+1)$ and $RR(i)$, and between $RR(i+2)$ and $RR(i+1)$) is lower than half of the bin width. That is:

$$S_k = \{(i, i+1, i+2)\} \tag{5.1}$$

$$where\big\{RR(i) \in I_k,$$
$$|RR(i+1) - RR(i)| \leq \tfrac{\delta}{2}, |RR(i+2) - RR(i+1)| \leq \tfrac{\delta}{2}\big\} \tag{5.2}$$

$$I_k = \big\{RR(i) : \mathrm{m}inRR + (k-1)\delta \leq RR(i) \leq \mathrm{m}inRR + k\delta\big\} \tag{5.3}$$

We set the bin width as δ=40 ms. In this step, basically triplets of consecutive beats that were preceded by a similar RR interval were selected, thus allowing the assumption of stability.

2. For each triplet of beats included in S_k, two T-wave variation waveforms, $\Delta T_1(n)$ and $\Delta T_2(n)$, were defined as the difference between each pair of consecutive ST-T complexes:

$$\Delta T_{(i,1)}(n) = T_{(i+1)}(n) - T_{(i)}(n) \tag{5.4}$$

$$\Delta T_{(i,2)}(n) = T_{(i+2)}(n) - T_{(i+1)}(n), \qquad n = 1, \ldots, N \tag{5.5}$$

where $T_i(n)$ denotes the ST-T complex of the i^{th} beat (Figure 5.1), defined as a fixed interval of 300 ms after the end of the QRS complex, with n the index of the sample within the complex.

3. From $\Delta T_1(n)$ and $\Delta T_2(n)$ waveforms, two measurements of ventricular variability were derived:

$$v_i^+(n) = \frac{\Delta T_{(i,1)}(n) + \Delta T_{(i,2)}(n)}{2} \tag{5.6}$$

$$v_i^-(n) = \frac{\Delta T_{(i,1)}(n) - \Delta T_{(i,2)}(n)}{2}, \tag{5.7}$$

where $v_i^+(n)$ quantifies the average repolarization variation in each triplet, and $v_i^-(n)$ measures the alternant repolarization variation along the three consecutive stable beats. In the following, we will use vector notation, being $\boldsymbol{v}_i^+$ and $\boldsymbol{v}_i^-$ the column vectors whose elements are the samples of $v_i^+(n)$ and $v_i^-(n)$, respectively.

4. Since this variation of the ventricular repolarization activity can be within the range of few microvolts, comparable to the noise level, we replicate the analysis already presented in the previous chapters in the context of TWA analysis, where all TWA waveforms were aligned in phase before final averaging. In this case, the phase-aligned waveforms, $\boldsymbol{v}_i^{a+}$ and $\boldsymbol{v}_i^{a-}$, were estimated as:

$$\boldsymbol{v}_i^{a+} = sign\left(\boldsymbol{v}_i^{+T}\mathbf{w}_1^+\right)\boldsymbol{v}_i^+ \tag{5.8}$$

$$\boldsymbol{v}_i^{a-} = sign\left(\boldsymbol{v}_i^{-T}\mathbf{w}_1^-\right)\boldsymbol{v}_i^- \tag{5.9}$$

where $\mathbf{w}_1^+$ corresponds to the first eigenvector associated to the greatest eigenvalue λ_1^+ of the correlation matrix $\mathbf{R}_{\boldsymbol{v}^+}$ estimated from all

variability vectors $\boldsymbol{v}_i^+$, and $\mathbf{w}_1^-$ is the first eigenvector associated to the greatest eigenvalue λ_1^- of the correlation matrix $\mathbf{R}_{\boldsymbol{v}^-}$ estimated from all variability vectors $\boldsymbol{v}_i^-$ (see section 3.3.1 for more details).

5. Finally, the average repolarization variation associated to the k^{th} bin, i.e. the subset S_k, denoted as $\overline{\boldsymbol{v}}_k^+$, is defined as the median waveform of all $\boldsymbol{v}_i^{a+}$ computed for the respective bin. In the same way, the alternant variation waveform associated to the same bin, denoted as $\overline{\boldsymbol{v}}_k^-$, is defined as the median waveform of all $\boldsymbol{v}_i^{a-}$.

5.3.3 The 3-beat indices of ventricular repolarization variation

Based on these two measurements, we propose two indices to characterize the repolarization variation in the 24-hour Holter recording: the index of average repolarization variation and the index of alternant variation within sequences of 3 beats, $\mathrm{I}_{\mathrm{V3}}^+$ and $\mathrm{I}_{\mathrm{V3}}^-$, respectively. They were defined as the mean absolute value of the final average waveform of all bins (of all $\overline{\boldsymbol{v}}_k^{a+}$ and $\overline{\boldsymbol{v}}_k^{a-}$, respectively). That is:

$$\mathrm{I}_{\mathrm{V3}}^+ = \frac{1}{N}\sum_{n=1}^{N}\left|\frac{1}{K}\sum_{k=1}^{K}\overline{v}_k^{a+}(n)\right| \tag{5.10}$$

$$\mathrm{I}_{\mathrm{V3}}^- = \frac{1}{N}\sum_{n=1}^{N}\left|\frac{1}{K}\sum_{k=1}^{K}\overline{v}_k^{a-}(n)\right| \tag{5.11}$$

with N the total number of samples in the ST-T complex.

Both indices were also computed on each individual lead, denoted as $\mathrm{I}_{\mathrm{V3X}}^+$, $\mathrm{I}_{\mathrm{V3Y}}^+$, $\mathrm{I}_{\mathrm{V3Z}}^+$, $\mathrm{I}_{\mathrm{V3X}}^-$, $\mathrm{I}_{\mathrm{V3Y}}^-$ and $\mathrm{I}_{\mathrm{V3Z}}^-$ for leads X, Y and Z, respectively. Additionally, we defined the heart-rate restricted indices $\mathrm{I}_{\mathrm{V3}}^{+90}$ and $\mathrm{I}_{\mathrm{V3}}^{-90}$ by including only bins associated to heart rates faster than 90 beats/min (i.e. RR <660 ms).

5.3.4 The 2-beat index of ventricular repolarization variation

Instantaneous beat-to-beat repolarization variation in 2-beat sequences, denoted as I_{V2}, is also computed, following a similar approach but considering

only pairs of 2 consecutive beats $(i, i+1)$ with similar RR. In that case, each subset S'_k was defined as:

$$S'_k = \{\, (i, i+1) \,\} \tag{5.12}$$

$$where \{ RR(i) \in I_k, |RR(i+1) - RR(i)| \leq \tfrac{\delta}{2} \} \tag{5.13}$$

A single T-wave variation waveform was computed for each pair of beats in S'_k as $\Delta T_i(n) = T_{(i+1)}(n) - T_{(i)}(n)$. Finally, the $\mathrm{I_{V2}}$ was defined as:

$$\mathrm{I_{V2}} = \frac{1}{N} \sum_{n=1}^{N} \left| \frac{1}{K} \sum_{k=1}^{K} \overline{\Delta T}^{a}_{k}(n) \right| \tag{5.14}$$

where $\overline{\Delta T}^{a}_{k}(n)$, analogous to the computation of the previous indices, is the median variation waveform of all $\Delta T_i(n)$ included in the corresponding subset S'_k, after being aligned in sign.

Also in this case, the index $\mathrm{I}^{90}_{\mathrm{V2}}$, including bins associated to heart rates faster than 90 beats/min, was computed.

5.3.5 Statistical analysis

Data are presented as median (25^{th}; 75^{th} percentiles) for continuous variables and as number (percentage) for categorical variables, unless otherwise specified. Two-tailed Mann-Whitney and Fisher exact tests were applied to evaluate differences between groups in quantitative and categorical data, respectively. Survival analysis was performed by using Kaplan-Meier estimator and comparison of cumulative events between groups by the log-rank test. Prognostic value of proposed indices in predicting SCD was determined with univariate and multivariate Cox proportional hazards analysis. For all tests, the null hypothesis was rejected for p≤0.05.

5.4 Results

Indices were computed for each available Holter recording. Distributions of $\mathrm{I^{+}_{V3}}$, $\mathrm{I^{-}_{V3}}$, $\mathrm{I^{+90}_{V3}}$ and $\mathrm{I^{-90}_{V3}}$ are presented in Figure 5.2, for both SCD and non-SCD groups of patients. As shown in the figure, SCD outcome was

associated in most cases with higher values, i.e, with higher repolarization variability.

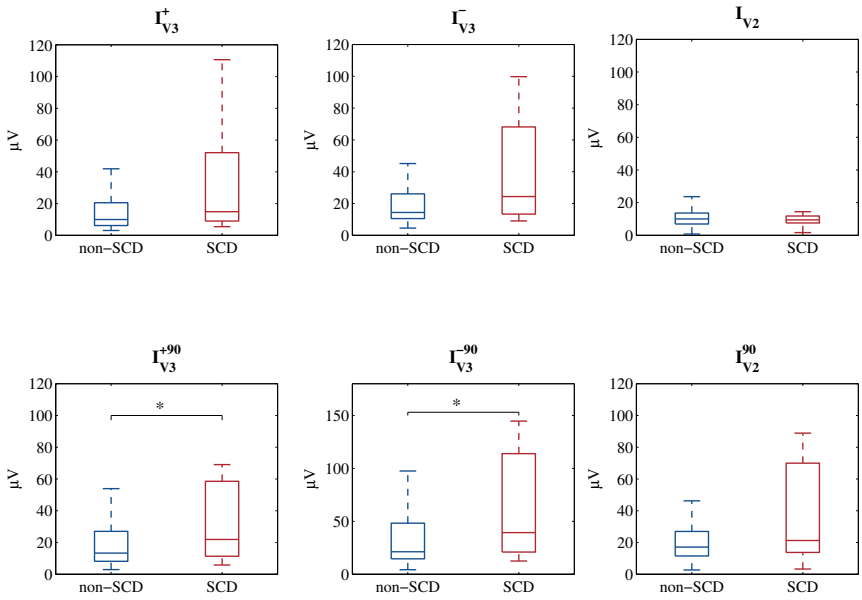

Figure 5.2: Distribution of I_{V3} and I_{V2} indices for non-SCD and SCD groups. *: p≤0.05 non-SCD vs SCD.

I^{+}_{V3} and I^{-}_{V3} were not computable in 8 out of 171 Holters (4.7%) as only 2 leads were available and the vector-magnitude of the VCG could not be computed. Moreover, the additional restriction imposed when computing I^{+90}_{V3} and I^{-90}_{V3}, by considering only bins of RRs associated to HRs $\geq$ 90 beats/min, led to the exclusion of 7 additional recordings (8.7% of the total population) in which there was not any suitable triplet of beats accomplishing the conditions in that range.

Both indices were also computed in each lead individually. The associated distributions, are shown in Figure 5.3. Also in this case, SCD group is associated to higher values, with significant differences between groups in case of using lead X and bins with HRs $\geq$ 90 beats/min.

Regarding the 2-beat indices, the distributions of I_{V2} and I^{90}_{V2} values for both groups are also presented in Figure 5.2 (right pannels). While I_{V2} values did not present significant differences between SCD and non-SCD groups, I^{90}_{V2} was higher in SCD group in comparison with the non-SCD group, though not statistically significant (21.21 (13.7;69.93) μV vs 17.1

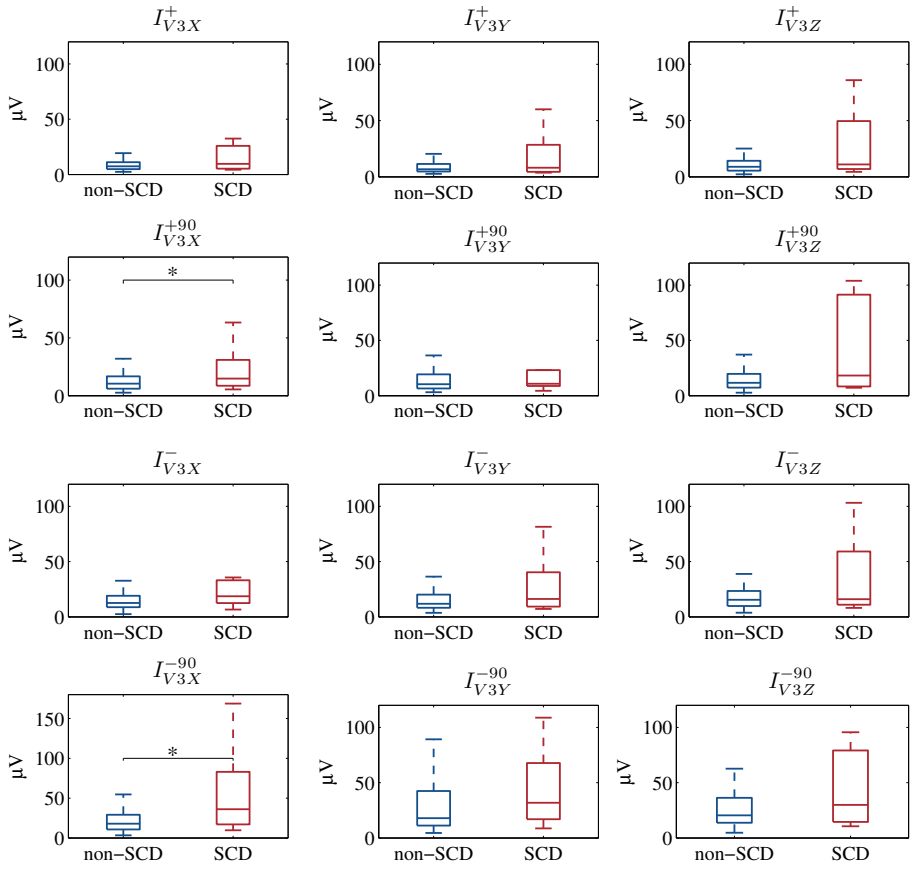

Figure 5.3: Distribution of I_{V3X}, I_{V3Y} and I_{V3Z} in left, middle and right pannels, for non-SCD and SCD groups. *: p≤0.05 non-SCD vs SCD.

(11.49;26.296) μV, NS). In this case, I^{90}_{V2} was not computable in 10 out of 171 recordings, either because only 2 leads were available (8 recordings) or because the methodology did not select any processable interval (2 recordings).

Then, the individual predictive value of each index was tested. To do that, the same strategy as in the previous study was followed, setting a risk threshold th_{risk} corresponding to the 75^{th} percentile of the total distribution of I_{V3} values (i.e. $I_{V3}(+)$ if $I_{V3} \geq th_{risk}$ and $I_{V3}(-)$, otherwise).

Univariate analysis demonstrated that I^{+}_{V3X}, I^{+90}_{V3X}, I^{-90}_{V3}, I^{+}_{V3X} and I^{-90}_{V3X} were successfully associated to SCD outcome (see Table 5.2).

Table 5.2: Association of I_{V3} and I_{V2}^{90} indices with sudden cardiac death in patients with heart failure and atrial fibrillation.

	Univariate		**M1**	
	HaR (95% CI)	**p-value**	**HaR** (95% CI)	**p-value**
$I_{V3}^{+} \geq 22.650\ \mu V$	2.45 (0.98,6.08)	0.054	2.25 (0.87,5.84)	0.096
$I_{V3}^{+90} \geq 32.517\ \mu V$	2.15 (0.83,5.55)	0.113	1.91 (0.70,5.23)	0.209
$I_{V3X}^{+} \geq 11.752\ \mu V$	**2.97** (1.21,7.31)	**0.018**	**2.85** (1.09,7.44)	**0.033**
$I_{V3X}^{+90} \geq 17.332\ \mu V$	**2.97** (1.17,7.53)	**0.022**	**2.81** (1.01,7.81)	**0.047**
$I_{V3}^{-} \geq 28.101\ \mu V$	2.38 (0.96,5.93)	0.062	2.22 (0.83,5.88)	0.111
$I_{V3}^{-90} \geq 56.334\ \mu V$	**2.91** (1.15,7.39)	**0.024**	2.53 (0.97,6.58)	0.057
$I_{V3X}^{-} \geq 20.287\ \mu V$	**2.88** (1.17,7.08)	**0.021**	**2.82** (1.09,7.33)	**0.033**
$I_{V3X}^{-90} \geq 34.133\ \mu V$	**3.76** (1.49,9.48)	**0.005**	**3.20** (1.21,8.48)	**0.020**
$I_{V2}^{90} \geq 28.86\ \mu V$	**2.66** (1.07,6.63)	**0.035**	**2.88** (1.10,7.57)	**0.032**

M1: Adjusted model includes age, gender, New York Heart Association class, left ventricular ejection fraction≤35%, diabetes, the use of antiarrhythmic drugs (beta-blockers, digoxin and amiodarone), and the proposed index

In addition to the univariate Cox proportional model, one multivariate model (M1) was also constructed by adjusting for significant clinical covariates including age, gender, NYHA class, LVEF≤35%, diabetes and the use of antiarrhythmic drugs (beta-blockers, digoxin and amiodarone). To note, the index I_{V3X}^{-90} preserves its predictive value with hazard ratios of 3.76 and 3.20 for univariate and M1 models, respectively.

Regarding to the I_{V2}^{90} index, patients classified as $I_{V2}^{90}(+)$ were successfully associated with SCD outcome, with hazard ratios of 2.66 and 2.88 for univariate and M1 models, respectively (see Table 5.2). However, the index lost its predictive value if no restriction in HR was imposed (I_{V2}).

Figure 5.4 shows the Kaplan-Meier survival curves for SCD associated to most significative indices. Clearly, mortality rates were always significantly higher in the positive (+) group in comparison to patients classified as negative (−) at the end of the follow-up period.

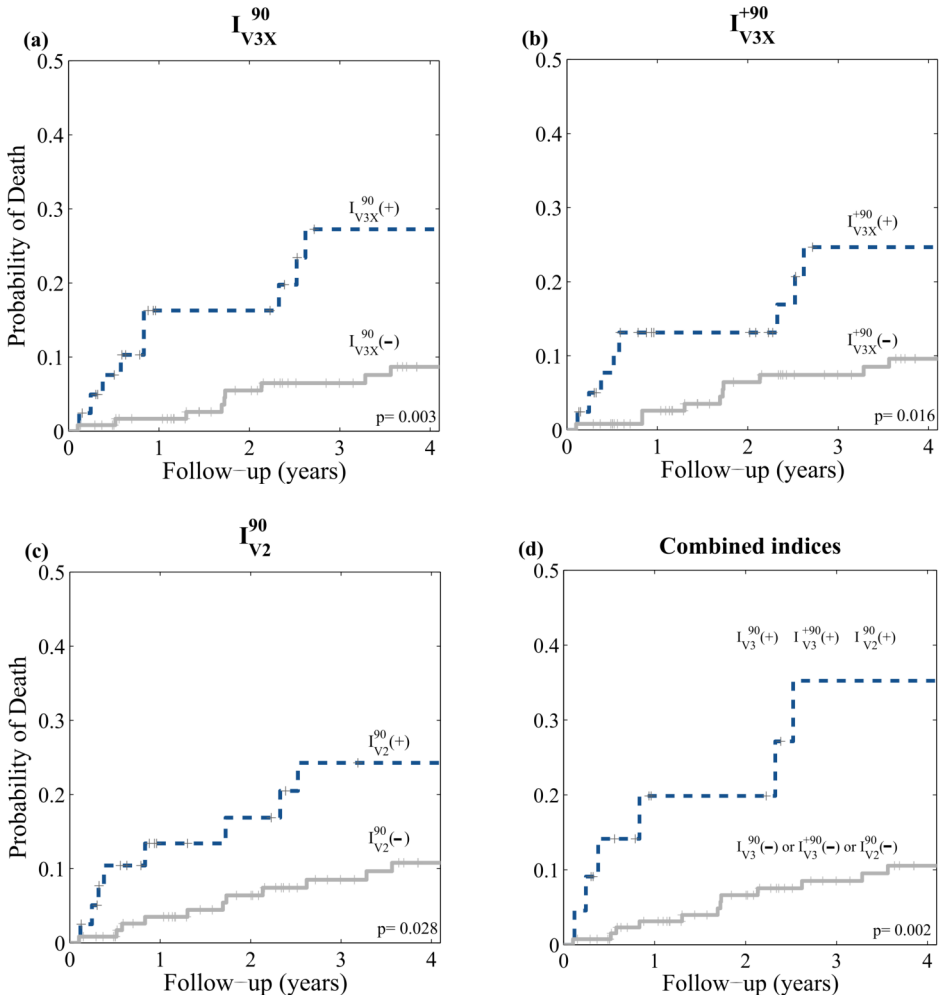

Figure 5.4: Cumulative probability curves of sudden cardiac death associated to (a) I^{-90}_{V3X} (b) I^{+90}_{V3X}, (c) I^{90}_{V2} and (d) combination of I^{+90}_{V3} & I^{-90}_{V3} & I^{90}_{V2} indices.

5.4.1 Combination of I_{V3} and I_{V2}

Finally, an additional analysis was performed to assess whether the use of combined indices would improve SCD risk stratification. First, results derived from the analysis of I^{-}_{V3} and I^{+}_{V3} were combined, then additional information from I^{90}_{V2} analysis was also included. Results from univariate and M1 multivariate models are shown in Table 5.3. The combination of I^{-}_{V3} and I^{+}_{V3} improved the single stratification performance of I^{-}_{V3} and I^{+}_{V3} in most of the cases. Nonetheless, the better prognostic values were obtained when I^{90}_{V2} was also considered: the combination of patients that were simultaneously classified as $I^{-}_{V3}(+)$, $I^{+}_{V3}(+)$ and $I^{90}_{V2}(+)$ in the individual analysis, identified patients with more than 4-fold increased risk of SCD in the univariate analysis. The best performance is obtained by considering patients at risk according to $I^{-}_{V3X}(+)$ and $I^{+}_{V3X}(+)$ and $I^{90}_{V2}(+)$ (i.e, the group of patients that were classified as positive in these three cases: $I^{-}_{V3X}(+)$ & $I^{+}_{V3X}(+)$ & $I^{90}_{V2}(+)$ group) which presented more than 6-fold increased risk of SCD in the two predictive models (univariate and M1). Kaplan-Meier survival curve is shown in Figure 5.4 (d).

5.5 Discussion

Non-invasive assessment of ventricular repolarization heterogeneities during atrial fibrillation is not a straightforward task, consequence of the irregular ventricular activity present under this particular condition. In this chapter, a new method able to quantify ventricular repolarization changes, suitable in the particular condition of AF was presented. The prognostic value of some derived indices was evaluated in a chronic heart failure population with AF. We found that both the 3-beat index of ventricular repolarization variation, I^{-90}_{V3}, and the 2-beat index of ventricular repolarization variation I^{90}_{V2}, restricted to heart rates ≥ 90 beats/min, which quantify consecutive T-wave variations based on a selective beat averaging methodology, independently predicted SCD in this study population. Interestingly, the computation of I_{V3} in a single-lead basis led to an improvement in the predictive value when using lead X (I^{-}_{V3X}, I^{-90}_{V3X}, I^{+}_{V3X} and I^{+90}_{V3X}). Moreover, risk stratification based on the combination of I_{V3} and I^{90}_{V2} indices rather than individual performance, provided the identification of patients at highest risk of SCD.

Table 5.3: Association of the combination of I_{V3} and I_{V2}^{90} indices with sudden cardiac death in patients with heart failure and atrial fibrillation.

	positive patients (%)	Univariate		M1	
		HaR (95% CI)	**p-value**	**HaR** (95% CI)	**p-value**
$I_{V3}^{+}(+)\&I_{V3}^{-}(+)$	37 (21.6%)	**2.72** (1.09,6.77)	**0.031**	**2.84** (1.07,7.56)	**0.036**
$I_{V3}^{+90}(+)\&I_{V3}^{-90}(+)$	36 (21.1%)	2.49 (0.96,6.42)	0.06	2.29 (0.86,6.10)	0.097
$I_{V3X}^{+}(+)\&I_{V3X}^{-}(+)$	32 (18.7%)	**3.59** (1.44,8.94)	**0.006**	**3.73** (1.40,9.93)	**0.008**
$I_{V3X}^{+90}(+)\&I_{V3X}^{-90}(+)$	32 (18.7%)	**3.22** (1.25,8.33)	**0.016**	**2.81** (1.00,7.93)	**0.050**
$I_{V3}^{+}(+)\&I_{V3}^{-}(+)\&I_{V2}^{90}(+)$	19 (11.1%)	**4.29** (1.63,11.30)	**0.003**	**4.07** (1.45,11.44)	**0.008**
$I_{V3}^{+90}(+)\&I_{V3}^{-90}(+)\&I_{V2}^{90}(+)$	22 (12.9%)	**4.22** (1.58,11.30)	**0.004**	**4.05** (1.42,11.52)	**0.009**
$I_{V3X}^{+}(+)\&I_{V3X}^{-}(+)\&I_{V2}^{90}(+)$	15 (8.8%)	**6.49** (2.46,17.14)	**<0.001**	**6.35** (2.16,18.73)	**0.001**
$I_{V3X}^{+90}(+)\&I_{V3X}^{-90}(+)\&I_{V2}^{90}(+)$	15 (8.8%)	**4.47** (1.59,12.61)	**0.005**	**3.67** (1.23,10.86)	**0.019**

M1: Adjusted model includes age, gender, New York Heart Association class, left ventricular ejection fraction≤35%, diabetes, the use of antiarrhythmic drugs (beta-blockers, digoxin and amiodarone) and the proposed index

The underlying mechanisms that associate AF and SCD are still intriguing. Actually, recent data have suggested SCD as the most common single cause of death in AF patients, rather than stroke or deaths from other cardiovascular origin [61, 217]. Indeed, some studies suggested that AF is intrinsically pro-arrhythmic in the ventricle, increasing susceptibility to ventricular arrhythmias (and, consequently, SCD) [80–83], whereas others support the hypothesis that AF is actually acting through other risk factors, like CHF, leading to the increase in SCD incidence [218, 219]. A more comprehensive understanding of this phenomenon is still needed to better plan treatment strategies. In this context, non-invasively ascertai-

ning in what patients this proarrhythmic risk is higher, is crucial for the question of therapy decision-making. However, it is the irregularity in the ventricular response during AF that makes the use of well-established electrocardiographic markers for SCD prediction not extensible to patients in this rhythm. Indices such as TWA, among others, require the patient to be under a sinus rhythm condition to be properly assessed [161], while there is not any standard method for measuring QT interval/dynamics or TWA when irregular ventricular rhythm is present. Data on SCD stratification in AF patients based on electrical instability in the ventricle are scarce.

The methodology, measurements based on selective beat averaging [216], selected consecutive beats preceded by a similar RR interval ($\leq \pm 20$ ms), from which beat-to-beat variations in ventricular repolarization were assessed under stable rhythm. First, selecting triplets of stable beats, two indices were computed: $\mathrm{I}_{\mathrm{V3}}^{+}$, measuring the average repolarization variation within the triplet, and $\mathrm{I}_{\mathrm{V3}}^{-}$, which could be considered as a measurement of the average alternant variation in the triplet. The later arises as a first attempt in the assessment of instantaneous local alternans, as the irregular ventricular rate contraction during AF prevent from the evaluation of sustained TWA. However, as the irregularity in HR increases, it can become challenging to find 3-beats sequences with similar RR along the Holter recording, and this can compromise the bin characterization. The I_{V2}, restricted to only two consecutive stable ventricular repolarizations, adds the advantage that more stable pairs than triplets resulted available to characterize each bin, leading to a potentially more robust estimation of the repolarization variations. In all cases, the positive association of higher ventricular variability with SCD outcome in our study population is in agreement with the fact that repolarization heterogeneity predispose to this fatal outcome in sinus rhythm patients [161].

It is known that ventricular repolarization is very influenced by the heart rate in previous beats, with a memory that can attain 2-3 min [123,220]. Therefore, it can be argued that beats that are averaged within a given bin may present different repolarization morphologies due to different RR histories. However, the QT/RR slope, which expresses adaptation of ventricular repolarization to HR, has been shown to be decreased in AF compared to sinus rhythm [221]. Also, the most important effect is that of the HR in the previous beat, which is similar in all averaged beats. In the proposed method, the beats selected for averaging have stable instantaneous HR and they are averaged with other beats with similar previous HR. Also, due to

the irregular series of RR intervals that characterizes AF, it can be expected that the effect of the different long-term histories will be small. Finally, the averaging will fade the possible morphological differences, compensating the different RR histories of the different pairs/triplets.

Several independent predictors associated to SCD in AF populations have been proposed, including male sex, diabetes, history of myocardial infarction, heart failure, higher heart rate and left ventricular hypertrophy, among others [61,217]. Also in a previous study based on the irregularity of the RR series extracted from high-resolution 20-minute ECG, which included a subset of 155 AF patients from our cohort, authors demonstrated that reduced irregularity of RR intervals in terms of approximate entropy (ApEn) during AF was also predictive of all-cause death and SCD, in contrast to traditional HRV indices [222]. However, to the best of our knowledge, this is the first study in the attempt to non-invasively stratify CHF patients with AF at risk of SCD by assessing ventricular repolarization instability from the ECG signal. These results open the door to further research in this field. For example, the evaluation of combined non-invasive indices of ventricular dispersion together with HR-derived indices may improve stratification performance.

5.5.1 Limitations

The study present some limitations that need to be acknowledged. Although results obtained in this study have shown prognostic value in our study population, this population is limited in terms of the number of SCD events (n=19). Therefore, further prospective studies in AF populations, with and without CHF, are needed in order to evaluate the actual clinical value of the indices. Moreover, this is a *post hoc* analysis and, as the MUSIC study was aimed at the evaluation of prognostic models in CHF not focused on the detailed analysis of the AF group, relevant information regarding the clinical course of AF patients, such as duration, were not available.

5.6 Conclusion

In this chapter, we have shown how increased ventricular repolarization beat-to-beat variation was associated to SCD in CHF patients with AF. We have introduced two new sets of indices, computed from triplets and pairs

of consecutive beats preceded by a similar RR, respectively, from which I_{V3}^{-90}, I_{V3X}^{-90} and I_{V2}^{90} best stratified AF patients according to their risk of SCD, with larger variability associated to lower survival probability. In addition, risk assessment based on the combination of the proposed indices led to an improved prognostic value compared to the individual performance, with a better identification of high-risk patients. Although results should be confirmed in additional prospective studies, these results encourage further research on the evaluation of ventricular repolarization ECG-derived markers in future studies on patients with AF.

Chapter 6

Conclusions and future work

6.1 Summary and main conclusions

The objective of this thesis was to propose methodological advances for the assessment of ventricular repolarization instability, in pathological and abnormal conditions, leading to an improvement in prediction of ventricular arrhythmias and, consequently, SCD risk. In particular, we have addressed this objective by developing robust algorithms for the assessment of T-wave alternans, in invasive and non-invasive cardiac signals. These methods have been applied and evaluated in both experimental and clinical conditions.

First, TWA was simultaneously characterized in body-surface ECG and intracardiac EGM signals during coronary artery occlusion. A multilead

strategy that linearly combines the information available in different leads maximizing the 2-beat periodicity (TWA periodicity) content was used. This approach allowed us to find the optimal combination of intracardiac leads usable for in-vivo monitorization of TWA directly from an ICD device.

Then, possible induced effects of simulated microgravity on cardiac electrical instability were also assessed in terms of TWA. Based on the same multilead approach, a long-term averaging technique for TWA estimation on Holter recordings was used, and adapted for shorter and non-stationary ECG recordings.

Finally, methodological advances in the assessment of ventricular repolarization instability in the presence of sporadic (VPCs) and sustained (AF) rhythm disturbances were proposed. On the one hand, a methodological improvement for the estimation of TWA amplitude is proposed, which deals with the possible phase reversal on the alternans sequence induced by the presence of VPCs. On the other hand, the high irregularity of the ventricular response in AF limits the use of TWA under this clinical condition. A new method for assessing ventricular repolarization changes based on a selective averaging technique was developed and new non-invasive indices of repolarization variation were proposed. The positive impact in the prognostic value of the computed indices was demonstrated in clinical studies.

6.1.1 Optimal detection of TWA in intracardiac electrogram signals

T-wave alternans, reflecting spatio-temporal repolarization heterogeneity, has been linked with electrical instability and an increased vulnerability of the myocardium, predisposing to the development of ventricular arrhythmias (VT/VF) [5]. It has been demonstrated that TWA can be inducible by coronary artery occlusion [147,153,162,175,176], and it has been widely characterized from body-surface ECG in both experimental models and humans. However, the analysis of TWA from intracardiac signals is scarcer and, in most, cases limited to the study of pacing-induced alternans [163–165, 167, 168].

Attention has been recently focused on the usefulness in continuous monitoring intracardiac alternans as a predictor of electrical instability and myocardial vulnerability [167–170], but a comprehensive intracardiac characterization of this phenomenon was first required.

In this thesis, TWA phenomenon was measured at both body-surface ECG and intracardiac EGM signals during coronary artery occlusion has been characterized. To do that, a multilead approach based on periodic component analysis (πCA) was used, that optimally combines the available leads in such a way that the 2-beat periodicity of the signal is maximized [156], together with the Laplacian Likelihood Ratio Method (LLRM). Intracardiac TWA was characterized by analyzing different leads in four different anatomical locations: the coronary sinus, epicardial space and the right and left ventricles.

Results obtained when analyzing TWA from the ECG leads were concordant with previous studies in both humans and experimental data [153,162]. A similar behavior with the progression of the occlusion period was observed on the intracardiac leads. TWA episodes in intracardiac signals appeared delayed and were shorter that in the body-surface ECG leads, with higher amplitudes. The comparison of multilead results with those obtained with individual unipolar and bipolar leads confirms the improved sensitivity for a given specificity that can be achieved by the multilead approach. Although the sensitivity for TWA detection was higher in ECG leads than in EGM leads from a single area, a linear combination of just two intracardiac leads from the right ventricle and the coronary sinus can detect intracardiac alternans with a similar performance. The potentiality of this study, as mentioned before, is that proper TWA monitorization using an ICD device, may provide real-time information of electrical instability and help in properly delivering ICD therapy.

6.1.2 Methodological advances for analysis of TWA and ventricular repolarization variations under rhythm disturbances

TWA tests are usually performed in the clinical routine under controlled heart rate, typically by exercise-induced stress. However, an important percentage of the test performed using the commercially available methods (SM and MMAM) still have indeterminate results [196–198]. One of the reasons is the presence of ventricular premature contractions (VPCs). Even if the LLRM has been shown to outperform estimation accuracy in the presence of impulsive noise, as a VPC appearing within the alternans sequence, it is known that VPCs may alter repolarization dynamics and introduce a phase

reversal on the alternans sequence [158]. In this case, TWA estimation and, consequently, its potential clinical value can be unfavourably affected.

The long-term averaging of alternans activity in ambulatory ECGs has been shown to provide prognostic value for SCD [157]. The advantages of this technique are that (i) it proceeds in a fully-automatic way, without the necessity of posterior visual inspection; and (ii) it avoids a hard detection stage and the need for a detection threshold definition.

In this thesis, we proposed the inclusion of a VPC processing step for the control of the alternans sequence before and after the VPC, in order to ensure its continuity in phase before TWA estimation. We have demonstrated how the inclusion of this step leads to an improved stratification performance of the index of average alternans (IAA) in a CHF population. In addition, this index showed to be sensitive to the circadian pattern, preserving its prognostic information when computed from 06.00 to 12.00 in the morning. Interestingly, this day interval is known to be the one with the highest incidence of SCD events.

If sporadic heart rhythm disturbances, as VPCs, compromised the usefulness of TWA, this phenomenon can not be assessed in the absence of a sinus rhythm condition. The irregular ventricular activity present in atrial fibrillation patients, therefore, is not suitable for TWA analysis. And to the best of our knowledge, there are not standard ECG-derived risk markers adapted to this particular condition.

With the aim of overcoming this limitation, we have developed a new method to quantify beat-to-beat variations in ventricular repolarization on ambulatory Holter recordings, during AF rhythm. Using a selective heart rate averaging technique, consecutive beats preceded by a similar RR interval were selected, and the average variation with in the ST-T complex for each RR range computed. We proposed two new sets of indices: (i) the 2-beat index of ventricular repolarization variation, ($\mathrm{I_{V2}}$), computed from pairs of stable consecutive beats; (ii) the 3-beat indices of ventricular repolarization variation, computed in triplets of stable consecutive beats, and from which the average variation with in the triplet ($\mathrm{I^{+}_{V3}}$) and the alternant variation within the triplet ($\mathrm{I^{-}_{V3}}$) were quantified.

These indices, when restricted to beats associated to HRs faster than 90 beats/min, were found to be significantly associated to SCD risk in CHF patients with AF, with a larger ventricular repolarization beat-to-beat va-

riation associated to lower survival probability. In addition, risk assessment based on the combination of the proposed indices improved stratification performance compared to their individual potential, providing with a better identification of high-risk AF patients. As far as we know, this is a pioneer study that attempts a non-invasive SCD stratification AF patients through the assessment of the ventricular repolarization instability using the ECG signal.

Nevertheless, the actual prognostic value of both methodologies needs to be confirmed in larger prospective studies, and extending the analysis to different clinical conditions.

6.1.3 Evaluation of changes on TWA activity induced by simulated microgravity

Apart from studying the prognostic value of ventricular repolarization in the pathologic heart, we have also studied the changes in the structurally normal heart induced by a prolonged exposure to simulated microgravity. This environmental condition affects the control of autonomic and cardiovascular systems, with a potential increase of cardiac risk.

Changes in ventricular repolarization in terms of TWA activity have been evaluated during and immediately after short- (5 days) mid- (21 days) and long-duration (60 days) head-down bed-rest campaigns. A comprehensive characterization of this phenomenon was provided by the analysis at rest conditions, selecting the night period from ambulatory Holter recordings, and during two stress induced manoeuvres: an orthostatic tolerance test by head-up tilt and a VO_{2max} exercise test. In this case, after πCA transformation, the long-term averaging technique was used for TWA estimation. An adapted methodology, suitable for the analysis of shorter, non-stationary ECG signals obtained during the two stress manoeuvres was proposed (short-term averaging).

We concluded that a 60-day exposure to simulated microgravity was not enough to induce significant changes in healthy myocardial substrate up to the point of manifesting electrical instability in terms of TWA. However, subjects from the long-duration campaign presented an increasing trend of TWA activity after 60 days of immobilization period. Although this results need to be confirmed with data from an ongoing campaign, they might be indicative, together with previous observations of a reversible increase in

repolarization heterogeneity after HDBR observed in other indices [180,181], of initial alterations in the repolarization phase.

6.1.4 Clinical significance

Accurate stratification of patients at risk of SCD is crucial for improving the actual cost-effectiveness of therapeutic strategies, which remains particularly low in the case of ICDs. Any efforts aimed at developing tools that can help in clinical decisions, especially in the proper identification of pro-arrhythmic factors, are, therefore, more than justified. The research presented in this thesis sheds some light in this context.

On the one hand, ICD technology could be improved by integrating algorithms for real-time monitoring of repolarization alternans that, if confirmed in further studies, may help in increasing the effectiveness rate of shock therapy. On the other hand, the ECG signal represents a non-invasive, easy and, most important, cheap solution for cardiac evaluation. The study of ventricular repolarization from the ECG, reflected on the ST-T complex, can provide valuable prognostic information when abnormalities are present. The computation of the indices proposed in this thesis using a simple ambulatory ECG recording, would help in the identification of patients at higher risk of suffering from SCD. All of that would present a positive impact in both, the patient and healthcare systems. Finally, the analysis of ECG signals recorded during reduced gravitational stimulus, as HDBR experiments, also provides interesting information which can be taken into account in immobilized or bedridden patients.

6.2 Future work

Some future research lines derived from this work are presented below. Some of them have been already proposed in the previous chapters as a possible solution to the acknowledged limitations; others arise from the obtained results.

An optimal intracardiac lead configuration for TWA detection has been proposed. In that study, TWA were induced by occlusion of the LCX artery. However, it is known that TWA prevalence and

magnitude are dependent on what and how myocardial region is affected by the occlusion. Therefore, investigation of the optimal lead combination when TWA are induced by occlusion in the left anterior descending and the right coronary arteries would allow to define the best configuration, also independent of the occlusion site.

The absence of significant changes in terms of TWA induced by long-term exposure to microgravity did not allow us to draw clear conclusions. Indeed, initial alterations were visible after 60 days of bed-rest, though not statistically significant. A deeper evaluation of ventricular instability through other markers, such as QT and Tpe interval dynamics, or the recently proposed index of T-wave morphology restitution would help to better elucidate possible electrical instabilities after long-duration exposure to simulated microgravity.

The prognostic value of the indices presented in chapters 4 and 5 has been validated in the MUSIC database, including patients with CHF in sinus rhythm and AF, respectively. Future prospective studies, extending also to other groups of patients, should validate their actual clinical value.

The indices of ventricular repolarization variation proposed in chapter 5, were computed using the three orthogonal leads, both independently and from the vector-magnitude of the VCG signal. It would be interesting to study if the use of multilead approaches, such as PCA, could help to better capture the repolarization instability, thus, improving predictability.

On the other hand, the joint evaluation of the proposed indices of ventricular repolarization, together with indices related to the autonomic nervous system, as those derived from HRV analysis or heart rate turbulence, may improve stratification performance.

References

[1] N Townsend, L Wilson, P Bhatnagar, K Wickramasinghe, M Rayner, and M Nichols. Cardiovascular disease in europe: epidemiological update 2016. *European Heart Journal*, 37(42):3232, 2016.

[2] LJ Laslett, P Jr Alagona, BA Clark, JP Jr Drozda, F Saldivar, SR Wilson, C Poe, and M Hart. The worldwide environment of cardiovascular disease: Prevalence, diagnosis, therapy, and policy issues: A report from the american college of cardiology. *Journal of the American College of Cardiology*, 60(25, Supplement):S1–S49, 2012.

[3] RM John, UB Tedrow, BA Koplan, CM Albert, LM Epstein, MO Sweeney, AL Miller, GF Michaud, and WG Stevenson. Ventricular arrhythmias and sudden cardiac death. *The Lancet*, 380(9852):1520–1529, 2012.

[4] P Laguna, JP Martínez, and E Pueyo. Techniques for ventricular repolarization instability assessment from the ECG. *Proceedings of the IEEE*, 104(2):392–415, 2016.

[5] RL Verrier, T Klingenheben, M Malik, et al. Microvolt T-wave alternans physiological basis, methods of measurement, and clinical utility – Consensus guideline by International Society for Holter and Noninvasive Electrocardiology. *Journal of the American College of Cardiology*, 58(13):1309–1324, 2011.

[6] AC Guyton and JE Hall. *Text book of medical physiology*. W. B. Saunders Co., 2006.

[7] L Sörnmo and P Laguna. *Bioelectrical Signal Processing in Cardiac and Neurological Applications*. Elsevier Science, 2005.

[8] E Pueyo, JP Martínez, and P Laguna. Cardiac repolarization analysis using the surface electrocardiogram. *Philosophical Transactions of the Royal Society*, 367:213–233, 2009.

[9] CE Conrath and T Opthof. Ventricular repolarization: An overview of (patho)physiology, sympathetic effects and genetic aspects. *Progress in Biophysics and Molecular Biology*, 92(3):269–307, 2006.

[10] FG Akar, KR Laurita, and DS Rosenbaum. Cellular basis for dispersion of repolarization underlying reentrant arrhythmias. *Journal of Electrocardiology*, (2):23–31, 2000.

[11] KM Holzem and IR Efimov. Arrhythmogenic remodelling of activation and repolarization in the failing human heart. *EP Europace*, 14:v50–v57, 2012.

[12] V Shusterman, R Lampert, and B London. The many faces of repolarization instability: Which one is prognostic? *Journal of Electrocardiology*, 42(6):511–516, 2009.

[13] R Hainsworth. The control and phisiological importance of heart rate. In M Malik and JA Camm, editors, *Heart Rate Variability*, chapter 1. Futura Publishing Company, Inc., 1995.

[14] E Frank. An accurate, clinically practical system for spatial vectorcardiography. *Circulation*, 13:737–749, 1956.

[15] JJ Goldberger and J Ng. *Practical Signal and Image Processing in Clinical Cardiology*. Springer-Verlag London, 2010.

[16] C Antzelevitch and A Burashnikov. Overview of basic mechanisms of cardiac arrhythmia. *Caridac Electrophysiology Clinics*, 3(1):23–45, 2011.

[17] JA Vasallo, DM Cassidy, KE Kindwall, FE Marchlinski, and ME Josephson. Non uniform recovery of excitability in the left ventricle. *Circulation*, 78(6):1365–1372, 1988.

[18] BJ Boukens, VM Christoffels, R Coronel, and AF Moorman. Developmental basis for electrophysiological heterogeneity in the ventricular and outflow tract myocardium as a substrate for lifethreatening ventricular arrhythmias. *Circulation Research*, 104(1):19–31, 2009.

[19] P Coumel. Cardiac arrhtyhmias and the autonomic nervous system. *Journal of Cardiovascular Electrophysiology*, 4(3):338–355, 1993.

[20] MJ Shen and DP Zipes. Role of the autonomic nervous system in modulating cardiac arrhythmias. *Circulation research*, 114(6):1004–1024, 2014.

[21] BA Koplan and WG Stevenson. Ventricular tachycardia and sudden cardiac death. *Mayo Clinic Proceedings*, 84(3):289–297, 2009.

[22] P Ponikowski, AA Voors, SD Anker, et al. 2016 ESC guidelines for the diagnosis and treatment of acute and chronic heart failure. The Task Force for the diagnosis and treatment of acute and chronic heart failure of the European Society of Cardiology (ESC) developed with the special contribution of the Heart Failure Association (HFA) of the ESC. *European Heart Journal*, 37(27):2129–2200, 2016.

[23] SG Priori, C Blomström-Lundqvist, A Mazzanti, et al. 2015 ESC Guidelines for the management of patients with ventricular arrhythmias and the prevention of sudden cardiac death. The Task Force for the management of patients with ventricular arrhythmias and the prevention of sudden cardiac death of the European Society of Cardiology (ESC) endorsed by: Association for European Paediatric and Congenital Cardiology (AEPC). *European Heart Journal*, 36(41):2793, 2015.

[24] A Mosterd and AW Hoes. Clinical epidemiology of heart failure. *Heart*, 93(9):1137–1146, 2007.

[25] Y Gerber, SA Weston, MM Redfield, AM Chamberlain, SM Manemann, R Jiang, JM Killian, and VL Roger. A contemporary appraisal of the heart failure epidemic in Olmsted County, Minnesota, 2000 to 2010. *JAMA Internal Medicine*, 175(6):996–1004, 2015.

[26] TE Owan, DO Hodge, RM Herges, SJ Jacobsen, VL Roger, and MM Redfield. Trends in prevalence and outcome of heart failure with preserved ejection fraction. *The New England Journal of Medicine*, 355(3):251–259, 2006.

[27] AP Maggioni, U Dahlström, G Filippatos, et al. EURObservational Research Programme: regional differences and 1-year follow-up results of the Heart Failure Pilot Survey (ESC-HF pilot). *European Journal of Heart Failure*, 15(7):808–817, 2013.

[28] SJ Pocock, CA Ariti, JJ McMurray, et al. Predicting survival in heart failure: a risk score based on 39372 patients from 30 studies. *European Heart Journal*, 34(19):1404–1413, 2013.

[29] EES van Riet, AW Hoes, A Limburg, MAJ Landman, H van der Hoeven, and FH Rutten. Prevalence of unrecognized heart failure in older persons with shortness of breath on exertion. *European Journal of Heart Failure*, 16(7):772–777, 2014.

[30] J Mant, J Doust, A Roalfe, et al. Systematic review and individual patient data meta-analysis of diagnosis of heart failure, with modelling of implications of different diagnostic strategies in primary care. *Health Tecnology Assessment*, 13(32):1–207, 2009.

[31] AP Davie, CM Francis, MP Love, L Caruana, IR Starkey, TR Shaw, GR Sutherland, and JJ McMurray. Value of the electrocardiogram in identifying heart failure due to left ventricular systolic dysfunction. *British Medical Journal*, 312(7025):222, 1996.

[32] JT Thomas, RF Kelly, SJ Thomas, TD Stamos, K Albasha, JE Parrillo, and JE Calvin. Utility of history, physical examination, electrocardiogram, and chest radiograph for differentiating normal from decreased systolic function in patients with heart failure. *The American Journal of Medicine*, 112(6):437–445, 2002.

[33] JN Kirkpatrick, MA Vannan, J Narula, and RM Lang. Echocardiography in heart failure: applications, utility, and new horizons. *Journal of the American College of Cardiology*, 50(5):381–396, 2007.

[34] SF Nagueh, R Bhatt, RP Vivo, SR Krim, SI Sarvari, K Russell, T Edvardsen, OA Smiseth, and JD Estep. Echocardiographic evaluation of hemodynamics in patients with decompensated systolic heart failure. *Circulation: Cardiovascular Imaging*, 4(3):220–227, 2011.

[35] RM Lang, LP Badano, V Mor-Avi, et al. Recommendations for cardiac chamber quantification by echocardiography in adults: an update from the american society of echocardiography and the european association of cardiovascular imaging. *European Heart Journal – Cardiovascular Imaging*, 16(3):233–270, 2015.

[36] NM Hawkins, MC Petrie, PS Jhund, GW Chalmers, FG Dunn, and JJV McMurray. Heart failure and chronic obstructive pulmonary dise-

ase: diagnostic pitfalls and epidemiology. *European Journal of Heart Failure*, 11(2):130–139, 2009.

[37] New York Heart Association. Criteria Committee. *Diseases of the Heart and Blood Vessels. Nomenclature and Criteria for diagnosis.* Boston, Little, Brown and Co., 6th edition edition, 1964.

[38] R Garg and S Yusuf. Overview of randomized trials of angiotensin-converting enzyme inhibitors on mortality and morbidity in patients with heart failure. *JAMA*, 273(18):1450–1456, 1995.

[39] M Packer, PA Poole-Wilson, PW Armstrong, et al. Comparative effects of low and high doses of the angiotensin-converting enzyme inhibitor, lisinopril, on morbidity and mortality in chronic heart failure. *Circulation*, 100(23):2312–2318, 1999.

[40] SOLVD Investigattors. Effect of enalapril on survival in patients with reduced left ventricular ejection fractions and congestive heart failure. *The New England Journal of Medicine*, 325(5):293–302, 1991.

[41] MERIT-HF Study Group. Effects of controlled-release metoprolol on total mortality, hospitalizations, and well-being in patients with heart failure: the Metoprolol CR/XL Randomized Intervention Trial in congestive Heart Failure (MERIT-HF). *JAMA*, 283(10):1295–1302, 2000.

[42] M Packer, AJ Coats, MB Fowler, et al. Effect of carvedilol on survival in severe chronic heart failure. *The New England Journal of Medicine*, 344(22):1651–1658, 2001.

[43] CIBIS-II Investigators and Committees. The cardiac insufficiency bisoprolol study II (CIBIS-II): a randomised trial. *Lancet*, 353(9146):9–13, 1999.

[44] MD Flather, MC Shibata, AJ Coats, et al. Randomized trial to determine the effect of nebivolol on mortality and cardiovascular hospital admission in elderly patients with heart failure (SENIORS). *European Heart Journal*, 26(3):215–225, 2005.

[45] B Pitt, F Zannad, WJ Remme, R Cody, A Castaigne, A Perez, J Palensky, and J Wittes. The effect of spironolactone on morbidity and mortality in patients with severe heart failure. *The New England Journal of Medicine*, 341(10):709–717, 1999.

[46] F Zannad, JJV McMurray, H Krum, DJ Van Veldhuisen, K Swedberg, H Shi, J Vincent, SJ Pocock, and B Pitt. Eplerenone in patients with systolic heart failure and mild symptoms. *The New England Journal of Medicine*, 364(1):11–21, 2011.

[47] JG Cleland, BM Massie, and M Packer. Sudden death in heart failure: vascular or electrical? *European Journal of Heart Failure*, 1:41–45, 1999.

[48] DP Zipes, AJ Camm, M Borggrefe, et al. ACC/AHA/ESC 2006 Guidelines for management of patients with ventricular arrhythmias and the prevention of sudden cardiac death. *Journal of the American College of Cardiology*, 48(5):e247–e346, 2006.

[49] GF Tomaselli, DJ Beuckelmann, HG Calkins, RD Berger, PD Kessler, JH Lawrence, D Kass, AM Feldman, and E Marban. Sudden cardiac death in heart failure. the role of abnormal repolarization. *Circulation*, 90(5):2534–2539, 1994.

[50] DAMJ Theuns, T Smith, MGM Hunink, GH Bardy, and L Jordaens. Effectiveness of prophylactic implantation of cardioverter-defibrillators without cardiac resynchronization therapy in patients with ischaemic or non-ischaemic heart disease: a systematic review and meta-analysis. *Europace*, 12(11):1564–1570, 2010.

[51] NR Cook and PM Ridker. Advances in measuring the effect of individual predictors of cardiovascular risk: the role of reclassification measures. *Annals of Internal Medicine*, 150(11):795–802, 2009.

[52] GH Bardy, KL Lee, DB Mark, et al. Amiodarone or an implantable cardioverterdefibrillator for congestive heart failure. *The New England Journal of Medicine*, 352(3):225–237, 2005.

[53] SMMA Sohaib, JA Finegold, SS Nijjer, R Hossain, C Linde, WC Levy, R Sutton, P Kanagaratnam, DP Francis, and ZI Whinnett. Opportunity to increase life span in narrow QRS cardiac resynchronization therapy recipients by deactivating ventricular pacing: evidence from randomized controlled trials. *JACC: Heart Failure*, 3(4):327–336, 2015.

[54] JGF Cleland, MJ Calvert, Y Verboven, and N Freemantle. Effects of cardiac resynchronization therapy on long-term quality of life: an

analysis from the Cardiac Resynchronisation-Heart Failure (CARE-HF) study. *American Heart Journal*, 157(3):457–466, 2009.

[55] V Fuster, LE Rydén, DS Cannom, et al. ACC/AHA/ESC 2006 Guidelines for the management of patients with atrial fibrillation. *Journal of the American College of Cardiology*, 48(4):e149 – e246, 2006.

[56] M Zoni-Berisso, F Lercari, T Carazza, and S Domenicucci. Epidemiology of atrial fibrillation: European perspective. *Clinical Epidemiology*, 16(6):213–220, 2014.

[57] P Kirchhof, S Benussi, D Kotecha, et al. 2016 ESC Guidelines for the management of atrial fibrillation developed in collaboration with EACTS. *European Heart Journal*, 37(38):2893–2962, 2016.

[58] S Colilla, A Crow, W Petkuun, DE Singer, T Simon, and X Liu. Estimates of current and future incidence and prevalence of atrial fibrillation in the U.S. adult population. *American Journal of Cardiology*, 112(8):1142–1147, 2013.

[59] SS Chugh, R Havmoeller, K Narayanan, et al. Worldwide epidemiology of atrial fibrillation: A Global Burden of Disease 2010 Study. *Circulation*, 129(8):837–847, 2014.

[60] G Thrall, D Lane, D Carroll, and GYH Lip. Quality of life in patients with atrial fibrillation: A systematic review. *The American Journal of Medicine*, 119(5):448.e1–e19, 2006.

[61] E Marijon, JY Le Heuzey, S Connolly, et al. Causes of death and influencing factors in patients with atrial fibrillation. Clinical perspective. *Circulation*, 128(20):2192–2201, 2013.

[62] BL Nguyen, MC Fishbein, LS Chen, PS Chen, and S Masroor. Histopathological substrate of chronic atrial fibrillation in humans. *Heart Rhythm*, 6(4):454–460, 2009.

[63] C Chimenti, MA Russo, A Carpi, and A Frustaci. Histological substrate of human atrial fibrillation. *Biomedicine and Pharmacotherapy*, 64(3):177–183, 2010.

[64] A Frustaci, C Chimenti, F Bellocci, E Morgante, MA Russo, and A Maseri. Histological substrate of atrial biopsies in patients with lone atrial fibrillation. *Circulation*, 96:1180–1184, 1997.

[65] GK Moe and JA Abildskov. Atrial fibrillation as a self-sustaining arrhtyhmia independent of focal discharge. *American Heart Journal*, 58(1):59–70, 1959.

[66] M Haissaguerre, P Jais, DC Shah, A Takahashi, M Hocini, G Quiniou, S Garrigue, A Le Mouroux, P Le Metayer, and J Clementy. Spontaneous initiation of atrial fibrillation by ectopic beats originating in the pulmonary veins. *The New England Journal of Medicine*, 339:659–666, 1998.

[67] M Haissaguerre, M Hocini, A Denis, et al. Driver domains in persistent atrial fibrillation. *Circulation*, 130:530–538, 2014.

[68] CS Fox, H Parise, RB D'Agostino, DM Lloyd-Jones, RS Vasan, TJ Wang, D Levy, PA Wolf, and EJ Benjamin. Parental atrial fibrillation as a risk factor for atrial fibrillation in offspring. *JAMA*, 291(23):2851–2855, 2004.

[69] N Oyen, MF Ranthe, L Carstensen, HA Boyd, MS Olesen, SP Olesen, J Wohlfahrt, and M Melbye. Familial aggregation of lone atrial fibrillation in young persons. *Journal of the American College of Cardiology*, 60(10):917–921, 2012.

[70] T Nikolaidou and KS Channer. Chronic atrial fibrillation: a systematic review of medical heart rate control management. *Postgraduate Medical Journal*, 85(1004):303–312, 2009.

[71] LJ Tamariz and EB Bass. Pharmacological rate control of atrial fibrillation. *Cardiology Clinics*, 22(1):35–45, 2004.

[72] JB Segal, RL McNamara, MR Miller, N Kim, SN Goodman, NR Powe, K Robinson, D Tu, and EB Bass. The evidence regarding the drugs used for ventricular rate control. *The Journal of Family Practice*, 49(1):47–49, 2000.

[73] P Kirchhof, L Eckardt, P Loh, K Weber, RJ Fischer, KH Seild, D Bocker, G Breithardt, W Haverkamp, and M Borggrefe. Anterior-posterior versus anterior-lateral electrode positions for external cardioversion of atrial fibrillation: a randomised trial. *Lancet*, 360(9342):1275–1279, 2002.

[74] S Mittal, S Ayati, KM Stein, D Schwartzman, D Cavlovich, PJ Tchou, SM Markowitz, DJ Slotwiner, MA Scheiner, and BB Lerman. Transthoracic cardioversion of atrial fibrillation: comparison of rectilinear

biphasic versus damped sine wave monophasic shocks. *Circulation*, 101:1282–1287, 2000.

[75] C Lafuente-Lafuente, MA Longas-Tejero, JF Bergmann, and J Belmin. Antiarrhythmics for maintaining sinus rhythm after cardioversion of atrial fibrillation. *The Cochrane Database of Systematic Reviews*, 16(5):CD005049, 2012.

[76] E Arbelo, J Brugada, G Hindricks, et al. Ther atrial fibrillation ablation pilot study: a European survey on methodology and results of catheter ablation for atrial fibrillation conducted by the European Heart Rhythm Association. *European Heart Journal*, 35(22):1466–1478, 2014.

[77] H Calkins, KH Kuck, R Cappato, et al. 2012 HRS/EHRA/ECAS Expert consensus statement on catheter and surgical ablation of atrial fibrillation: Recommendations for patient selection, procedural techniques, patient management and follow-up, definitions, endpoints, and research trial design. *EP Europace*, 14(4):528, 2012.

[78] JL Cox, JP Boineau, RB Schuessler, TB Ferguson, ME Cain, BD Lindsay, PB Corr, KM Kater, and DG Lappas. Succesful surgical treatment of atrial fibrillation. Review and clinical update. *JAMA*, 266(14):1976–1980, 1991.

[79] MP Van den Berg, AE Tuinenburg, HJ Crijns, IC Van Gelder, AT Gosselink, and KI Lie. Heart failure and atrial fibrillation: current concepts and controversies. *Heart*, 77(4):309–313, 1997.

[80] LY Chen, N Sotoodehnia, P Bůžková, et al. Atrial fibrillation and the risk of sudden cardiac death: The atherosclerosis risk in communities study and cardiovascular health study. *JAMA Internal Medicine*, 173(1):29–35, 2013.

[81] LY Chen, DG Benditt, and A Alonso. Atrial fibrillation and its association with sudden cardiac death. *Circulation Journal*, 78(11):2588–2593, 2014.

[82] PM Okin, CN Bang, K Wachtell, DA Hille, SE Kjeldsen, B Dahlöf, and RB Devereux. Relationship of sudden cardiac death to new-onset atrial fibrillation in hypertensive patients with left ventricular hypertrophy. Clinical perspective. *Circulation: Arrhythmia and Electrophysiology*, 6(2):243–251, 2013.

[83] A Bardai, MT Blom, DA van Hoeijen, HWM van Deutekom, HJ Brouwer, and HL Tan. Atrial fibrillation is an independent risk factor for ventricular fibrillation: large-scale population-based case-control study. *Circulation: Arrhythmia and Electrophysiology*, 7(6):1033–1039, 2014.

[84] WH Maisel and LW Stevenson. Atrial fibrillation in heart failure: epidemiology, pathophysiology, and rationale for therapy. *The American Journal of Cardiology*, 91(6):2–8, 2003.

[85] F Sanchís-Gomar, C Pérez-Quilis, R Leischik, and A Lucia. Epidemiology of coronary heart disease and acute coronary syndrome. *Annals of Translational Medicine*, 4(13):256, 2016.

[86] SD Fihn, JM Gardin, J Abrams, et al. 2012 ACCF/AHA/ACP/AATS/PCNA/SCAI/STS Guideline for the diagnosis and management of patients with stable ischemic heart disease. *Circulation*, 126(25):e354–e471, 2012.

[87] N Townsend, M Nichols, P Scarborough, and M Rayner. Cardiovascular disease in Europe - Epidemiological update 2015. *European Heart Journal*, 36(40):2696–2705, 2015.

[88] G Montalescot, U Sechtem, S Achenbach, et al. 2013 ESC Guidelines on the management of stable coronary artery disease. The Task Force on the management of stable coronary artery disease of the European Society of Cardiology. *European Heart Journal*, 34(38):2949–3003, 2013.

[89] DB Gillis and DR Hamilton. Estimating outcomes of astronauts with myocardial infarction in exploration class space missions. *Aviation, Space and Environmental Medicine*, 83(2):79–91, 2012.

[90] V Convertino and GW Hoffler. Cardiovascular physiology. Effects of microgravity. *The Journal of the Florida Medical Association*, 79(8):517–524, 1992.

[91] JA Ptak, NA Yazinski, CA Block, and JC Jr Buckey. Unusual neurological syndrome induced by atmospheric pressure change. *Aviation, Space and Environmental Medicine*, 84(5):522–524, 2013.

[92] EK Zawadzka-Bartczak and LH Kopka. Cardiac arrhythmias during aerobatic flight and its simulation on a centrifuge. *Aviation, Space and Environmental Medicine*, 82(6):599–603, 2011.

[93] JD Rogge, JF Meyer, and WK Brown. Comparison of the incidence of cardiac arrhythmias during +Gx acceleration, treadmill exercise and tilt table testing. *Aerospace Medicine*, 40(1):1–5, 1969.

[94] DE Torphy, SD Jr Leverett, and LE Lamb. Cardiac arrhythmias occurring during acceleration. *Aerospace Medicine*, 37(1):52–58, 1966.

[95] MB Sides, J Vernikos, VA Convertino, et al. The Bellagio Report: Cardiovascular risks of spaceflight: implications for the future of space travel. *Aviation, Space and Environmental Medicine*, 76(9):877–895, 2005.

[96] RS Johnson, LF Dietlein, and CA Berry. *Biomedical Results of Apollo*. National Aeronautics and Space Administration. Washington, DC., 1st edition, 1975.

[97] T Anzai, MA Frey, and A Nogami. Cardiac arrhythmias during long-duration spaceflights. *Journal of Arrhythmia*, 30(3):139–149, 2014.

[98] JM Fritsch-Yelle, UA Leuenberger, DS D'Aunno, AC Rossum, TE Brown, ML Wood, ME Josephson, and AL Goldberger. An episode of ventricular tachycardia during long-duration spaceflight. *The American Journal of Cardiology*, 81(11):1391–1392, 1992.

[99] T Russomano, JH Baers, R Velho, RB Cardoso, A Ashcroft, L Rehnberg, RD Gehrke, MKP Dias, and RR Baptista. A comparison between the 2010 and 2005 basic life support guidelines during simulated hypogravity and microgravity. *Extreme Physiology & Medicine*, 2:11, 2013.

[100] DS D'Aunno, AH Dougherty, HF DeBlock, and JV Meck. Effect of short- and long-duration spaceflight on QTc intervals in healthy astronauts. *The American Journal of Cardiology*, 91(4):494–497, 2003.

[101] JM Fritsch-Yelle, PA Whitson, RL Bondar, and TE Brown. Subnormal norepinephrine release relates to presyncope in astronauts after spaceflight. *Journal of Applied Physiology*, 81(5):2134–2141, 1996.

[102] JM Fritsch, JB Charles, BS Bennett, MM Jones, and DL Eckberg. Short-duration spaceflight impairs human carotid baroreceptor-cardiac reflex responses. *Journal of Applied Physiology*, 73(2):664–671, 1992.

[103] JV Meck, CJ Reyes, SA Perez, AL Goldberger, and MG Ziegler. Marked exacerbation of orthostatic intolerance after long- vs. short-duration spaceflight in veteran astronauts. *Psychosomatic Medicine*, 63(6):865–873, 2001.

[104] AC Rossum, MG Ziegler, and JV Meck. Effect of spaceflight on cardiovascular responses to upright posture in a 77-year-old astronaut. *The American Journal of Cardiology*, 88(11):1335–1337, 2001.

[105] J Liu, Y Li, B Verheyden, et al. Is autonomic modulation different between European and Chinese astronauts? *PLoS One*, 10(3):e0120920, 2015.

[106] TN James. Normal and abnormal consequences of apoptosis in the human heart. *Annual Review of Physiology*, 60:309–325, 1998.

[107] Z Mallat, A Tedgui, F Fontaliran, R Frank, M Durigon, and G Fontaine. Evidence of apoptosis in arrhythmogenic right ventricular dysplasia. *The New England Journal of Medicine*, 335(16):1190–1196, 1996.

[108] SH Platts, MB Stenger, TR Phillips, NM Arzeno, AK Brown, B Levine, and R Summers. Evidence Based Review: Risk of cardiac rhythm problems during space flight. 2010.

[109] FA Cucinotta, MHY Kim, and L Ren. Managing Lunar and Mars mission radiation risks part I: Cancer risks, uncertainties, and shielding effectiveness. 2005.

[110] N Kanas, V Salnitskiy, V Gushin, DS Weiss, EM Grund, C Flynn, O Kozerenko, A Sled, and CR Marmar. Asthenia – does it exist in space? *Psychosomatic Medicine*, 63(6):874–880, 2001.

[111] A Pavy-Le Traon, M Heer, MV Narici, J Rittweger, and J Vernikos. From space to Earth: advances in human physiology from 20 years of bed rest studies (1986–2006). *European Journal of Applied Physiology*, 101(2):143–194, 2007.

[112] PJ Schwartz and S Wolf. QT interval prolongation as predictor of sudden death in patients with myocardial infarction. *Circulation*, 57(6):1074–1077, 1978.

[113] EG Schouten, JM Dekker, P Meppelink, FJ Kok, JP Vandenbroucke, and J Pool. QT interval prolongation predicts cardiovascular mortality in an apparently healthy population. *Circulation*, 84(4):1516–1523, 1991.

[114] A Montanez, JN Ruskin, PR Hebert, GA Lamas, and CH Hennekens. Prolonged QTc interval and risks of total and cardiovascular mortality and sudden death in the general population: a review and qualitative overview of the prospective cohort studies. *Archives of Internal Medicine*, 164(9):943–948, 2004.

[115] PM Okin, RB Devereux, BV Howard, RR Fabsitz, ET Lee, and TK Welty. Assessment of QT interval and QT dispersion for prediction of all-cause and cardiovascular mortality in American Indians. *Circulation*, 101(1):61–66, 2000.

[116] CP Day, JM McComb, and RWF Campbell. QT dispersion: an indication of arrhythmia risk in patients with long QT intervals. *Circulation*, 1:335–343, 1990.

[117] M Malik, B Acar, Y Gang, YG Yap, K Hnatkova, and AJ Camm. QT dispersion does not represent electrocardiographic interlead heterogeneity of ventricular repolarization. *Journal of Cardiovascular Electrophysiology*, 11(8):835–843, 2000.

[118] M Baumert, A Porta, MA Vos, M Malik, JP Couderc, P Laguna, G Piccirillo, GL Smith, LG Tereshchenko, and PG Volders. QT interval variability in body surface ECG: measurement, physiological basis, and clinical value: Position statement and consensus guidance endorsed by the European Heart Rhythm Association jointly with the ESC Working Group on Cardiac Cellular Electrophysiology. *Europace*, 18(6):925–944, 2016.

[119] MC Haigney, W Zareba, PJ Gentlesk, et al. QT interval variability and spontaneous ventricular tachycardia or fibrillation in the Multicenter Automatic Defibrillator Implantation Trial (MADIT) II patients. *Journal of the American Collage of Cardiology*, 44(7):1481–1487, 2004.

[120] G Piccirillo, D Magrì, S Matera, et al. QT variability strongly predicts sudden cardiac death in asymptomatic subjects with mild or moderate

left ventricular systolic dysfunction: a prospective study. *European Heart Journal*, 28(11):1344–1350, 2007.

[121] S Ahnve and H Vallin. Influence of heart rate and inhibition of autonomic tone on the QT interval. *Circulation*, 65(3):435–439, 1982.

[122] E Pueyo, Z Husti, T Hornyik, I Baczkó, P Laguna, A Varró, and B Rodríguez. Mechanisms of ventricular rate adaptation as a predictor of arrhythmic risk. *American Journal of Physiology: Heart and Circulatory Physiology*, 289(5):H1577–H1587, 2010.

[123] E Pueyo, P Smetana, P Caminal, A Bayés-de Luna, M Malik, and P Laguna. Characterization of QT interval adaptation to RR interval changes and its use as a risk-stratifier of arrhythmic mortality in amiodarone-treated survivors of acute myocardial infarction. *IEEE Transactions on biomedical engineering*, 51(9):1511–1520, 2004.

[124] A Grom, TS Faber, M Brunner, C Bode, and M Zehender. Delayed adaptation of ventricular repolarization after sudden changes in heart rate due to conversion of atrial fibrillation. A potential risk factor for proarrhythmia? *Europace*, 7(2):113–121, 2005.

[125] P Smetana, E Pueyo, K Hnatkova, V Batchvarov, P Laguna, and M Malik. Individual patterns of dynamic QT/RR relationship in survivors of acute myocardial infarction and their relationship to antiarrhythmic efficacy of amiodarone. *Journal of Cardiovascular Electrophysiology*, 15(10):1147–1154, 2004.

[126] A Pathak, D Curnier, J Fourcade, et al. QT dynamicity: a prognostic factor for sudden cardiac death in chronic heart failure. *European Journal of Heart Failure*, 7(2):269–275, 2005.

[127] M Iacoviello, C Forleo, P Guida, R Romito, A Sorgente, S Sorrentino, S Catucci, F Mastropasqua, and M Pitzalis. Ventricular repolarization dynamicity provides independent prognostic information toward major arrhythmic events in patients with idiopathic dilated cardiomyopathy. *Journal of the American College of Cardiology*, 50(3):225–231, 2007.

[128] K Szydlo, M Trusz-Gluza, K Wita, A Filipecki, W Orszulak, D Urbanczyk, J Krauze, J Kolasa, and Z Tabor. QT/RR relationship in

patients after remote anterior myocardial infarction with left ventricular dysfunction and different types of ventricular arrhythmias. *Annals of Noninvasive Electrocardiology*, 13(1):60–66, 2008.

[129] JA Kors, HJ Ritsema van Eck, and G van Herpen. The meaning of the Tp-Te interval and its diagnostic value. *Journal of Electrocardiology*, 41:575–580, 2008.

[130] M Yamaguchi, M Shimizu, H Ino, H Terai, K Uchiyama, K Oe, T Mabuchi, T Konno, T Kaneda, and H Mabuchi. T wave peak-to-end interval and QT dispersion in acquired long QT syndrome: a new index for arrhythmogenicity. *Clinical Science*, 105(6):671–676, 2003.

[131] T M Abdelrahman. Prognostic value of Tpeak-to-end interval for risk stratification after acute myocardial infarction. *The Egyptian Journal of Critical Care Medicine*, 2(1):19 – 27, 2014.

[132] R Panikkath, K Reinier, A Uy-Evanado, C Teodorescu, J Hattenhauer, R Mariani, K Gunson, J Jui, and SS Chugh. Prolonged Tpeak-to-Tend interval on the resting ECG is associated with increased risk of sudden cardiac deathclinical perspective. *Circulation: Arrhythmia and Electrophysiology*, 4(4):441–447, 2011.

[133] R Coronel, FJ Wilms-Schopman, T Opthof, and MJ Janse. Dispersion of repolarization and arrhythmogenesis. *Heart Rhythm*, 6(4):537–543, 2009.

[134] MP Nash, CP Bradley, PM Sutton, RH Clayton, P Kallis, MP Hayward, DJ Paterson, and P Taggart. Whole heart action potential duration restitution properties in cardiac patients: A combined clinical and modelling study. *Experimental Physiology*, 91(2):339–354, 2006.

[135] A Mincholé, E Pueyo, JF Rodríguez, E Zacur, M Doblaré, and P Laguna. Quantification of restitution dispersion from the dynamic changes of the T-wave peak to end, measured at the surface ECG. *IEEE Transactions on Biomedical Engineering*, 58(5):1172–1182, 2011.

[136] A Mincholé, A Bueno-Orovio, P Laguna, E Pueyo, and B Rodríguez. ECG-based estimation of dispersion of APD restitution as a tool to stratify sotalol-induced arrhythmic risk. *Journal of Electrocardiology*, 48:867–873, 2015.

[137] A Mincholé, R Ariga, S Neubauer, H Watkins, and B Rodríguez. Electrocardiographic abnormalities of hypertrophic cardiomyopathy. In *Computing in Cardiology*, volume 41, pages 387–400, 2014.

[138] J Ramírez, V Monasterio, A Mincholé, et al. Automatic SVM classification of sudden cardiac death and pump failure death from autonomic and repolarization ECG markers. *Journal of Electrocardiology*, 48(4):551–557, 2014.

[139] J Ramírez, P Laguna, A Bayés-de Luna, M Malik, and E Pueyo. QT/RR and T-peak-to-end/RR curvatures and slopes in chronic heart failure: Relation to sudden cardiac death. *Journal of Electrocardiology*, 47:842–848, 2014.

[140] A Oehler, T Feldman, CA Henrikson, and LG Tereshchenko. QRS-T angle: A review. *Annals of Noninvasive Electrocardiology*, 19(6):534–542, 2014.

[141] JA Kors, I Kardys, IM van der Meer, G van Herpen, A Hofman, DAM van der Kuip, and JCM Witteman. Spatial QRS-T angle as a risk indicator of cardiac death in an elderly population. *Journal of Electrocardiology*, 36(1):113–114, 2003.

[142] T Yamazaki, VF Froelicher, J Myers, S Chun, and P Wang. Spatial QRS-T angle predicts cardiac death in a clinical population. *Heart Rhythm*, 2(1):73–78, 2005.

[143] JJ Goldberger, ME Cain, SH Hohnloser, et al. American Heart Association/American College of Cardiology Foundation/Heart Rhythm Society Scientific Statement on Noninvasive Risk Stratification Techniques for Identifying Patients at Risk for Sudden Cardiac Death. *Circulation*, 118(14):1497–1518, September 2008.

[144] HE Hering. Experimentelle studien an sugetieren ber das elektrocardiogram. *Zeitschrift fr experimentelle Pathologie und Therapie*, (7):363–378, 1909.

[145] JP Martínez and S Olmos. Methodological principles of T wave alternans analysis: a unified framework. *IEEE Transactions on Biomedical Engineering*, 52(4):599–613, April 2005.

[146] DS Rosenbaum, LE Jackson, JM Smith, H Garan, JN Ruskin, and RJ Cohen. Electrical Alternans and Vulnerability to Ventricular Arrhythmias. *New England Journal of Medicine*, 330(4):235–241, January 1994.

[147] BD Nearing and RL Verrier. Modified moving average analysis of T-wave alternans to predict ventricular fibrillation with high accuracy. *Journal of Applied Physiology*, 92(2):541–549, 2002.

[148] G Turitto, EB Caref, G El-Attar, M Helal, A Mohamed, RP Pedalino, and N El-Sherif. Optimal target heart rate for exercise-induced T-wave alternans. *Annals of Noninvasive Electrocardiology*, 6(2):123–128, 2001.

[149] S Maeda, M Nishizaki, N Yamawake, et al. Ambulatory ECG-based T-wave alternans and heart rate turbulence predict high risk of arrhythmic events in patients with old myocardial infarction. *Circulation Journal*, 73(12):2223–2228, 2009.

[150] PK Stein, D Sanghavi, PP Domitrovich, RA Mackey, and P Deedwania. Ambulatory ECG-based T-wave alternans predicts sudden cardiac death in high-risk post-MI patients with left ventricular dysfunction in the EPHESUS study. *Journal of Cardiovascular Electrophysiology*, 19(10):1037–1042, 2008.

[151] RL Verrier, K Kumar, and BD Nearing. Basis for Sudden Cardiac Death Prediction by T-Wave Alternans from an Integrative Physiology Perspective. *Heart Rhythm*, 6(3):416–422, 2009.

[152] RL Verrier, BD Nearing, and KF Kwaku. Noninvasive sudden death risk stratification by ambulatory ECG-based T-wave alternans analysis: Evidence and methodological guidelines. *Annals of Noninvasive Electrocardiology*, 10(1):110–120, 2005.

[153] JP Martínez, S Olmos, G Wagner, and P Laguna. Characterization of repolarization alternans during ischemia: time-course and spatial analysis. *IEEE Transactions on Biomedical Engineering*, 53(4):701–711, 2006.

[154] M Orini, B Hanson, V Monasterio, JP Martínez, M Hayward, P Taggart, and P Lambiase. Comparative Evaluation of Methodologies for T-Wave Alternans Mapping in Electrograms. *IEEE Transactions on Biomedical Engineering*, 61(2):308–316, 2014.

[155] V Monasterio, P Laguna, and JP Martínez. Multilead Analysis of T-Wave Alternans in the ECG Using Principal Component Analysis. *IEEE Transactions on Biomedical Engineering*, 56(7):1880–1890, 2009.

[156] V Monasterio, GD Clifford, P Laguna, and JP Martínez. A multilead scheme based on periodic component analysis for T-wave alternans analysis in the ECG. *Annals of Biomedical Engineering*, 38(8):2532–2541, 2010.

[157] V Monasterio, P Laguna, I Cygankiewicz, R Vázquez, A Bayés-Genís, A Bayés-de Luna, and JP Martínez. Average T-wave alternans activity in ambulatory ECG records predicts sudden cardiac death in patients with chronic heart failure. *Heart Rhythm*, 9(3):383–389, 2012.

[158] H Hashimoto, K Suzuki, and M Nakashima. Effects of the ventricular premature beat on the alternation of the repolarization phase in ischemic myocardium during acute coronary occlusion in dogs. *Journal of Electrocardiology*, 17(3):229–238, 1984.

[159] AA Armoundas, T Mela, and FM Merchant. On the estimation of T-wave alternans using the spectral fast fourier transform method. *Heart Rhythm*, 9(3):449–456, 2012.

[160] SM Narayan and JM Smith. Spectral analysis of periodic fluctuations in electrocardiographic repolarization. *IEEE Transactions on Biomedical Engineering*, 46(2):203–212, 1999.

[161] HJJ Wellens, PJ Schwartz, FW Lindemans, et al. Risk stratification for sudden cardiac death: current status and challenges for the future. *European Heart Journal*, 35(25):1642–1651, 2014.

[162] MM Demidova, A Martín-Yebra, JP Martínez, V Monasterio, S Koul, J van der Pals, D Romero, P Laguna, D Erlinge, and PG Platonov. T-wave alternans in experimental myocardial infarction: Time course and predictive value for the assessment of myocardial damage. *Journal of Electrocardiology*, 46:263–269, 2013.

[163] DL Carson, R Cardinal, P Savard, and M Vermeulen. Characterisation of unipolar waveform alternation in acutely ischaemic porcine myocardium. *Cardiovascular Research*, 20:521–527, 1986.

[164] O Paz, X Zhou, J Gillberg, HJ Tseng, E Gang, and C Swerdlow. Detection of T-wave alternans using an implantable cardioverted-defibrillator. *Heart Rhythm*, 3(7):791–797, 2006.

[165] MA Kwofie, AK Chaudhary, and JB Martins. Association among intracardiac T-wave alternans, ischemia, and spontaneous ventricular arrhythmias after coronary artery occlusion in a canine model. *Translational Research*, 158:265–272, 2011.

[166] BD Nearing and RL Verrier. Tracking cardiac electrical instability by computing interlead heterogeneity of T-wave morphology. *Journal of Applied Physiology*, 95:2265–2272, 2003.

[167] EH Weiss, FM Merchant, A d'Avila, L Foley, VY Reddy, JP Singh, T Mela, JN Ruskin, and AA Armoundas. A novel lead configuration for optimal spatio-temporal detection of intracardiac repolarization alternansclinical perspective. *Circulation: Arrhythmia and Electrophysiology*, 4(3):407–417, 2011.

[168] RK Sandhu, O Costantini, JE Cummings, S Poelzing, DS Rosenbaum, and KJ Quan. Intracardiac alternans compared to surface T-wave alternans as a predictor of ventricular arrhythmias in humans. *Heart Rhythm*, 5(7):1003 – 1008, 2008.

[169] J Tsai, JM CAo, S Zhou, M Swissa, AW Cates, BH Kenknight, LS Chen, HS Karagueuzian, and PS Chen. T-wave alternans as a predictor of spontaneous ventricular tachycardia in a canine model of sudden cardiac death. *Journal of Cardiovascular Electrophysiology*, 13:51–55, 2002.

[170] AA Armoundas, CM Alber, RJ Cohen, and T Mela. Utility of implantable cardioverter defibrillator electrograms to estimate repolarization alternans preceding a tachyarrhythmic event. *Journal of Cardiovascular Electrophysiology*, 15:594–597, 2004.

[171] DJ Christini, KM Stein, SC Hao, SM Markowitz, S Mittal, DJ Slotwiner, S Iwai, MK Das, and BB Lerman. Endocardial detection of repolarization alternans. *IEEE Transactions on Biomedical Engineering*, 50(7):855–862, 2003.

[172] JP Martínez, R Almeida, S Olmos, AP Rocha, and P Laguna. A wavelet-based ECG delineator: evaluation on standard databases. *IEEE Transactions on Biomedical Engineering*, 51(4):570–581, 2004.

[173] LK Saul and JB Allen. Periodic component analysis: an eigenvalue method for representing periodic structure in speech. In *Advances in Neural Information Processing Systems 13 - Proceedings of the 2000 Conference, NIPS 2000*, volume 14, pages 807–813, 2000.

[174] R Sameni, C Jutten, and MB Shamsollahi. Multichannel electrocardiogram decomposition using periodic component analysis. *IEEE Transactions on Biomedical Engineering*, 55(8):807–813, 2008.

[175] S Okamoto, M Inden, T Konishi, and T Nakano. ST segment alternans during percutaneous transluminal coronary angioplasty – A case report. *Angiology*, 42(1):30–34, 1991.

[176] BD Nearing, SN Oesterle, and RL Verrier. Quantification of ischaemia induced vulnerability by precordial T wave alternans analysis in dog and human. *Cardiovascular Research*, 28(9):1440–1449, 1994.

[177] E Kaplinsky, S Ogawa, CW Balke, and LS Dreifus. Two periods of early ventricular arrhythmia in the canine acute myocardial infarction model. *Circulation*, 60:397–403, 1979.

[178] AE Nicogossian, RS Williams, CL Huntoon, CR Doarn, JD Polk, and VS Schneider. *Space Physiology and Medicine: From Evidence to Practice*. Springer, 4th edition, 2016.

[179] BM Mitchell and JV Meck. Short-duration spaceflight does not prolong QTc intervals in male astronauts. *The American Journal of Cardiology*, 93(8):1051 – 1052, 2004.

[180] EG Caiani, A Pellegrini, J Bolea, M Sotaquira, R Almeida, and P Vaïda. Impaired T-wave amplitude adaptation to heart-rate induced by cardiac deconditioning after 5-days of head-down bed-rest. *Acta Astronautica*, 91:166–172, 2013.

[181] C Sakowski, V Starc, SM Smith, and TT Schlegel. Sedentary long-duration head-down bed rest and ECG repolarization heterogeneity. *Aviation, Space and Environmental Medicine*, 82:416–423, 2011.

[182] SM Grenon, X Xiao, S Hurwitz, CD Ramsdell, N Sheynberg, C Kim, GH Williams, and RJ Cohen. Simulated microgravity induces microvolt T wave alternans. *Annals of Noninvasive Electrocardiology*, 10(3):363–370, 2005.

[183] D Linnarsson, RL Hughson, KS Fraser, G Clément, LL Karlsson, E Mulder, WH Paloski, J Rittweger, FL Wuyts, and J Zange. Effects of an artificial gravity countermeasure on orthostatic tolerance, blood volumes and aerobic power after short-term bed rest (BR-AG1). *Journal of Applied Physiology*, 118(1):29–35, 2015.

[184] R Bailón, N Garatachea, I de la Iglesia, JA Casajús, and P Laguna. Influence of running stride frequency in heart rate variability analysis during treadmill exercise testing. *IEEE Transactions on Biomedical Engineering*, 60(7):1796–1805, 2013.

[185] F Castells, P Laguna, L Sörnmo, A Bollmann, and J Millet-Roig. Principal component analysis in ECG signal processing. *EURASIP Journal on Advances in Signal Processing*, 2007(1):074580, 2007.

[186] D Hernando, R Bailón, P Laguna, and L Sörnmo. Heart rate variability during hemodialysis and its relation to hypotension. In *Computing in Cardiology 2011*, volume 38, pages 189–192, 2011.

[187] Task Force of the European Society of Cardiology Electrophysiology and the North American Society of Pacing and. Heart rate variability: standards of measurement, physiological interpretation and clinical use. *Circulation*, 93(5):1043–1065, 1996.

[188] EG Caiani, P Massabuau, L Weinert, P Vaïda, and RM Lang. Effects of 5 days of head-down bed rest, with and without short-arm centrifugation as countermeasure, on cardiac function in males (BR-AG1 study). *Journal of Applied Physiology*, 117(6):624–632, 2014.

[189] PJ Schwartz and A Malliani. Electrical alternation of the T-wave: clinical and experimental evidence of its relationship with the sympathetic nervous system and with the long QT syndrome. *American Heart Journal*, 89(1):45–50, 1975.

[190] ES Kaufman, JA Mackall, B Julka, C Drabek, and DS Rosenbaum. Influence of heart rate and sympathetic stimulation on arrhythmogenic T wave alternans. *American journal of physiology. Heart and circulatory physiology*, 279(3):H1248–55, 2000.

[191] M Baumert, E Lambert, G Vaddadi, CI Sari, M Esler, G Lambert, P Sanders, and E Nalivaiko. Cardiac repolarization variability in patients with postural tachycardia syndrome during graded head-up tilt. *Clinical Neurophysiology*, 122(2):405–409, 2011.

[192] K Iwasaki, T Shiozawa, A Kamiya, D Michikami, K Hirayanagi, K Yajima, S Iwase, and T Mano. Hypergravity exercise against bed rest induced changes in cardiac autonomic control. *European Journal of Applied Physiology*, 94(3):285–291, 2005.

[193] MB Stenger, JM Evans, CF Knapp, SM Lee, TR Phillips, SA Perez, AD Jr Moore, WH Paloski, and SH Platts. Artificial gravity training reduces bed rest-induced cardiovascular deconditioning. *European Journal of Aapplied Physiology*, 112(2):605–616, 2012.

[194] D Duplyakov, G Golovina, E Sysuenkova, and S Garkina. Can the result of a tilt test be predicted in the first five minutes? *Cardiology Journal*, 18(5):521–526, 2011.

[195] P Albrecht, J Arnold, S Krishnarnachari, and RJ Cohen. Exercise recordings for the detection of T-wave alternans: Promises and pitfalls. *Journal of Electrocardiology*, 29(1):46–51, 1996.

[196] T Chow, DJ Kereiakes, J Onufer, A Woelfel, S Gursoy, BJ Peterson, ML Brown, W Pu, DG Benditt, and MASTER Trial Investigators. Does microvolt T-wave alternans testing predict ventricular tachyarrhythmias in patients with ischemic cardiomyopathy and prophylactic defibrillators? The MASTER (Microvolt T Wave Alternans Testing for Risk Stratification of Post-Myocardial Infarction Patients) trial. *Journal of the American College of Cardiology*, 52(20):1607–1615, 2008.

[197] O Costantini, SH Hohnloser, MM Kirk, BB Lerman, JH Baker, B Sethuraman, MM Dettmer, and DS Rosenbaum. The ABCD (Alternans Before Cardioverter Defibrillator) Trial: Strategies Using T-Wave Alternans to Improve Efficiency of Sudden Cardiac Death Prevention. *Journal of the American College of Cardiology*, 53(6):471–479, 2009.

[198] MR Gold, JH Ip, O Costantini, JE Poole, S McNulty, DB Mark, KL Lee, and GH Bardy. Role of microvolt T-wave alternans in assessment of arrhythmia vulnerability among patients with heart failure and systolic dysfunction: Primary results from the T-wave alternans sudden cardiac death in heart failure trial substudy. *Circulation*, 118(20):2022–2028, 2008.

[199] DM Bloomfield, SH Hohnloser, and RJ Cohen. Interpretation and classification of microvolt T-wave alternans tests. *Journal of Cardiovascular Electrophysiology*, 13(5):502–512, 2002.

[200] T Nieminen and RL Verrier. Usefulness of T-wave alternans in sudden death risk stratification and guiding medical therapy. *Annals of Noninvasive Electrocardiology*, 15(3):276–288, 2010.

[201] X-Q Quan, H-L Zhou, L Ruan, J-G Lv, J-H Yao, F Yao, K Huang, and C-T Zhang. Ability of ambulatory ECG-based T-wave alternans to modify risk assessment of cardiac events: A systematic review. *BMC Cardiovascular Disorders*, 14, 2014.

[202] GB Moody, WE Muldrow, and RG Mark. A noise stress test for arrhythmia detectors. In *Computers in Cardiology 1984*, volume 11, pages 381–384, 1984.

[203] R Vázquez, A Bayés-Genís, I Cygankiewicz, et al. The MUSIC Risk score: a simple method for predicting mortality in ambulatory patients with chronic heart failure. *European Heart Journal*, 30(9):1088–1096, 2009.

[204] GB Moody and RG Mark. Development and evaluation of a 2-lead ECG analysis program. In *Computers in Cardiology 1982*, volume 9, pages 39–44, 1982.

[205] F Extramiana, P Maison-Blanche, F Badilini, J Pinoteau, T Deseo, and P Coumel. Circadian modulation of QT rate dependence in healthy volunteers. *Journal of Electrocardiology*, 32(1):33 – 43, 1999.

[206] E Watanabe, T Arakawa, T Uchiyama, M Tong, K Yasui, H Takeuchi, T Terasawa, I Kodama, and H Hishida. Prognostic significance of circadian variability of RR and QT intervals and QT dynamicity in patients with chronic heart failure. *Heart Rhythm*, 4(8):999 – 1005, 2007.

[207] JE Muller, PL Ludmer, SN Willich, GH Tofler, G Aylmer, I Klangos, and PH Stone. Circadian variation in the frequency of sudden cardiac death. *Circulation*, 75(1):131–138, 1987.

[208] SM Narayan, BD Lindsay, and JM Smith. Demonstration of the Pro-arrhythmic Preconditioning of Single Premature Extrastimuli by Use

of the Magnitude, Phase, and Distribution of Repolarization Alternans. *Circulation*, 100(18):1887–1893, 1999.

[209] O Sayadi, FM Merchant, D Puppala, T Mela, JP Singh, EK Heist, C Owen, and AA Armoundas. A novel method for determining the phase of T-wave alternans: Diagnostic and therapeutic implications. *Circulation: Arrhythmia and Electrophysiology*, 6(4):818–826, 2013.

[210] VN Batchvarov, II Christov, G Bortolan, II Simova, and AJ Camm. Post-extrasystolic changes of the vectorcardiographic T loop in healthy subjects. In *2007 Computers in Cardiology*, pages 451–454, 2007.

[211] VN Batchvarov, A Bajpai, and AJ Camm. Post-extrasystolic changes of the T wave in a patient with congestive heart failure. *EP Europace*, 9(11):1093, 2007.

[212] G Lenis, T Baas, and O Dössel. Ectopic beats and their influence on the morphology of subsequent waves in the electrocardiogram. *Biomedical Engineering / Biomedizinische Technik*, 58(2):109–119, 2013.

[213] RL Verrier and BD Nearing. Ambulatory ECG monitoring of T-wave alternans for arrhythmia risk assessment. *Journal of Electrocardiology*, 36:193–197, 2003.

[214] T Nieminen, T Lehtimäki, J Viik, et al. T-wave alternans predicts mortality in a population undergoing a clinically indicated exercise test. *European Heart Journal*, 28(19):23332–2337, 2007.

[215] K Nademanee, V Intarachot, MA Josephson, and BN Singh. Circadian variation in occurrence of transient overt and silent myocardial ischemia in chronic stable angina and comparison with Prinzmetal angina in men. *American Journal of Cardiology*, 60(7):494–498, 1987.

[216] F Badilini, P Maison-Blanche, R Childers, and P Coumel. QT interval analysis on ambulatory electrocardiogram recordings: a selective beat averaging approach. *Medical & Biological Engineering & Computing*, 37(1):71–79, 1999.

[217] A Eisen, CT Ruff, E Braunwald, et al. Sudden cardiac death in patients with atrial fibrillation: Insights from the ENGAGE AFTIMI 48 trial. *Journal of the American Heart Association*, 5(7):e003735, 2016.

[218] K Reinier, E Marijon, A Uy-Evanado, C Teodorescu, K Narayanan, H Chugh, K Gunson, J Jui, and SS Chugh. The association between atrial fibrillation and sudden cardiac death: the relevance of heart failure. *JACC. Heart failure*, 2(3):221–227, 2014.

[219] JP Piccini and JP Daubert. Atrial fibrillation and sudden cardiac death: Is heart failure the middleman? *JACC: Heart Failure*, 2(3):228–229, 2014.

[220] CP Lau, AR Freedman, S Flemming, M Malik, AJ Camm, and DE Ward. Hysteresis of the ventricular paced QT interval in response to abrupt changes in pacing rate. *Cardiovascular Research*, 22(2):67–72, 1988.

[221] A Fujiki, R Yoshioka, M Sakabe, and S Kusuzaki. QT/RR relation during atrial fibrillation based on a single beat analysis in 24-h holter ECG: The role of the second and further preceding RR intervals in QT modification. *Journal of Cardiology*, 57(3):269 – 274, 2011.

[222] I Cygankiewicz, V Corino, R Vazquez, A Bayés-Genis, L Mainardi, W Zareba, A Bayés-de Luna, PG Platonov, and MUSIC Trial Investigators. Reduced irregularity of ventricular response during atrial fibrillation and long-term outcome in patients with heart failure. *The American Journal of Cardiology*, 116(7):1071–1075, 2015.

List of Publications

Journal Publications

A Martín-Yebra, EG Caiani, V Monasterio, A Pellegrini, P Laguna, JP Martínez. Evaluation of T-wave alternans activity under stress conditions after 5 days and 21 days of sedentary head-down bed-rest. *Physiological measurement*, 2015;(36):pp. 2041-2055.

EG Caiani, **A Martín-Yebra**, F Landreani, J Bolea, P Laguna, P Vaïda. Weightlessness and cardiac rhythm disorders: current knowledge from space flight and bed-rest studies. *Frontiers in Astronomy and Space Sciences*,2016;(3):27

A Martín-Yebra, V Monasterio, I Cygankiewicz, A Bayés-de-Luna, EG Caiani, P Laguna and JP Martínez. Post-Ventricular Premature Contraction Phase Correction Improves the Predictive Value of Average T-wave Alternans in Ambulatory ECG Recordings. *IEEE Transactions on Biomedical Engineering*, 2017; DOI: 10.1109/TBME.2017.2711645.

Submitted Publications

A Martín-Yebra, P Laguna, I Cygankiewicz, A Bayés-de-Luna, EG Caiani, JP Martínez. Indices of Ventricular Repolarization Variation for Sudden Cardiac Death Prediction in Atrial Fibrillation Patients. Submitted to IEEE Transactions on Biomedical Engineering. *Under review.*

Conference Proceedings

A Martín-Yebra, V Monasterio, A Pellegrini, P Laguna, E Caiani, JP Martínez. Effect of Simulated Microgravity by Head-Down Bed-Rest on T wave Alternans. *XXXIX International Conference on Computing in Cardiology*, pp. 377-380, Krakow (Poland), September 2012.

A Martín-Yebra, E Caiani, V Monasterio, A Pellegrini, P Laguna, JP Martínez. T-Wave Alternans and Autonomic Nervous System Activity During Orthostatic Stress after 5 Days of Head-Down Bed-Rest. *Cardiovascular Oscillations (ESGCO), 2014 8th Conference of the European Study Group on;*, pp. 115-116, Fai della Paganella, (Italy), May 2014.

A Martín-Yebra, EG Caiani, P Laguna, V Monasterio and JP Martínez. Circadian Modulation on T-wave Alternans Activity in Chronic Heart Failure Patients. *XLII International Conference on Computing in Cardiology, 2015*, pp. 845-848, Nice (France). September, 2015.

A Martín-Yebra, I Cygankiewicz, A Bayés-de-Luna, P Laguna, EG Caiani, JP Martínez. Index of T-wave Variation as a Predictor of Sudden Cardiac Death in Chronic Heart Failure Patients with Atrial Fibrillation. *XLIII International Conference on Computing in Cardiology, 2016*, pp. 5-8, Vancouver (Canada). September, 2016.

A Martín-Yebra, V Monasterio, P Laguna, JP Martínez, EG Caiani. Evaluation of changes in T-wave alternans induced by 60-days of immobilization by head-down bed-rest. *XLIV International Conference on Computing in Cardiology, 2017.* Acepted.

Abstracts

A Martín-Yebra, JP Martínez, V Monasterio, A Pellegrini, P Laguna, E Caiani. Evaluation of T-wave alternans during exercise and orthostatic stress testing after 5 days of head-down bed-rest. *Life in space for life on earth symposium.* Waterloo (Canada). June, 2014. Abstract.

E Caiani, A Pellegrini, J Bolea, **A Martín-Yebra**, A Auricchio, P Laguna, P Vaïda. Ventricular Repolarization Changes Driven by Deconditioning after 21Days of HeadDown BedRest. *Life in space for life on earth symposium.* Waterloo (Canada). June, 2014. Abstract.

A Martín-Yebra, JP Martínez, V Monasterio, P Laguna, EG Caiani. Evaluation of changes in T-wave alternans induced by 21-days of bedridden immobilization by head-down bed-rest. *(European Heart Journal, suppl. 1: Abstracts of the ESC Congress 2015, London, UK, P1545, 2015).* August, 2015.

Publications indirectly related to the thesis

MM Demidova, **A Martín-Yebra**, JP Martínez, V Monasterio, Sasha Koul, J van der Pals, D Romero, P Laguna, D Erlinge, P Platonov. T wave alternans in experimental myocardial infarction: Time course and predictive value for assessment of myocardial damage. *Journal of Electrocardiology* 46(3):pp. 263–9. 2013.

MM Demidova, **A Martín-Yebra**, J van der Pals, S Koul, D Erlinge, P Laguna, JP Martínez, P G Platonov. Transient and rapid QRS widening associated with J-wave pattern predicts impending ventricular fibrillation in experimental myocardial infarction." *Heart Rhythm* 11(7). pp. 1195-1201, 2014.

MM Demidova, **A Martín-Yebra**, S Koul, H Engblom, JP Martínez, D Erlinge, PG Platonov. QRS broadening due to terminal distortion is associated with the size of myocardial injury in experimental myocardial infarction. *Journal of Electrocardiology*; 49:pp. 300–306. March, 2016.

A Martín-Yebra, F Landreani, C Casellato, E Pavan, P-F Migeotte, C Frigo, JP Martínez, EG Caiani. Evaluation of respiratory- and postural-induced changes on the Ballistocardiogram signal by time warping averaging. *Physiological measurement*; 38(7):1426–1440. Jun, 2017

A Martín-Yebra, F Landreani, C Casellato, E Pavan, C Frigo, P-F Migeotte, E G Caiani. Studying Heart Rate Variability from Ballistocardiography Acquired by Force Platform: Comparison with Conventional ECG. *XLII International Conference on Computing in Cardiology*, pp. 929-932, Nice (France). September, 2015.

EG Caiani, **A Martín-Yebra**, A Pellegrini, J Bolea, A Auricchio, E Pueyo, P Vaïda. High protein intake supplementation to compensate changes in ventricular repolarization due to 21-days of bedridden immobilization *European Heart Journal, suppl. 1: Abstracts of the ESC Congress 2015, London, UK, P6443 2015).* August, 2015.

F Landreani, **A Martín-Yebra**, C Casellato, E Pavan, C Frigo, P-F Migeotte, E G Caiani. Feasibility Study for Beat-to-beat Heart Rate detection by Smartphones Accelerometers. *The 5th IEEE International Conference on E-Health and Bioengineering - EHB 2015*, Iasi, pp. 1-4, 2015.

F Landreani, **A Martín-Yebra**, C Casellato, C Frigo, E Pavan, P-F Migeotte, EG Caiani Beat-to-beat Heart Rate Detection by Smartphones Accelerometers: Validation with ECG. *38th Annual International Conference of the IEEE Engineering in Medicine and Biology Society (EMBC)*, Orlando, FL, 2016, pp. 525-528. August, 2016.

F Landreani, M Morri, **A Martín-Yebra**, C Casellato, E Pavan, C Frigo, EG Caiani. Ultra-Short-Term Heart Rate Variability Analysis on Accelerometric Signals from Mobile Phone. *2017 E-Health and Bioengineering Conference (EHB)*, pp. 241-244, Sinaia (Romania), 2017.

F Landreani, **A Martín-Yebra**, C Casellato, E Pavan, C Frigo, P-F Migeotte, A Faini, G Parati, EG Caiani. Respiratory Frequency Estimation From Acceleromet-ric Signals Acquired by Mobile Phone in a Controlled Breathing Protocol. *XLIV International Conference on Computing in Cardiology 2017*. Accepted.